

Removal of steroid hormones from water by permeate-side polymer-based spherical activated carbon assisted membrane filtration

Zur Erlangung des akademischen Grades eines DOKTORS DER
INGENIEURWISSENSCHAFTEN (DR.-ING.)

von der KIT-Fakultät für Chemieingenieurwesen und Verfahrenstechnik des
Karlsruher Instituts für Technologie (KIT)

genehmigte

DISSERTATION

von

M. Sc. Matteo Tagliavini

Tag der mündlichen Prüfung: 22.10.2021

Erstgutachter: Prof. Dr.-Ing. Hermann Nirschl

Zweitgutachter: Prof. Dr.-Ing. Hans Hasse

Erstbetreuerin: Prof. Dr.-Ing. Andrea Iris Schäfer

“Da ist schon viel gefunden, aber da ist mehr, was noch gefunden werden kann. Und so gibt es wieder zu tun für neue Geschlechter.”

“Molto è già stato trovato, ma quello che è ancora da trovare, è di più. E questo significa altro lavoro per le nuove generazioni.”

Bertold Brecht *“Leben des Galilei”*

“Vita di Galileo”

Abstract

The presence of micropollutants in surface waters constitutes a serious concern both to the environment and human health. Among micropollutants, hormones emerge as one of the most dangerous due to their high estrogenic potential. After a lengthy monitoring strategy, the European Commission has proposed restricting environmental and drinking water quality standards (0.4 and 1 ng L^{-1} , respectively) for the most estrogenic hormone, estradiol.

Activated carbon adsorption is the most established and long-time used technology to remove a vast range of contaminants from water. High-pressure membranes and advanced oxidation processes, on the other hand, are receiving increasing consideration to address the issue of micropollutants due to their high removal efficiency. However, the high energy consumption and the risk of by-product formation are the main drawbacks of such promising technologies.

In this thesis, a novel approach is proposed to remove hormones from water. The approach relies on the combination of low-pressure membranes and activated carbon adsorption. The novelty is that polymer-based spherical activated carbon is used as a millimetric layer, placed on the permeated side of an ultrafiltration membrane.

Initially, a commercial activated carbon textile filter with a thickness of 2.2 mm is used. The filter is demonstrated to remove significantly hormones, reducing their concentrations from 100 ng L^{-1} in the feed to 20 to 40 ng L^{-1} in the permeate in a contact time of only 1 min . Stacking five filters on the permeate side of the membrane allows reducing the concentration down to 7 ng L^{-1} . When loose activated carbon is packed in a millimetric layer (e.g., not using the commercial filter), the adsorption process improves its performance and estradiol permeate concentration can be reduced to 7 ng L^{-1} with an adsorbing layer of only 2 mm .

This promising performance is still not enough to reduce estradiol below the target concentration. For this reason, the material characteristics (size, porous morphology and oxygen content) were systematically investigated to improve the kinetics of adsorption and, thus, the performance of the process. The activated carbon size emerges as the most critical factor that can be exploited to improve the adsorption kinetics. Estradiol concentration can be reduced (from 100 ng L^{-1} in the feed) below the drinking water standard of 1 ng L^{-1} with a layer of 2 mm and 4 mm packed with activated carbon of diameter 80 and $200 \mu\text{m}$, respectively.

Further, the mass transport of a trace solute in such a thin packed-layer is investigated by formulating and validating a breakthrough model. Axial dispersion is a transport mechanism that cannot be neglected in a thin packed-bed. Reported empirical correlations to estimate the axial dispersion coefficient (developed for packed-column) are not valid. The axial dispersion coefficient, estimated by fitting the model to the experimental data, depends on the ratio between the activated carbon diameter and the layer thickness. The model can be used to predict the required activated

carbon layer thickness required to meet the drinking water standard at different feed concentrations.

Finally, the impact of dissolved organic carbon present in surface waters on the adsorption of estradiol is considered. Direct competition leading to an early breakthrough is not observed. The narrow pore size of the activated carbon used reveals to be an important factor. Indeed, a major fraction of organic carbon is (size-)excluded by the internal activated carbon porosity. On the other hand, minor indirect competition related to the binding of estradiol to organic carbon occurs. In this sense, the integration with the ultrafiltration membrane is beneficial in that the larger fraction of organic carbon is rejected and they cannot enter the activated carbon layer.

Ultrafiltration-polymer-based spherical activated carbon is demonstrated to be a promising technology. It can compete with high-pressure membranes and oxidation processes in terms of micropollutant removal efficiency, a crucial characteristic considering the extremely low concentration required in the permeate for micropollutants. In addition, this process presents a small footprint, it requires low pressure and does not generate harmful by-products. Nevertheless, investigations at a more realistic scale are necessary to claim the effectiveness of the process here presented.

Zusammenfassung

Das Vorhandensein von Mikroverunreinigungen in Oberflächengewässern stellt ein ernsthaftes Problem sowohl für die Umwelt als auch für die menschliche Gesundheit dar. Hormone zählen unter diesen Mikroverunreinigungen, aufgrund ihres hohen östrogenen Potentials, zu den gefährlichsten Verunreinigungen. Nach einer umfangreichen Langzeitstudie über Wasserqualität hat die Europäische Kommission für das östrogenhaltigste Hormon, Östradiol, restriktive Umwelt- und Trinkwasserqualitätsstandards (0.4 bzw. 1 ng L^{-1}) vorgeschlagen.

Die Aktivkohleadsorption ist die etablierteste und am längsten angewandte Technologie zur Filtration einer Vielzahl von Verunreinigungen aus dem Wasser. Hochdruckmembranen und erweiterte Oxidationsverfahren hingegen werden, aufgrund ihrer hohen Verunreinigungsentfernungseffizienz zunehmend in Betracht gezogen, um Mikroverunreinigungen aus dem Wasser zu filtern. Der hohe Energieverbrauch und das Risiko der Nebenproduktbildung sind jedoch die Hauptnachteile dieser vielversprechenden Technologien.

In dieser Arbeit wird ein neuartiger Ansatz zur Entfernung von Hormonen aus Wasser vorgestellt. Der Ansatz beruht auf der Kombination von Niederdruckmembranen und Aktivkohleadsorption. Die Neuheit besteht darin, dass eine millimeterdünne Schicht polymerbasierter sphärischer Aktivkohle, die auf der Permeationsseite einer Ultrafiltrationsmembran platziert ist, zur Filtration verwendet wird.

Zunächst wird ein kommerzieller Textil-Aktivkohlefilter mit einer Dicke von 2.2 mm verwendet. Der Filter entfernt nachweislich signifikant Hormone und reduziert deren Konzentrationen von 100 ng L^{-1} im Zulauf auf 20 bis 40 ng L^{-1} im Permeat in einer Kontaktzeit von nur 1 min . Durch Stapeln von fünf Filtern auf der Permeatseite der Membran kann die Konzentration bis auf 7 ng L^{-1} reduziert werden. Wenn lose Aktivkohle in eine millimeterdicke Schicht gepackt wird (z. B. ohne Verwendung des kommerziellen Filters), verbessert sich die Leistung des Adsorptionsprozesses und die Estradiol-Permeatkonzentration kann auf 7 ng L^{-1} bereits bei einer Adsorptionsschicht von nur 2 mm reduziert werden.

Diese vielversprechende Leistung reicht jedoch noch nicht aus, um die Estradiolkonzentration unter die vorgegebene Konzentration zu senken. Aus diesem Grund wurden die Materialeigenschaften (Größe, Porenmorphologie und Sauerstoffgehalt) systematisch untersucht, um die Kinetik der Adsorption und damit die Leistung des Prozesses zu verbessern. Die Aktivkohlegröße entpuppt sich als der kritischste Faktor, der zur Verbesserung der Adsorptionskinetik ausgenutzt werden kann. Die Estradiolkonzentration kann, (von 100 ng L^{-1} im Zulauf) mit einer Schicht von in 2 mm und 4 mm gepackten Aktivkohle von 80 bzw. $200 \text{ }\mu\text{m}$ Durchmesser, unter den Trinkwasserstandard von 1 ng L^{-1} reduziert werden.

Weiterhin wird der Stofftransport eines Spurenstoffes in einer solch dünn gepackten Schicht durch Formulierung und Validierung eines Durchbruchmodells untersucht. Axiale Dispersion ist ein Transportmechanismus, der in einem dünnen Schüttbett nicht vernachlässigt werden kann. Berichten zufolge sind empirische Korrelationen zur Abschätzung des axialen Dispersionskoeffizienten (entwickelt für Packsäulen) nicht gültig. Der axiale Dispersionskoeffizient, der durch Anpassung des Modells an die experimentellen Daten geschätzt wird, hängt vom Verhältnis zwischen dem Aktivkohledurchmesser und der Schichtdicke ab. Das Modell kann zur Vorhersage der erforderlichen Aktivkohleschichtdicke verwendet werden, die zur Einhaltung der Trinkwassernorm bei unterschiedlichen Zulaufkonzentrationen erforderlich ist.

Schließlich wird der Einfluss von gelöstem organischem Kohlenstoff, der in Oberflächengewässern vorhanden ist, auf die Adsorption von Estradiol betrachtet. Eine direkte Konkurrenz, die zu einem frühen Durchbruch führt, wird nicht beobachtet. Die enge Porengröße der verwendeten Aktivkohle erweist sich als ein wichtiger Faktor. Tatsächlich wird ein Großteil des organischen Kohlenstoffs durch die interne Aktivkohle-Porosität (durch seine Größe) ausgeschlossen. Andererseits tritt eine geringe indirekte Konkurrenz durch die Bindung von Estradiol an organischen Kohlenstoff auf. In diesem Sinne ist die Integration mit der Ultrafiltrationsmembran insofern vorteilhaft, als dass der Großteil des organischen Kohlenstoffs abgelehnt wird und es nicht in die Aktivkohleschicht eindringen kann.

Ultrafiltrations-Polymer-basierte sphärische Aktivkohle erweist sich als eine vielversprechende Technologie. Sie kann mit Hochdruckmembranen und Oxidationsverfahren in Bezug auf die Effizienz der Entfernung von Mikroverunreinigungen konkurrieren, eine entscheidende Eigenschaft, wenn man bedenkt, dass die Konzentration der Mikroverunreinigungen im Permeat extrem niedrig sein muss. Darüber hinaus weist dieses Verfahren einen geringen Platzbedarf auf, es benötigt einen niedrigen Druck und erzeugt keine schädlichen Nebenprodukte. Dennoch sind Untersuchungen in einem realistischeren Maßstab notwendig, um die Effektivität des hier vorgestellten Verfahrens zu belegen.

Acknowledgements

I would first like to thank the head of the Institute for Advanced Membrane Technology (IAMT), Professor Andrea Schäfer, for the great opportunity she gave to do a PhD at the Karlsruhe Institute of Technology, for the possibility to access to IAMT exclusive research facilities.

Blücher gmbh, the Helmholtz Association and the Science and Technology of Nanosystems (STN, Nanomembrane initiative) are acknowledged for the funding received. It has always been a major concern to me to honor the funding and make the most out of it.

Professor Enders is acknowledged for her tenacity in helping me to get from the dissertation to the PhD defense. Professor Nirschl, Professor Hasse and Professor Wetzel are acknowledged for the time and effort in reviewing my thesis and for being part of my PhD committee.

I further would like to acknowledge all the collaborators that support my research in these years; my Master student Julia Wolters for effort provided, the Blücher team for the provision of the material, related information and the constructive feedbacks on the project development; Christian Njel and Julia Maibach for the precious XPS measurements and discussion; Peter Weidler for the huge effort and time he has put in the characterization of the material. I also would like to thank Professor Vlad Tarabara for the nice discussion about the results we had at Euromembrane 2018. All the members of IFG-MT (now IAMT) are highly acknowledged for different aspects of my experience: from the fruitful discussion during the group meetings to the nice international and culturally rich environment, I had the opportunity to live.

From the personal side, I am really thankful to Mitra that has always supported me and my ambitions even in the hardest time. My family is particularly acknowledged for the continuous support given and for the desire to invest in my education and my personal growth. The great time spent with Patrick, Rene and Thomas (and family) and all their friends was much appreciated as they helped me to distract and to get in touch with Germany and its culture. My friends from Bologna are acknowledged for the good time I have always had when I went there during my PhD.

Contents

| | |
|--|------------|
| Abstract | iii |
| Zusammenfassung | v |
| Acknowledgements | vii |
| 1 Introduction | 1 |
| 1.1 Motivation | 1 |
| 1.2 Current options to remove estrogens | 4 |
| 1.2.1 Pressure-driven membrane processes | 5 |
| 1.2.2 Activated carbon adsorption | 6 |
| 1.2.3 Advanced oxidation processes | 6 |
| 1.2.4 Novel membrane processes | 7 |
| 1.3 Research proposal | 8 |
| 2 Polymer-based activated carbon assisted membrane filtration | 9 |
| 2.1 Introduction | 10 |
| 2.2 Material and methods | 12 |
| 2.2.1 Membranes | 12 |
| 2.2.2 Polymer-based spherical activated carbon particles and textile mat | 12 |
| 2.2.3 Solution chemistry and steroid hormones | 13 |
| 2.2.4 Analytical methods | 14 |
| 2.2.5 Stirred-cell filtration set-up | 14 |
| 2.2.6 Dynamic adsorption of hormones in the UF-PBSAC mat | 14 |
| 2.2.7 Dynamic adsorption of hormones in the UF-PBSAC packed-layer | 16 |
| 2.2.8 Static adsorption | 17 |
| 2.2.9 Data analysis | 17 |
| 2.3 Results and discussion | 17 |
| 2.3.1 Permeability / flow properties of the UF-PBSAC mat | 17 |
| 2.3.2 Breakthrough curves of hormones for the UF-PBSAC mat | 18 |
| 2.3.3 Influence of the contact time | 21 |
| 2.3.4 Comparison between PBSAC mat and packed-layer | 23 |
| 2.3.5 Considerations about the lifetime of the layer | 24 |
| 2.3.6 Nanofiltration-PBSAC mat | 26 |
| 2.4 Conclusions | 28 |

| | | |
|----------|---|-----------|
| 3 | Influence of PBSAC material characteristics on the adsorption of hormones in the thin packed-layer | 29 |
| 3.1 | Introduction | 30 |
| 3.2 | Materials and methods | 32 |
| 3.2.1 | Membrane | 32 |
| 3.2.2 | Polymer-based spherical activated carbon | 32 |
| 3.2.3 | Chemicals and analytical methods | 33 |
| 3.2.4 | Dynamic adsorption experiments | 34 |
| 3.2.5 | Static adsorption experiments | 35 |
| 3.2.6 | Material characterization | 35 |
| 3.2.7 | Data analysis | 35 |
| 3.3 | Results and discussion | 36 |
| 3.3.1 | External surface area in a PBSAC layer | 36 |
| 3.3.2 | Influence of PBSAC diameter on the dynamic adsorption of E2 | 37 |
| 3.3.3 | Implication of PBSAC diameter on the required layer thickness | 38 |
| 3.3.4 | Considerations about the pressure drop in the UF-PBSAC | 39 |
| 3.3.5 | Characterization of the porous morphology of PBSAC at different activation | 39 |
| 3.3.6 | Influence of the activation degree on the dynamic adsorption of E2 | 42 |
| 3.3.7 | Implication of PBSAC activation on the expected lifetime of the layer | 43 |
| 3.3.8 | Characterization of PBSAC surface chemistry | 44 |
| 3.3.9 | Influence of oxygen content of the adsorption of hormones | 46 |
| 3.4 | Conclusions | 49 |
| 4 | Modeling the adsorption of estradiol in the UF-PBSAC packed-layer | 51 |
| 4.1 | Introduction | 52 |
| 4.2 | Analysis of transport/adsorption mechanisms in the UF-PBSAC | 53 |
| 4.2.1 | Film diffusion | 53 |
| 4.2.2 | Diffusion inside PBSAC | 55 |
| 4.2.3 | Relative importance of film transport and PBSAC diffusion | 56 |
| 4.2.4 | Axial dispersion | 56 |
| 4.2.5 | System dispersion | 58 |
| 4.3 | Model formulation | 58 |
| 4.3.1 | Mass balance in the UF membrane | 58 |
| 4.3.2 | Mass balance in the PBSAC layer | 58 |
| 4.3.3 | Mass balance in the PBSAC phase | 59 |
| 4.3.4 | Solution of the model | 60 |
| 4.4 | Experimental methodology | 61 |
| 4.5 | Parameters determination | 62 |
| 4.5.1 | Layer porosity and apparent PBSAC density | 62 |

| | | |
|----------|---|-----------|
| 4.5.2 | E2 adsorption isotherms | 63 |
| 4.5.3 | Mass transport parameters | 64 |
| 4.6 | Model validation | 64 |
| 4.6.1 | Convection – film transport – adsorption | 65 |
| 4.6.2 | Convection – dispersion - film transport – adsorption | 66 |
| 4.6.3 | Axial dispersion at different layer thicknesses | 66 |
| 4.7 | Example of model application | 68 |
| 4.8 | Conclusions | 69 |
| 5 | Impact of dissolved organic matter on the removal of estradiol by the UF-PBSAC | 71 |
| 5.1 | Introduction | 72 |
| 5.2 | Materials and methods | 73 |
| 5.2.1 | Membranes | 73 |
| 5.2.2 | Polymer-based activated carbon mat and particles | 74 |
| 5.2.3 | Dissolved organic matter feed solution | 74 |
| 5.2.4 | Analytical methodology for DOC | 75 |
| 5.2.5 | Chemicals and analytical method | 77 |
| 5.2.6 | Dynamic adsorption of E2 in the presence of DOC for the UF-PBSAC mat | 77 |
| 5.2.7 | Static adsorption experiments | 78 |
| 5.2.8 | Data analysis | 79 |
| 5.3 | Results and discussion | 79 |
| 5.3.1 | Feed water characteristics | 79 |
| 5.3.2 | Breakthrough curves of E2 for the UF membranes | 80 |
| 5.3.3 | Breakthrough curves of E2 for the UF-PBSAC mat | 81 |
| 5.3.4 | Analysis of the mass adsorbed in the PBSAC mat | 82 |
| 5.3.5 | Impact of the DOC type on the rejection of E2 | 84 |
| 5.3.6 | Adsorbability of DOC on PBSAC | 85 |
| 5.3.7 | Adsorption isotherms of dyes with different MW | 86 |
| 5.3.8 | Considerations about membrane cleaning | 88 |
| 5.4 | Conclusions | 88 |
| 6 | Conclusion and outlook | 91 |
| A | Supporting information on analytical methodology | 95 |
| A.1 | Hormones solution preparation | 95 |
| A.2 | Calibration curves of hormones | 96 |
| A.3 | Ethanol interference in LC-OCD analysis | 97 |
| B | Supporting information on experimental methodology | 99 |
| B.1 | Filtration protocols | 99 |
| B.2 | Repeatability analysis of E2 breakthrough curve | 102 |

| | | |
|----------|---|------------|
| C | Supporting results | 105 |
| C.1 | Influence of the thickness on E2 removal for the UF-PBSAC mat | 105 |
| C.2 | Estimation of the mass of PBSAC in the mat | 105 |
| C.3 | Estimation of PBSAC lifetime (breakthrough volume) | 106 |
| C.4 | Considerations about pressure drop | 106 |
| C.5 | Electrokinetic surface potential of UF membranes | 108 |
| C.6 | Real breakthrough curves for high-pressure UF | 109 |
| D | Supporting information on modeling | 111 |
| D.1 | Membrane and system dispersion | 111 |
| D.2 | Solution of the model | 113 |
| D.3 | Conceptual flow diagram | 116 |
| | Bibliography | 117 |

List of Figures

| | | |
|------|---|----|
| 1.1 | Schematic representation of the different sources of estrogens. | 3 |
| 1.2 | Maximum E2 concentration detected in water worldwide. | 4 |
| 1.3 | Conceptual description of the permeate side AC membrane filtration. Adapted from [68]. | 8 |
| 2.1 | Graphical abstract of Chapter 2. | 9 |
| 2.2 | Schematic of the filtration-adsorption set-up | 15 |
| 2.3 | Schematic of PBSAC layer preparation | 16 |
| 2.4 | Flux and EBCT as a function of applied pressure | 19 |
| 2.5 | Relative concentration and uptake of hormones in the UF-PBSAC . . . | 19 |
| 2.6 | Long term relative concentration and uptake of E2 in the UF-PBSAC . | 20 |
| 2.7 | E2 removal and permeate concentration as a function of flux | 21 |
| 2.8 | E2 removal and permeate concentration as a function of number of PBSAC mats | 22 |
| 2.9 | Comparison BTC in PBSAC mat and packed layer | 23 |
| 2.10 | MB adsorption isotherm for loose PBSAC and PBSAC mat | 24 |
| 2.11 | Treatable volume estimation of a PBSAC mat and a packed layer . . . | 25 |
| 2.12 | BTC of E2 in the nanofiltration-PBSAC mat | 26 |
| 2.13 | Concentration profile in the nanofiltration-PBSAC mat | 27 |
| 3.1 | Graphical abstract of Chapter 3. Adapted from [80]. | 29 |
| 3.2 | Limit of quantification of E2 | 34 |
| 3.3 | E2 removal, uptake and permeate conc. as a function of PBSAC diam- eter | 38 |
| 3.4 | E2 permeate conc. as a function of PBSAC layer thickness / diameter . | 39 |
| 3.5 | Specific surface area and pore volume of PBSAC | 40 |
| 3.6 | Pore size distribution of PBSAC | 41 |
| 3.7 | E2 removal, uptake and permeate conc. as a function of PBSAC activation | 42 |
| 3.8 | MB adsorption isotherm for different PBSAC activation | 44 |
| 3.9 | XPS spectra of PBSAC | 45 |
| 3.10 | E2 removal and permeate conc. for different PBSAC oxygen content . . | 46 |
| 3.11 | Static adsorption kinetics at different PBSAC oxygen content | 47 |
| 3.12 | E2 permeate conc. as a function of layer thickness / oxygen content . . | 49 |
| 4.1 | Graphical abstract of Chapter 5. | 51 |
| 4.2 | Relevant transport mechanisms in the UF-PBSAC | 54 |
| 4.3 | Example of BTC in a short bed | 56 |
| 4.4 | PBSAC bed density and PBSAC density | 62 |
| 4.5 | E2 isotherm for PBSAC 200 μm | 63 |

| | | |
|------|--|-----|
| 4.6 | E2 isotherm for PBSAC 80 μm and 640 μm | 63 |
| 4.7 | Simulated and experimental BTCs: convection-film-adsorption | 65 |
| 4.8 | Simulated and experimental BTCs: convection-dispersion-film-adsorption | 66 |
| 4.9 | D_{ax} estimated by best-fit at increasing PBSAC layer thickness. | 67 |
| 4.10 | D_{ax} estimated by best-fit as a function of L/d_p | 68 |
| 4.11 | Predicted required layer thickness to meet the guideline | 69 |
| | | |
| 5.1 | Graphical abstract of Chapter 5. Adapted from [144]. | 71 |
| 5.2 | Possible retention mechanism of E2 in presence of DOC | 73 |
| 5.3 | Flux and permeability as a function of applied pressures | 75 |
| 5.4 | UV-vis - TOC correlation of DOC | 76 |
| 5.5 | E2 activity detected by LSC in presence of DOC | 77 |
| 5.6 | LC-OCD-UV analysis of DOC | 79 |
| 5.7 | E2 BTCs in presence for HP UF-PBSAC mat | 82 |
| 5.8 | E2 BTCs in presence for LP UF-PBSAC mat | 83 |
| 5.9 | E2 adsorbed to PBSAC in presence of DOC | 84 |
| 5.10 | E2 and DOC retentate conc. as a function of UF MWCO | 85 |
| 5.11 | Static adsorption kinetic of DOC fractions | 86 |
| 5.12 | Dyes adsorption isotherms | 87 |
| | | |
| A.1 | Impact of methanol on static adsorption | 96 |
| A.2 | Hormones calibration curves (Chapter 2) | 96 |
| A.3 | Hormones calibration curve (Chapter 3) | 97 |
| A.4 | E2 calibration curve (Chapter 5) | 97 |
| A.5 | Impact of ethanol on LC-OCD analysis | 98 |
| | | |
| B.1 | BTC repetition in the UF-PBSAC mat | 103 |
| B.2 | BTC repetition in the UF-PBSAC packed layer | 103 |
| B.3 | BTC repetition in the UF-PBSAC mat in presence of DOC | 104 |
| | | |
| C.1 | Comparison real and ideal removal | 105 |
| C.2 | Real and ideal BTC in a packed bed | 106 |
| C.3 | Estimated pressure drop for membranes and a PBSAC layer | 108 |
| C.4 | Estimated pressure drop for a PBSAC layer and a column | 108 |
| C.5 | Electrokinetic potential of the UF membranes | 109 |
| C.6 | BTC accounting for feed concentrating in the HP UF-PBSAC mat | 110 |
| | | |
| D.1 | Components contributing to system dispersion | 111 |
| D.2 | Superficial velocity increase in the first 300 s | 112 |
| D.3 | Effect of membrane and system dispersion on the BTC | 113 |
| D.4 | Conceptual work flow of Chapter 4 | 116 |

List of Tables

| | | |
|-----|---|-----|
| 1.1 | Examples of common estrogenic chemicals. | 2 |
| 1.2 | Comparison between the reported PNEC and occurrence | 3 |
| 1.3 | Summary of the existing technologies to remove estrogens from water. | 7 |
| 2.1 | Approaches to integrate carbon adsorbent in a fixed-bed | 11 |
| 2.2 | Physicochemical properties of hormones | 12 |
| 2.3 | Properties of the PBSAC in Chapter2 | 13 |
| 2.4 | Parameters used in Chapter 2 | 18 |
| 2.5 | Characteristics of PBSAC mat and packed layer | 25 |
| 3.1 | Properties of PBSACs in Chapter 3 | 33 |
| 3.2 | Parameters used in Chapter 3 | 36 |
| 3.3 | External surface area of PBSAC in the packed layer | 37 |
| 3.4 | PBSAC micropores volume and micropores fraction | 41 |
| 3.5 | Treatable volume at different PBSAC activation | 44 |
| 3.6 | Oxygen content of PBSAC | 45 |
| 3.7 | Hormone characteristics and kinetics constants | 48 |
| 4.1 | Correlations for the film mass transfer coefficient | 55 |
| 4.2 | Conditions for the validity of the axial dispersion coefficient estimated through empirical correlations. | 57 |
| 4.3 | Re, Sc and k_f estimated through empirical correlations. | 64 |
| 4.4 | Comparison of k_f from correlation and best-fitting | 65 |
| 4.5 | Comparison of D_{ax} from correlation and best-fitting | 66 |
| 5.1 | List of the membranes used in Chapter 5 | 74 |
| 5.2 | Parameters used in Chapter 5 | 78 |
| 5.3 | HA and NOM composition | 80 |
| 5.4 | Characteristics of HS from HA and NOM | 80 |
| 5.5 | List of dyes used | 87 |
| 5.6 | UF cleaning frequency and typical condition | 88 |
| A.1 | Impact of ethanol on LC-OCD analysis | 98 |
| B.1 | Filtration protocol for the UF-PBSAC mat | 99 |
| B.2 | Filtration protocol for the UF-PBSAC packed layer | 101 |
| B.3 | E2 mass adsorbed in presence of DOC - repetition | 104 |
| C.1 | Permeability of commercial UF and MF membranes | 107 |
| D.1 | Dealy times due to permeate tube and support layer | 112 |

List of Abbreviations

| | |
|--------------|--|
| AC | Activated carbon |
| ADI | Acceptable daily intake |
| AOP | Advanced oxidation process |
| BTC | Breakthrough curve |
| CNP | Carbon nanoparticle |
| E1 | Estrone |
| E2 | 17 β -estradiol |
| E3 | Estriol |
| EBCT | Empty bed contact time |
| EDC | Endocrine disrupting compounds |
| EE2 | 17 β -ethinylestradiol |
| EQS | Environmental quality standard |
| GAC | Granular activated carbon |
| MB | Methylene blue |
| MF | Microfiltration |
| MP | Micropollutant |
| MW | Molecular weight |
| MWCO | Molecular weight cut-off |
| NF | Nanofiltration |
| ODE | Ordinary differential equation |
| P | Progesterone |
| PAC | Powdered activated carbon |
| PBSAC | Polymer-based spherical activated carbon |
| PDE | Partial differential equations |
| PNEC | Predicted-no-effect concentration |

| | |
|-----------|-----------------|
| RO | Reverse osmosis |
| T | Testosterone |
| UF | Ultrafiltration |

Chapter 1

Introduction

1.1 Motivation

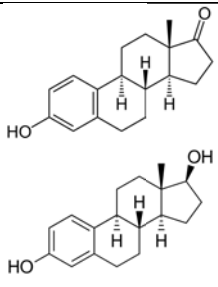
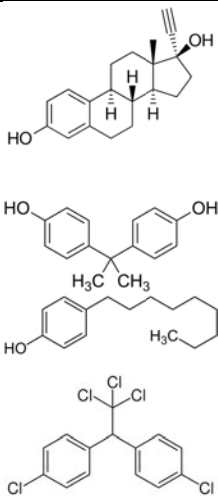
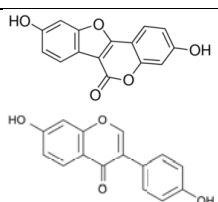
The term micropollutant (MP) defines a broad class of molecules of anthropogenic origin that can be found in water at a concentration in the ng to pg per liter range [1]. The presence of such pollutants in water is known for over 20 years [2]. The advancement in analytical techniques has allowed us to detect an always-increasing number of MPs in wastewater, surface water, drinking water, and even in seawater.

Estrogenic MPs are known to interfere with the endocrine (hormones) system, and they are harmful to any living organisms. For example, they can bind to the hormone receptor causing an unjustified response either at the wrong time or at an excessive extent. On the other hand, they can bind but not activate the receptor, preventing the binding of the natural-occurring hormone. Considering that hormones are present in the ng L^{-1} range in the blood, even small variations can have a negative effect. MPs with estrogenic potential include (i) natural and synthetic hormones, (ii) human-made chemicals that mimic the action of hormones (xenoestrogens), and (iii) plant hormones (phytoestrogens). A summary of the most common ones is reported in Table 1.1.

Estrogens accumulation in aquatic eco-systems, such as lakes and rivers, brings adverse effects on fish physiology and other aquatic wildlife. The feminization of the fish population of lakes and rivers has been reported in several publications [1, 3–5]. Eco-toxicological studies were carried out to assess which level of estrogens is sufficient to disrupt the aquatic-system, hence to derive a predicted-no-effect-concentration (PNEC) for each estrogen found in water. These studies usually follow this protocol: i) definition of a critical end-point (e.g., reproductivity or vitellogenesis production), ii) exposure of the fish population at increasing estrogen concentrations and iii) observation of the highest level at which no effect is present. Caldwell and coworkers [6] proposed PNECs of 6, 2, and 60 ng L^{-1} for the natural hormones estrone (E1), estradiol (E2), and estriol (E3), respectively. The synthetic hormones 17 β -ethinylestradiol (EE2) is at least 20 times more estrogenic than E2 and its reported PNEC ranges from 0.035 to 0.1 ng L^{-1} .

Beyond the effect on the environment, estrogens are suspected of causing reproductive disorders in humans [7] as well as several other diseases such as intellectual disability, autism, attention-deficit disorder, and obesity [3, 8]. Further, increasing evidence correlates the unnatural amounts of estrogens in the body to breast and

Table 1.1: Examples of common estrogenic chemicals.

| Category | Class | Category | Chemical structures |
|-------------------|--|---|---|
| Natural estrogens | Steroid hormones | Estrone 17 β -Estradiol |  |
| Xenoestrogens | Synthetic hormones Plasticizers Detergents Insecticides | Ethinylestradiol Bisphenol 4-n-Nonylphenol DDT |  |
| Phytoestrogens | Coumestans Isoflavones | Coumestrol Daidzein |  |

other types of cancer [3, 9]. Transande *et al.* [8] estimated an estrogens-related disease cost of hundreds of billions per year in the European Union. Acceptable daily intake (ADI) is used to define the limit of the ingestion of a hazardous compound. For E2, the World Health Organization (WHO) has estimated an ADI of 0-50 ng per kg of body weight. Apart from the concentration of single estrogens, the total estrogenic activity can be determined by bio-assays to characterize the hazardous potential of a water source [10, 11]. The result of these studies is reported as E2-equivalent; E1 and EE2 have about 0.33 and 20 times the estrogenic potential of E2.

Estrogenic MPs enter the water cycle by multiple routes (Fig. 1.1). Municipal wastewater is a source of many classes of MPs, including hormones. The human body continuously excretes natural hormones, pregnant women excrete between 280–600 μg per day of 17 β -estradiol [3]. Municipal landfills may also contain leachate with a significant amount of estrogens partially bounded to dissolved organic matter

1.1. Motivation

[12]. Further sources of estrogens are hospital effluent water [13], where concentrations up to 30 ng L^{-1} were detected [14], and dairy livestock industry that regularly used growth-regulating steroids to enhance cattle growth rates. Pharmaceutical factories are likely the primary source of estrogens from industrial activity [15]. In the waste effluent from a factory producing steroid contraceptives, E2 and EE2 were measured up to 85 and 155 ng L^{-1} . These concentrations were reduced only to 23 and 51 ng L^{-1} , respectively, after the water treatment plant [16]. Estrogenic activity was also detected in wastewater from the chemical and petrochemical industry [17].

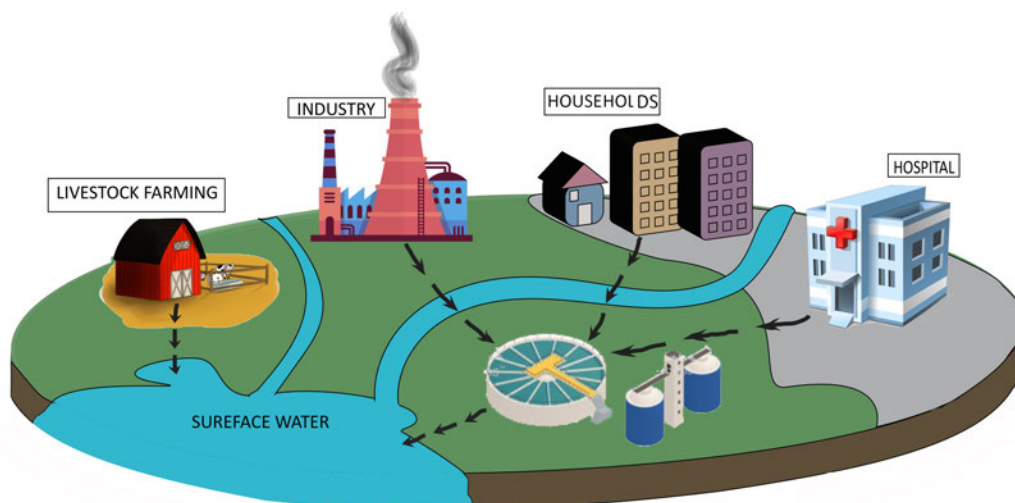


Figure 1.1: Schematic representation of the different sources of estrogens.

Discharge of estrogens in the water cycle results in the ubiquitous occurrence of estrogenic MPs in water resources: from surface to drinking water and even in groundwater and seawater [12, 18–20]. Fig. 1.2 shows that E2 is found in water in many developed counties in the world, highlighting how the quality of the water may be in issue, especially in countries where water scarcity is not. The maximum concentration of estradiol in European surface water was detected in Germany, in the inflow of Lake Constance [21]. In general, hormones are occurring in surface water at concentrations higher than their PNEC values as highlighted in Table 1.2.

Table 1.2: Comparison between the reported PNEC for estrogens (hormones) and the occurrence in surface water in Europe and the world.

| Compound | Reported PNEC ng L^{-1} | Occurrence in Europe | | Global occurrence | |
|-----------------------------------|--|----------------------|----------------|--------------------|----------------|
| | | ng L^{-1} | | ng L^{-1} | |
| | | <i>Average</i> | <i>Maximum</i> | <i>Average</i> | <i>Maximum</i> |
| Estrone (E1) | 6 | 3.6 | 1250 | 16 | 5000 |
| 17β -estradiol (E2) | 0.4-2 | 4.6 | 320 | 3 | 13450 |
| 17β -ethinylestradiol (EE2) | 0.035-1 | 4.9 | 280 | 43 | 5900 |
| Estriol (E3) | 60 | 2 | 480 | 9 | 480 |

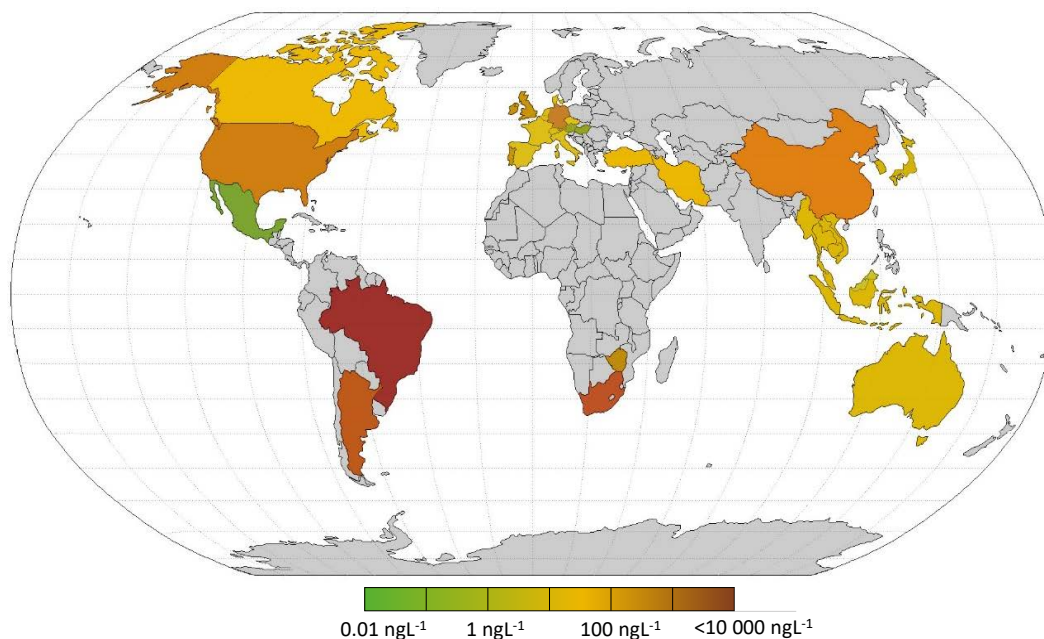


Figure 1.2: Maximum E2 concentration detected in surface, tap, drinking, and groundwater worldwide. Adapted from [19].

The first step of the European towards awareness and control of estrogenic (or endocrine disrupting compounds, EDC) took place in 1999 [22]. The "Community strategy for endocrine disruptors" defines a series of actions that would have been taken to address the potential environmental and health impact of EDC. In the short term, the strategy was based on the definition of a "Priority List" of substances suspected to be estrogenic. From the list that initially included over 500 chemicals, 12 substances were selected for their evidence of endocrine disruption. Among these 12 chemicals, 3 steroid hormones were included: E1, E2, and EE2 [23]. Environmental quality standards (EQS) of many priority substances were proposed in 2011. For E2 and EE2, maximum allowable concentration for discharge in surface water was set to 0.4 and 0.035 ng L⁻¹, respectively [24]. These values were decided based on the study from [25] and the opinion of a committee of independent scientists [26]. Regarding the water intended for human consumption, a target value of 1 ng L⁻¹ was proposed for E2 [27].

1.2 Current options to remove estrogens

Conventional wastewater treatment plants (WWTPs) usually consist of a primary step (clarification) and a secondary treatment (biological degradation). Tertiary treatment can be added to address the removal of specific compounds [28]. Despite WWTPs being designed to remove mainly nitrogen, carbon and phosphorous, MPs are also removed to a variable extent [29].

Estrogens are partially eliminated in the secondary treatment due to adsorption

to the sewage sludge and subsequent biodegradation [29, 30]. Focusing on the estrogens of environmental concern E1, E2, and EE2: E2 is reported to be easily biodegradable with removal ranging from 60 to 99 % while E1 is relatively weak removed (25-60 %). Indeed, the first step of E2 bio-degradation brings to the formation of E1 [31]. For this reason, higher E1 concentration in the effluent compared to the influent of the WWTP was measured in some cases [29, 32]. Finally, all the works considered concluded that the synthetic hormone EE2 is the most persistent (e.g., difficult to degrade)[29, 30, 33].

Other than the water effluent, estrogens can accumulate in the sludge due to their high adsorption affinity. The fate of estrogens in the sludge digestion process needs also be addressed more carefully [29]. In summary, conventional WWTPs are not considered reliable in achieving the complete elimination of hormones [30, 34]. In the following sections, alternative processes that are considered promising to tackle the challenge of estrogens in water will be presented.

1.2.1 Pressure-driven membrane processes

Due to ease of operation and small footprint, membranes are nowadays widely used in the field of water treatment and reuse [35, 36]. Pressure-driven membranes are a size-exclusion-based process where the pore size of the active layer is the most critical factor. Depending on it, a wide range of water contaminants can be retained from viruses and bacteria to salts. Membranes are classified based on the pore size in microfiltration (MF, 0.05-10 μm), ultrafiltration (UF, 5-100 nm), nanofiltration (NF, 1-10 nm) and reverse osmosis (RO, <2 nm). On the other hand, smaller pores lead to the need for higher pressure (hence energy consumption), which ranges from 0.05 bar for MF to over 100 bar for RO [35]. Besides the size of the pores, the membrane material plays a role in that charge repulsion between the contaminant and the membrane enhances the separation efficiency [37].

Many publications can be found on the rejection of organic MPs, including estrogens, by membranes. Removal of MPs by UF is generally poor [38], although minor retention occurs, mainly attributed to adsorption to the polymer matrix [39, 40]. In contrast, excellent removal can be achieved with the RO membrane [38, 41]. Nghiem *et al.* [42] and Semião *et al.* [43] investigated the rejection of hormones by NF. Lower retention than the one expected based on the NF pore size was explained in terms of adsorption. The hydrophobic nature of hormones favors the partition to the membrane followed by the diffusion on the permeate side [44].

Later on, the modification of the NF active layer was investigated by several authors to improve the rejection of MPs. Hydrophilization was demonstrated to reduce the adsorption of MPs, hence enhancing the rejection performance [45–47]. Alternatively, Guo *et al.* [48] managed to decrease from 0.44 to 0.40 nm the estimated effective pore size of NF when the coordination complex of tannic acid and ferric ion was introduced in the active layer via self-polymerization.

1.2.2 Activated carbon adsorption

Adsorption processes are based on the phase transfer of the target contaminant from the water phase to the solid adsorbent phase. The use of carbon material for treating water dates back to ancient times. Activated carbon (AC) process, as we know it today, starts in the 20th century [49]. AC can be produced from many different precursors such as coal, agricultural waste, and polymers. The process consists of carbonization (elimination of non-carbon component) and activation (removal of more reactive carbon species). AC can be classified based on the mean particle size in granular (GAC, 0.4-5 mm), powdered (PAC, < 40 μm) and super powdered (SPAC, 1 μm -100 nm) activated carbon [50, 51]. The size of AC is strongly related to the application technique. GAC is typically used as a fixed-bed in a column while PAC is applied as a slurry. AC can be combined with membranes in the so-called hybrid processes, which will be considered in detail in Chapter 2.

The performance of AC in the adsorption of MPs is determined by the intrinsic properties of the AC such as specific surface area and surface chemistry and the physicochemical properties of the target contaminant. The surface chemistry of an AC is highly dependent on the precursor used while the porous morphology (e.g. pore volume and surface area) depends on the activation step in the production process. The relevance of the material characteristics of AC in the adsorption of MPs will be discussed in Chapter 3. Finally, the presence of background organic matter is a factor that needs to be taken into account in the design of an AC process. Organic matter is present in water at a concentration much higher compared to MPs. It can interfere in different ways with the adsorption process, as it will be explained in Chapter 5.

In general, AC is considered a suitable adsorbent for estrogens due to their hydrophobic nature. Adsorbability of E2 at its environmentally-relevant concentration was demonstrated on both GAC [52] and PAC [53]. Recently, polymer-based spherical activated carbon (PBSAC) were investigated for the adsorption of steroid hormones, showing fast adsorption kinetics in batch experiments [54]. In the last decades, the use of carbon nanoparticle (CNP) has received increasing attention in the research community. Many publications have focused on the adsorption performances of carbon nanotube and graphene. Due to the small size, using these particles in a real process is still challenging despite many options were proposed for their safe integration in polymeric membranes.

1.2.3 Advanced oxidation processes

Advanced oxidation processes (AOPs) include a set of chemical treatments where the degradation of virtually any contaminants can be achieved via reaction with the hydroxyl radical ($\text{OH}\cdot$) [55]. The classification of these processes is based on how $\text{OH}\cdot$ is generated. In ozonation, one of the most investigated AOP, $\text{OH}\cdot$ is formed from the decomposition of ozone (O_3) via a chain reaction mechanism [56]. Other

examples are UV, H₂O₂, Fenton process as well as combinations of these [57]. AOP is a promising technology to tackle the challenge of MPs in water because of the high removal achievable. Further, OH· can oxidize unspecifically almost any molecules that makes it very suitable to treat heterogeneous mixtures of MPs. Sun *et al.* [58] and Pesoutova *et al.* [59] reported complete degradation of E1, E2 and EE2 from municipal wastewater using ozone-based AOP. Removal of estrogens in the range 70-100 % was observed by other authors using H₂O₂/UV and Fenton process [60]. However, many authors have also reported low mineralization despite high removal efficiency, a sign of the formation of persistent byproducts that may be as harmful as the target contaminant [57, 61]. Byproducts formation is indeed the central issue of AOPs to the point where activated carbon adsorption is considered more suitable for sensitive receiving water (e.g. drinking water) [62].

1.2.4 Novel membrane processes

In recent times, many researchers have focused on novel membranes where MPs are not eliminated by size-exclusion but by kinetic processes such as adsorption or degradation. Besides the advantage in terms of footprint, membranes may present a favorable mass transfer regime with no diffusion limitations typical of fixed-bed adsorbers (e.g., AC column). The active surface area of the material is directly exposed to the flow (convectively accessible) of the target contaminants. Commercial membranes need to be modified or novel membranes synthesized to introduce adsorptive or catalytic properties. Many different strategies have been proposed in the literature in this direction. The integration of functional nanoparticles in the membrane matrix is promising. One option is to mix the NP inside the polymer before the casting procedure [63, 64], alternatively NP can be physically loaded in the membrane [65, 66]. CNPs, such as CNT and graphene, are an ideal candidate for adsorption purposes. Polymeric NP can also be tailored to enhance specific interaction with the target MP [67].

Table 1.3: Summary of the existing technologies to remove estrogens from water.

| Technology | Removal range | Pros / Cons |
|------------------------------|-------------------|--|
| Conventional water treatment | 20 - 99 % | Established technology / incomplete removal |
| High-pressure membrane | 80 - 99 % | Small footprint / high energy requirements |
| Activated carbon column | n.a. ^a | Established technology / large footprint |
| Advanced oxidation process | 70 - 100 % | Unspecific and complete removal / byproducts formation |

^anot applicable: the performance of an AC column is defined by the breakthrough time rather than the removal

1.3 Research proposal

In this thesis, a new approach is proposed to remove estrogens, steroid hormones in particular, from water. A millimetric AC layer is placed on the permeate side of a membrane (Fig. 1.3). PBSAC was selected as the adsorbent layer due to its superior performance in adsorbing steroid hormones. Regarding the membrane, the main focus is on the use of a UF because it can reject other water contaminants such as viruses, bacteria and organic matter at high permeability. This approach is convenient compared to the other options to remove estrogens presented above. It needs low pressure, hence low energy consumption, compared to the NF/RO membranes. A small footprint and carbon consumption characterize it compared to AC columns. It does not present the risk of harmful by-product formation, as in the case of AOPs. Finally, adsorption can be integrated into a membrane process in a simple way, where the adsorption step occurs independently of the filtration one avoiding the challenges presented by nano-composite membranes.

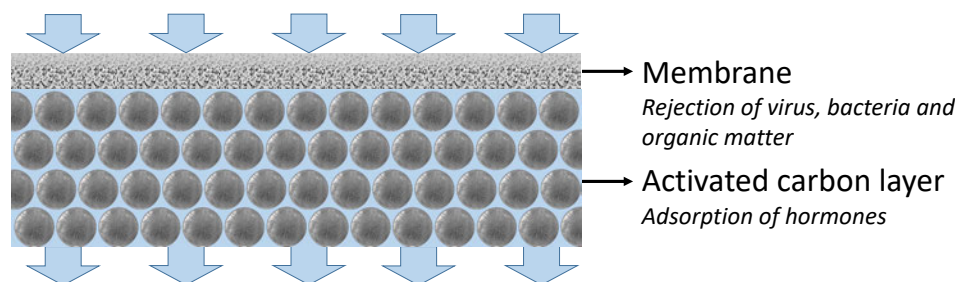


Figure 1.3: Conceptual description of the permeate side AC membrane filtration. Adapted from [68].

In principle, the UF-PBSAC can simultaneously remove organic matter and MPs in a single step. The removal of organic matter, viruses and bacteria by UF is an established process, proven from the research to the industrial scale. On the other side, the adsorption of MPs in a thin adsorbent layer was never proposed and it brings some challenges. First, using of a thin layer translates in low contact time compared to an AC column, which represents a challenge to the adsorption kinetic. Second, the lower amount of AC in the thin layer may be related to a small total adsorption capacity. Saturation may occur really quickly, compromising the feasibility of using a thin AC layer in a real process.

The thesis starts in Chapter 2 with an assessment of the feasibility of using a millimetric PBSAC layer to remove steroid hormones from water. In Chapter 3, a systematic investigation of the intrinsic properties of PBSAC is carried out to find room for improvement of the mass transport/adsorption kinetic of the thin layer. Chapter 4 has the goal to provide a solid understanding of the mass transport and adsorption process through mathematical modeling. Finally, the impact of organic matter is investigated in order to define the potential of the UF-PBSAC in a real process (Chapter 5).

Chapter 2

Polymer-based activated carbon assisted membrane filtration*

The presence of estrogens in surface and drinking water is an issue recognized by the World Health Organization. Steroid hormones are one of the most common classes of estrogens. With conventional water treatment plants only partially removing hormones, new technologies need to be explored. This chapter presents a novel approach where a millimetric polymer-based spherical activated carbon (PBSAC) layer is placed on the permeate side of an ultrafiltration membrane (UF-PBSAC). The feasibility of this approach was tested by obtaining the breakthrough curves of four hormones with a particular focus on the most estrogenic estradiol. The use of realistic hormones concentration (100 ng L^{-1}) resulted in a peculiar breakthrough curve characterized by a constant permeate concentration as a function of filtered volume. Relevant hormone removal (60-80 %) could be achieved using a commercial PBSAC filter mat at a contact time of only $\approx 1 \text{ min}$. The removal could be further increased to 94 % employing five PBSAC mats on the permeate side of the membrane. Using a PBSAC packed-layer (rather than the commercial mat) as the adsorbing layer led to a significant improvement of the adsorption performance. Indeed, removal of 94 % was achieved using a packed-layer of only 2 mm (corresponding to a contact time of $\approx 1 \text{ min}$). The UF-PBSAC is a promising approach to remove hormones, characterized by many positive aspects such as high permeability process, small footprint and low carbon consumption. However, the high removal demonstrated is still not enough to reach the water quality standards under development by environmental organizations.



Figure 2.1: Graphical abstract of Chapter 2.

* This chapter is based on the following publication: "Removal of steroid micropollutants by polymer-based spherical activated carbon (PBSAC) assisted membrane filtration", Journal of Hazardous Materials, 2018, 353, 514-521. For this thesis chapter, part of the content has been rewritten and some of the graphs have been adapted by the author.

2.1 Introduction

Membrane filtration and activated carbon (AC) adsorption can be combined in the so-called hybrid processes [69]. Different layouts are possible: the AC adsorption step can be introduced as a separated treatment unit either as a pre-treatment or post-treatment. The addition of an AC adsorption before membrane filtration is known to be effective in reducing fouling [70–72]. In this case, AC can be used both as a granular activated carbon (GAC) column and as powdered activated carbon (PAC) suspension. On the other hand, an AC post-treatment has the main goal to remove soluble organic contaminants such as micropollutants (MPs) and it is limited to the use of a GAC column [69]. Indeed, fixed-bed PAC is problematic because the fine particles could be exported with the treated water. AC can also be coupled with membranes in a single treatment unit, which presents an evident advantage in terms of process footprint. The most common example is the UF/MF-PAC reactor, where PAC is added as a slurry directly on the feed side of the membrane. This process is effective in both (MPs) removal and fouling control [73, 74]. In summary, the integration of AC adsorption on the permeate side of the membrane in a single step was never reported in literature.

Fixed-bed processes are generally considered more convenient compared to batch processes [75], especially at low pollutant's concentration as is the case for MPs [76]. Besides the traditional GAC columns, other approaches can be found in the literature to use AC and other carbon-based adsorbents in a fixed-bed configuration (summarized in Table 2.1). For example, Ruhl *et al.* [75] have integrated PAC in a deep pumice filter, recalling the so-called Haberer process published in 1991 [77]. Immobilized PAC showed enhanced adsorption efficiency for several pharmaceutical and other MPs compared to the same adsorbent used in batch. Other examples demonstrate the integration of PAC, SPAC and CNP in a polymeric membrane. This was achieved either by coating the membrane on the feed side (e.g., the active layer side) or by loading the adsorbent in the support layer of the membrane (e.g., on the permeate side) [65, 66, 78]. With these approaches, effective removal of compounds such as methylene blue, atrazine and estradiol could be achieved. Another interesting strategy was presented by Wu *et al.* [79] that introduced the concept of PAC dynamic membrane where the PAC is deposited as a "fouling layer" on the feed side of microfiltration.

The performance of the adsorption process depends primary on the affinity between pollutant and adsorbent as well as operative parameters such as flow rate and length of the column. These operative parameters determine the contact time between AC and target contaminant. The empty bed contact time (EBCT) is defined as the ratio between the volume of the reactor (containing the adsorbent particles) and the volumetric flow rate. On the other side, the real contact time takes into account the porosity of the adsorbent bed. Considering the difficulty in determining

2.1. Introduction

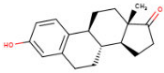
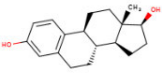
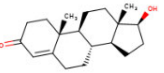
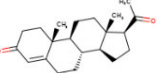
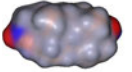
Table 2.1: Summary of the different approaches to integrate AC or CNP adsorption in a fixed-bed process (nr: not reported) [80].

| Process | Bed thickness and EBCT | MP tested and conc. range | Scale | Ref. |
|--|------------------------------|---|----------------------|-----------|
| GAC filter | 0.5 – 2 m 7 to 380 min | Pharmaceutical, personal care product and other MPs $1 \mu\text{g L}^{-1}$ to $5 \mu\text{g L}^{-1}$ | Full and pilot scale | [81–84] |
| PAC deep-bed filter | 1 m 4.5 min | Pharmaceutical, personal care product and other MPs $1 \mu\text{g L}^{-1}$ to $5 \mu\text{g L}^{-1}$ | Pilot scale | [75] |
| UF-PBSAC | 0.2 to 1 cm 1 to 6 min | Steroid MPs 100 ng L^{-1} | Bench scale | This work |
| Dynamic membrane | PAC 0.18 to 0.32 cm nr | not tested with MPs | Bench scale | [79] |
| AC fibers and CNP loading inside membranes | nr | Steroid MPs 100 ng L^{-1} | Bench scale | [85–87] |
| SPAC and CNP coating on membranes | nr | Methylene blue and atrazine 0.9 mg L^{-1} and $1.5 \mu\text{g L}^{-1}$ | Bench scale | [65, 66] |

the porosity of the bed reliably, EBCT can be used for practical application. In fixed-bed adsorption, higher EBCT can be achieved either by decreasing the feed flow rate or increasing the length of the bed.

In this chapter, the feasibility of using only a thin (millimetric) polymer-based spherical activated carbon (PBSAC) layer to adsorb estrogenic MPs will be assessed. Estrone (E1) and estradiol (E2) are selected as model estrogens MPs, but other two steroid hormones, namely testosterone (T) and progesterone (P), will also be used. The physicochemical properties of these compounds are shown in Table 2.2. The PBSAC layer, initially used in the form of a commercial PBSAC textile mat, is coupled with an ultrafiltration (UF) membrane. The selected UF has a molecular weight cut-off of 10 kDa, meaning that no rejection can be expected for the selected MPs (MW of 0.270 to 0.314 kDa as shown in Table 2.2). This allows us to focus on the adsorption process occurring in the thin PBSAC layer. Later, the contact time is varied either by changing the flow rate or the thickness of the PBSAC layer. Finally, the adsorbent layer will be placed on the permeate side of a nanofiltration (NF) membrane that is known to reject the selected MPs partially. The aim to investigate the potential of using a thin adsorbent layer to remove the residual MPs that are not rejected by the NF.

Table 2.2: Relevant physicochemical properties of the four hormones used obtained using ChemAxon Marvin.

| Hormone | Estrone | 17 β -estradiol | Testosterone | Progesterone |
|-----------------------------------|---|---|--|---|
| Molecular weight (Da) | 270.4 | 272.4 | 288.4 | 314.5 |
| Chemical structure |  |  |  |  |
| Max/min projection radius (nm) | 0.70 / 0.41 | 0.73 / 0.41 | 0.75 / 0.49 | 0.69 / 0.41 |
| Electrostatic molecular potential |  |  |  |  |
| H bonding donor / acceptor | 1 / 2 | 2 / 2 | 1 / 2 | 0 / 2 |

2.2 Material and methods

2.2.1 Membranes

In this chapter, three polymeric membranes are used: one UF and two NF. Most experiments are carried out using the UF membrane (Merck-Millipore, PLGC) that is chosen based on negligible hormones adsorption and retention of other water parameters such as organics, viruses and bacteria. It consists of a support layer of non-woven polypropylene and an active layer made of regenerated cellulose. The molecular weight cut-off (MWCO) is 10 kDa, and the total thickness of 230 μm . On the other hand, the NF membranes, NF270 and NF90 (provided as flat sheet samples by the Dow Chemical Company, Germany) are thin-film composites. They have been largely investigated for the retention of steroid hormones. They are made of a semi-aromatic piperazine-based polyamide (NF270) and a fully aromatic polyamide active layer (NF90) on top of a polysulfone support reinforced with a polyester non-woven backing layer.

2.2.2 Polymer-based spherical activated carbon particles and textile mat

PBSAC is provided by Blücher gmbh. It is produced from cross-linked polystyrene precursor. The synthesis is carried out in a batch process by means of a first carbonization step and a subsequent activation step with oxidizing agents to establish pore volume by controlled oxidation of carbon at 1173 K [88]. PBSAC used in this chapter has a mean diameter of 450 μm (Table 2.3). The PBSAC mat is a commercial material (mainly used for air treatment). A water-soluble glue is used to stick the PBSAC together and obtain a dense filter mat with a thickness of 2.2 mm. The diameter of PBSAC in the mat has a size of 450 μm .

2.2. Material and methods

Table 2.3: Properties of the PBSAC sample used in Chapter 2 provided by the manufacturer.

| Sample label | Particle diameter | Tap density | BET specific surface area |
|--------------|-------------------|-------------------|----------------------------|
| | μm | g L^{-1} | $\text{m}^2 \text{g}^{-1}$ |
| P450 | 450 | 355 | 2045 |

2.2.3 Solution chemistry and steroid hormones

A background electrolyte solution consisting of 1 mM NaHCO_3 (Bernd Kraft, Germany, 99.7 % purity) and 10 mM NaCl (VWR Chemicals, Germany, 99.9 % purity) is used in all experiments. For the standard feed volume of 0.7 L, 0.41 and 0.08 g of NaCl and NaHCO_3 are weighted on a microbalance (Explorer EX225D/AD, Ohaus, Germany) and dissolved in Milli-Q Type 1 water (Merck Millipore, Germany; resistivity of $18.2 \text{ M } \Omega\text{cm}$ at 25°C). The final background solution has a pH of about 8 (measured with a pH meter, WTW InoLab pH720, Germany).

Tritium-labeled MPs were used for high quality mass balance facilitated by a low detection limit [54, 89]. Estradiol [2,4,6,7-3H], estrone [2,4,6,7-3H], progesterone [1,2,6,7-3H] and testosterone [1,2,6,7-3H] were purchased from Perkin Elmer (USA) dissolved in 100 % ethanol. Native hormone solutions are all characterized by a total activity of 1 mCi mL^{-1} while the specific activity varies between 70-98 Ci mmol^{-1} depending on the batch that corresponds to concentration in the range 2.8-4.4 mg L^{-1} (calculated as shown in Appendix A.1). In particular, the hormones used in this chapter have specific activity of 70, 94, 98 and 80 Ci mmol^{-1} for E2, E1, P and T respectively. Stock solutions of $10 \mu\text{g L}^{-1}$ were first prepared for each hormone by dilution with Milli-Q Type 1 water. These stock solutions were further diluted with the background solution to achieve the "standard" hormone feed concentration of 100 ng L^{-1} . The final hormone feed solution has a pH of 8 (measured with a pH meter, WTW InoLab pH720, Germany).

When a concentration higher than 100 ng L^{-1} is used, radio-labeled hormones are mixed with non-labeled ones. Due to the low solubility in water, a non-labeled hormones stock solution of 10 mg L^{-1} is prepared by dissolving the proper amount of hormone powder in methanol. For the preparation of E2 solution of $100 \mu\text{g L}^{-1}$, 9.99 mL of non-labeled E2 stock (10 mg L^{-1}) per L of solution is added as shown in Appendix A.1.

In addition, the textile dye Methylene blue (MB) is used to measure the maximum adsorption capacity (e.g., the maximum possible uptake) of PBSAC. MB has a high solubility in water and it was already used in the literature as an indicator of the maximum uptake of an adsorbent [90].

2.2.4 Analytical methods

The concentration of tritium-labeled hormones was measured using a Liquid Scintillation Counter (LSC; 2550 TR/AB, Packard, USA). The instrument detects the activity of tritium in the sample. The activity can be correlated to the hormone concentration by means of an external calibration curve. Considering that each native tritium-labeled hormone solution has a different specific activity, calibration curves need to be performed for each hormone and even for different native solution of the same hormone. This method provides reliable results down to concentration lower than 1 ng L^{-1} . The calibration curves for E2, E1, T and P used in this chapter are reported in Appendix A.2 (Fig. A.2).

A UV-vis spectrophotometer (Lambda 25, Perkin Elmer, USA) was used to measure the absorbance of MB solution at the wavelength of 664 nm. MB concentration was determined from absorbance through a calibration curve.

2.2.5 Stirred-cell filtration set-up

The stirred-cell filtration set-up is typically used for dead-end membrane filtration. In this work, it was adapted to perform dynamic adsorption experiments in the membrane-PBSAC. The system is composed of a bottom part, a cell and a top part (Fig. 2.2A). The bottom part contains the filtration medium (membrane or membrane + PBSAC) as it will describe in more detail in the following sections. Bottom parts with different heights were produced (KIT, Germany) to hold PBSAC layers of thickness from 1 to 13 mm (the diameter of the layer is always 65 mm). The cell (volume of 0.99 L) contains a stir bar (Millipore, UK) and is filled with contains the feed the solution and is sealed on the top of the bottom part employing two o-rings (Fig. 2.2B). Last, the system is sealed with the top part connected to a synthetic air tank used to pressurize the cell. A pressure regulator and an On/Off valve are mounted on the line that connects the top part and the synthetic air tank. In the top part, a thermocouple (TJ2-CPSS-M60U-250-SB, Omega Engineering, Germany) and a pressure transducer (PX219-30V85G5V, Omega Engineering, Germany) are located to monitor the temperature and the pressure inside the cell. Permeate mass is measured by an electronic balance (Adventurer Pro AV 2102, Ohaus, Germany). A computer collects data with a data acquisition module (Labview®2014 National Instruments, Germany).

2.2.6 Dynamic adsorption of hormones in the UF-PBSAC mat

For dynamic filtration experiments in the membrane-PBSAC mat, the filtration medium (Fig. 2.2C) is prepared as follows. First, a stainless steel support layer (2 mm thickness) is placed inside the bottom part. One or more PBSAC mats are then placed on the top of the porous support. Finally, the membrane is placed on the top of the PBSAC mat and the bottom part is sealed with the cell. The cell is filled with the feed solution prepared as described in previous sections. As the synthetic air valve

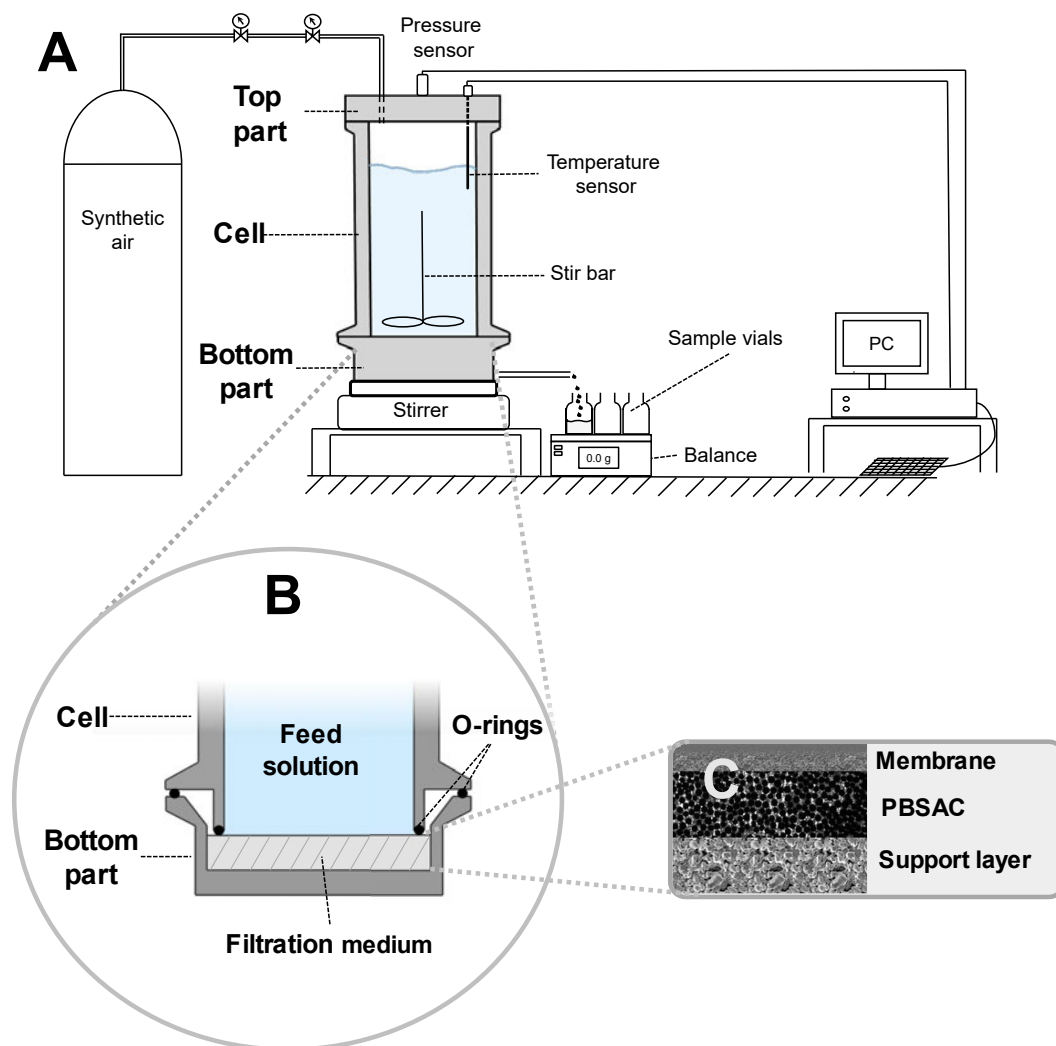


Figure 2.2: Schematic of the stirred-cell set-up used for dead-end filtration-adsorption experiments (A) with a focus on the sealing of the bottom part with the cell (B) and the filtration medium (C). Adapted from [80].

is opened, the pressure inside the cell increases and the feed solution starts to flow through the membrane-PBSAC filter.

A detailed filtration protocol is reported in Appendix B.1. As a first step, MilliQ water is filtered for 90 min to achieve compaction of the membrane and wetting of the PBSAC layer. In the last 30 min of this step, the pure water flux is also measured and compared to the expected values (either provided by the manufacturer of the membrane or by the experience of the user). In case, the pure flux is higher than the one expected, the filtration medium is replaced because it means either the membrane used is damaged or the sealing is not properly working. After the pure water flux measurement, the system is depressurized, the top part is removed and the cell is filled with the solution containing hormones (0.7 L). The filtration of the hormone solution is started, the permeated water is collected on the glass beakers placed on the balance. Every 0.1 L of permeate collected in one beaker, the permeate tube is moved manually on the next beaker. The filtration of hormones is carried out until

0.6 L of permeated is collected in six different beakers. After that, the system is depressurized, the top part removed and 5 mL of the feed solution remained in the cell collected (retentate). The feed, permeate and retentate samples are then analyzed with the LSC to obtain the breakthrough curve. During the filtration of hormones, the stirring rate is set to 400 rpm in the case of NF-PBSAC. In contrast, no stirring is used for the UF-PBSAC.

2.2.7 Dynamic adsorption of hormones in the UF-PBSAC packed-layer

When a packed-bed of PBSAC is coupled with the membrane, the preparation of the filtration medium is different (Fig. 2.3). The porous stainless steel support is inserted inside the bottom part in the same way. Then, a disk is placed on the top of the support. This disk has a thickness of 2 mm, an internal diameter of 65 mm and an external diameter of 75 mm (same as the internal diameter of the bottom part). The packed-layer is obtained by pouring the desired amount of PBSAC particles inside, followed by gentle tapping to achieve a uniform layer. The volume inside the disk to be filled with PBSAC is 6.6 cm³, the mass of PBSAC poured inside the disk depends on the tap density of the sample (reported in Table 2.3). For the PBSAC sample used in this work, a mass of 2.4 g is used in the layer (calculated from Eq. (2.1)). The membrane is then placed on the top of the PBSAC layer. The system is sealed with an o-ring sitting directly on the membrane.

$$\begin{aligned} \text{mass of PBSAC in the layer} &= \\ &= \text{Volume of the layer} \cdot \text{Tap density of PBSAC} \quad (2.1) \end{aligned}$$

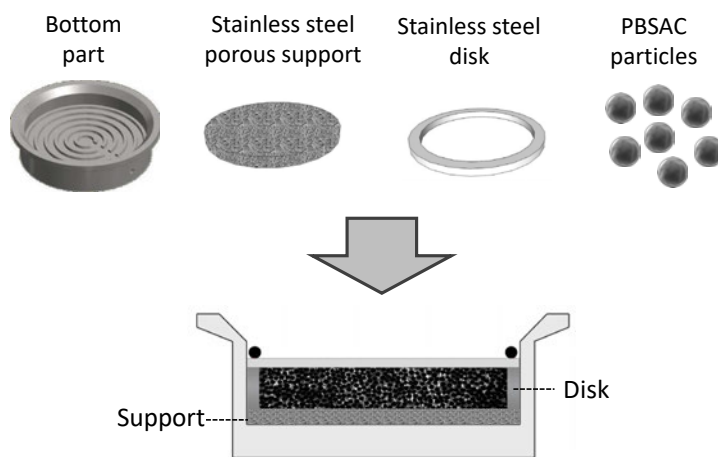


Figure 2.3: Schematic representation of the materials needed to prepare a packed-layer of PBSAC inside the bottom part of the stirred cell.

The filtration protocol for the UF-PBSAC packed layer is similar the one for the UF-PBSAC mat and is reported in Appendix B.1.

2.2.8 Static adsorption

The adsorption isotherms of MB for the loose particles and the PBSAC embedded in the mat are measured in static conditions. MB solutions from 10 mg L⁻¹ to 500 mg L⁻¹ are poured inside the flasks (Duran Group, Germany). The desired amount of PBSAC (for a final 0.5 g L⁻¹) or a piece of PBSAC mat (75 mg) is added into the flask. The flasks are placed inside the incubator shaker (Innova 43 R, New Brunswick Scientific, USA) at 260 rpm and 20 °C. A sample is collected from the flask after 96 h and 120 h for the loose PBSAC and the PBSAC mat, respectively. The uptake at the end is calculated by Eq. (2.2) and it is plotted as a function of the remaining MB concentration in the liquid phase to obtain the adsorption isotherm.

$$q = \frac{V(c_{initial} - c_{final})}{mass\ of\ PBSAC\ or\ mat} \quad (2.2)$$

2.2.9 Data analysis

The parameters used to characterize the process are summarized in Table 2.4. An important parameter that influences the dynamic adsorption of hormones in the UF-PBSAC is the contact time. EBCT is calculated from Eq. (2.3). The permeate volume is calculated from the mass of permeate (measured by the balance), considering the density of water at the temperature of the experiment [92]. The main performance parameter selected to characterize the UF-PBSAC process is hormone removal (Eq. (2.7)). The hormone uptake (Eq. (2.9)) will also be discussed.

2.3 Results and discussion

2.3.1 Permeability / flow properties of the UF-PBSAC mat

Permeability is an important performance parameter in membrane processes. In the UF-PBSAC, removal of estrogens is expected to occur by adsorption in the AC layer. Thus, permeability also has a significant influence on the contact time of the adsorption process. For this reason, the pure water flux was measured at increasing pressure both for the UF and the UF-PBSAC. The empty bed contact time (EBCT) in the UF-PBSAC was calculated based on Eq. (2.3).

Fig. 2.4A shows that the flux increases with pressure in the same way for the UF and the UF-PBSAC. It means that permeability of the process is determined by the membrane as expected, considering its much smaller pore size (for UF \approx 5 nm, for the PBSAC-mat the characteristics pore size can be estimated to be in the range 0.3-0.7 mm based on Eq. (2.10)). The permeability of the process is then between 70 and 90 L m⁻² h⁻¹ bar⁻¹ for a UF MWCO of 10 kDa. By increasing the pressure from 0.5 to 3.5 bar, the flux through the PBSAC mat increases from 50 to 360 L m⁻² h⁻¹. As a consequence, the EBCT varies between 175 and 20 seconds, depending

Table 2.4: Summary of the parameters used in Chapter 2 together with the units and the formulae for their calculation [91].

| Parameter | Unit | Formula | |
|--|----------------------------|--|--------|
| Empty bed contact time | s | $EBCT = \frac{V_{PBSAC}}{\dot{V}_P}$ | (2.3) |
| Flux | $L m^{-2} h^{-1}$ | $J_w = \frac{\dot{V}_P}{t_F A_{memb.}}$ | (2.4) |
| Permeability | $L m^{-2} h^{-1} bar^{-1}$ | $A = \frac{J_w}{\Delta P}$ | (2.5) |
| Relative concentration | – | $Relative\ conc. = \frac{c_P}{c_F}$ | (2.6) |
| Removal | % | $R = \left(1 - \frac{c_P}{c_F}\right) 100$ | (2.7) |
| Mass of MP adsorbed | ng | $m_{ads} = V_F c_F - \sum_{i=1}^{n.samples} V_{P,i} c_{P,i} - V_R c_R$ | (2.8) |
| Uptake | $ng g^{-1}$ | $q_{ads} = \frac{m_{ads}}{m_{PBSAC}}$ | (2.9) |
| Characteristic pore length of a packed-bed | mm | $l_\beta = d_P \left(\frac{\varepsilon_b}{1 - \varepsilon_b}\right)$ | (2.10) |
| V_P : volume of the permeate collected | | \dot{V}_P : volumetric flow rate of the permeate | |
| c_P : MP concentration in the permeate | | t_F : filtration time | |
| V_F : volume of the feed | | $A_{memb.}$: area of the membrane | |
| c_F : MP concentration in the feed | | ΔP : applied pressure | |
| V_R : volume of the retentate | | d_P : diameter of PBSAC | |
| c_R : MP concentration in the retentate | | ε_b : porosity of the packed bed | |
| V_{PBSAC} : volume of the PBSAC mat /layer | | | |

on the pressure applied. These values confirm that the adsorption process in the UF-PBSAC may be challenged by such low EBCT.

2.3.2 Breakthrough curves of hormones for the UF-PBSAC mat

The feasibility of using a thin PBSAC mat for MPs adsorption was assessed by measuring the breakthrough curves of 4 hormones until 0.6 L of permeate collected. For comparison, filtration through the UF only was also carried out.

The relative concentration (Eq. (2.6)) of the 4 hormones is reported in Fig. 2.5A. When only the UF is used, hormones break through quickly reaching the concentration of the feed after 0.2 L. The lower concentration in the first sample (0.1 L)

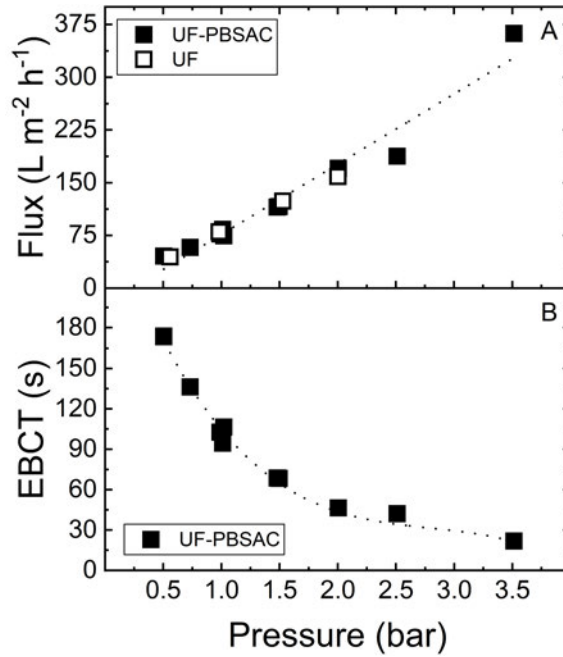


Figure 2.4: (A) Flux as a function of applied pressure for the UF and the UF-PBSAC; (B) empty bed contact time in the UF-PBSAC mat as a function of applied pressure. Temperature 25°C. Adapted from [91].

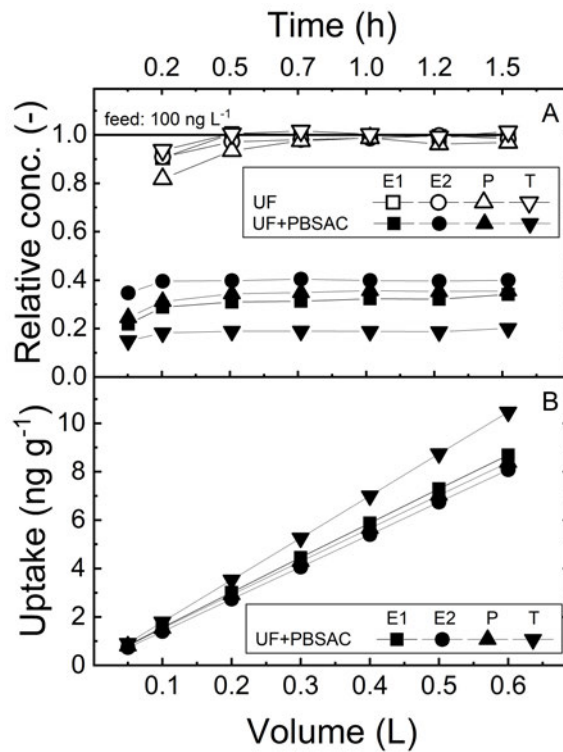


Figure 2.5: Relative concentration (A) and uptake (B) of E1, E2, T and P as a function of permeate volume. Feed concentration: 100 ng L⁻¹. Flux 125 L m⁻² h⁻¹. Temperature: 25 °C. Adapted from [91].

can be attributed to mixing with the water in the system (mainly permeate tube) and minor adsorption to the membrane. On the other hand, the addition of the

PBSAC mat brings an evident reduction in the permeate concentration of all hormones. The concentration in the permeate varies between 40 ng L^{-1} (E2) to 20 ng L^{-1} (T), corresponding to removals of 60 to 80 %. Although complete removal is not achieved, these results demonstrate that adsorption of MPs can occur in a thin layer with an EBCT of 1 min only. The shape of the breakthrough is also unusual in that the permeate concentration quickly stabilizes to a constant value and does not further change. This peculiar behavior is related to the linear increase of the uptake (Eq. (2.9)) during the process (Fig. 2.5B). This is not surprising considering the low concentration of hormones in the feed (100 ng L^{-1}) compared to the high specific surface area (hence saturation uptake) of PBSAC. Indeed, the adsorption isotherm of E2 on PBSAC was shown to be linear at least up to 1 mg g^{-1} in static adsorption in previous work [54]. In dynamic adsorption anyway, the permeate concentration can increase with the volume filtered not only because of saturation but also due to mass transport limitation.

Considering the low uptake ($<10 \text{ ng g}^{-1}$) that can be achieved in these conditions, filtration of E2 in the UF-PBSAC is carried out for a longer time until 9 L of permeate is collected. Besides the standard concentration of 100 ng L^{-1} for the feed, a feed concentration three orders of magnitude higher ($100 \text{ }\mu\text{g L}^{-1}$) was also tested.

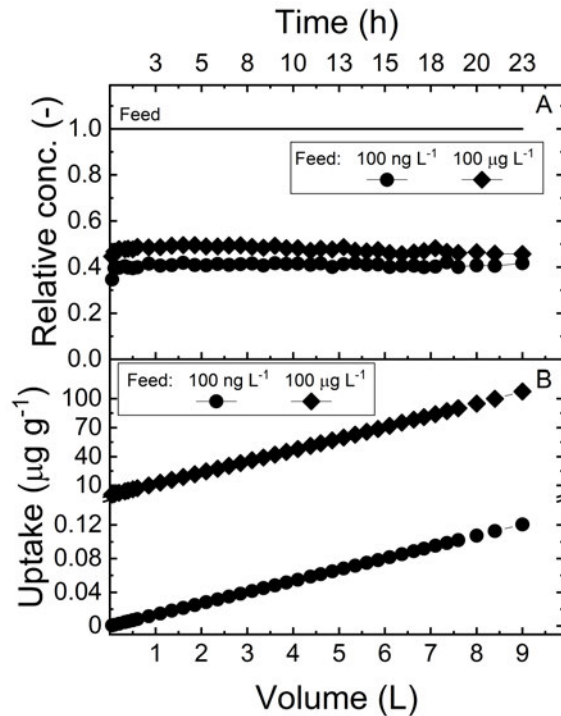


Figure 2.6: Relative concentration (A) and uptake (B) of E2 as a function of permeate volume for feed concentration of 100 ng L^{-1} and $100 \text{ }\mu\text{g L}^{-1}$. Flux $125 \text{ L m}^{-2} \text{ h}^{-1}$. Temperature: $25 \text{ }^\circ\text{C}$. Adapted from [91].

The shape of the breakthrough curve remains the same even after 9 L of solution filtered (Fig. 2.6A). The uptake increases linearly until $0.12 \text{ }\mu\text{g g}^{-1}$ for a feed of 100 ng L^{-1} and $107 \text{ }\mu\text{g g}^{-1}$ for a feed of $100 \text{ }\mu\text{g L}^{-1}$. The removal decreases slightly

at the highest concentration that could also be related to experimental error (Appendix B.2). Interference of methanol (used to increase the solubility of E2 in the feed) may also explain the slightly lower removal at the high concentration (Appendix A.1).

From these first results some consideration can be made about the feasibility of using a thin AC layer. First, at environmentally-relevant concentrations, the exhaustion uptake of the adsorbent is far, thus the use of the thin layer (with the related lower AC content compared to a column) may not be an issue. Second, the complete removal cannot be achieved in a PBSAC mat at an EBCT of 1 min. For this reason, the EBCT will be varied either by changing the flux or the thickness of the PBSAC layer.

2.3.3 Influence of the contact time

The applied pressure to the UF-PBSAC mat during filtration was varied between 0.5 bar to 3.5 bar to vary the flux (or superficial velocity). The removal of E2 at the end of the experiment (0.6 L of permeate collected) is plotted against the flux in Fig. 2.7.

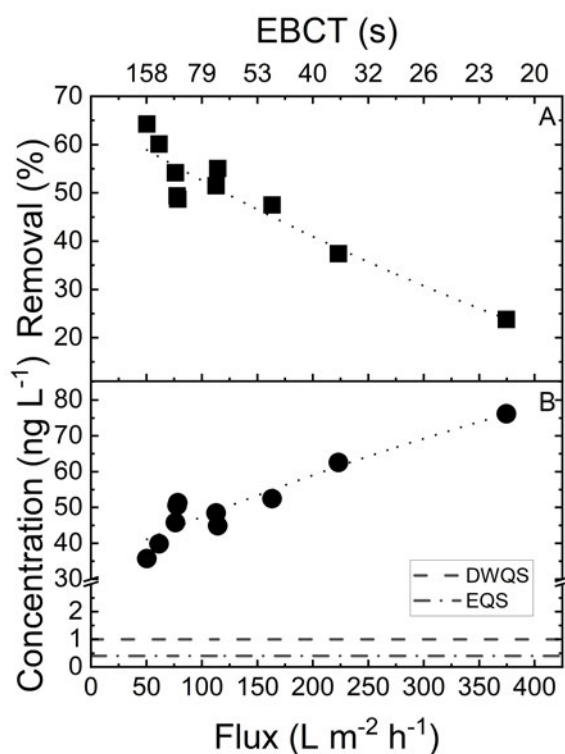


Figure 2.7: Removal (A) and corresponding permeate concentration (B) of E2 as a function of the flux for the UF-PBSAC mat. Feed concentration: 100 ng L⁻¹. Temperature: 25 °C. DWQS: drinking water quality standard. EQS: environmental quality standard. Adapted from [91].

An effect of the flux (hence the contact time) on the removal of E2 can be observed in Fig. 2.7A. The maximum removal of 65 % is achieved at the lowest flux of 50 L m⁻² h⁻¹. On the other side, the removal drops down to 23 % at the highest flux. The increase in the removal at low flux is related to the higher contact time.

However, from Fig. 2.7B, it can be noticed that even at the lowest flux, the permeate concentration is far from meeting the requirement for E2 level in surface and drinking water.

To increase the thickness of the adsorbing layer, an increasing number of PBSAC mats were placed on the permeate side of the UF membrane. From 1 single mat up to 6 mats, the thickness of the layer increases from 2.2 mm to 13.2 mm. This translates into an increase of the EBCT from 1 to 6 minutes. The removal and permeate concentration of E2 at increasing PBSAC mats is reported in Fig. 2.8.

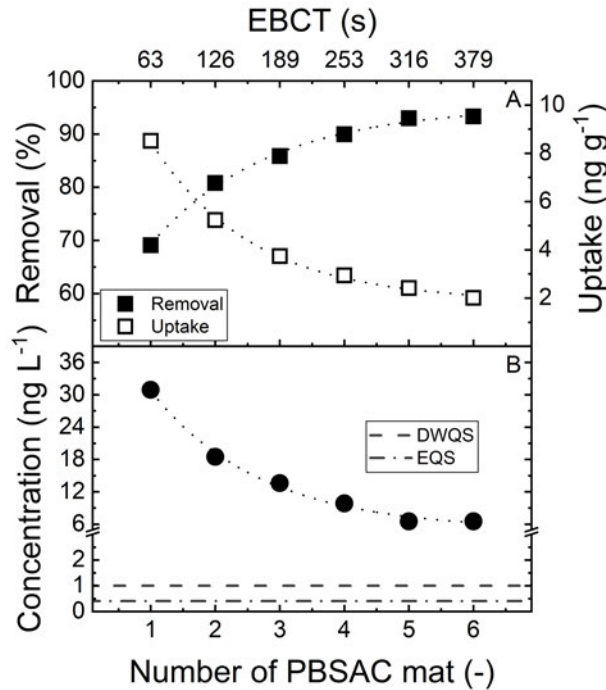


Figure 2.8: Removal and uptake (A) and corresponding permeate concentration (B) of E2 as a function of the number of PBSAC mats used. Flux $125 \text{ L m}^{-2} \text{ h}^{-1}$. Feed concentration: 100 ng L^{-1} . Temperature: $25 \text{ }^\circ\text{C}$. DWQS: drinking water quality standard. EQS: environmental quality standard. Adapted from [91].

Increasing the number of mats leads to clear improved performance, with E2 reaching 94 % removal for five mats (corresponding to 1 cm of adsorbing layer), as shown in Fig. 2.8A. The addition of one further mat (resulting in a thickness of 13.2 mm) does not further improve the process. The uptake (Eq. (2.9)) decreases with increasing number of mats, although a higher mass of E2 is adsorbed to PBSAC. This is simply related to the fact that a higher amount (mass) of the PBSAC mat is used.

The increase in the removal was compared to that expected, assuming that the adsorption process is independent in each layer (e.g., as if they act as separated layers in series). From Fig. C.1 in Appendix C.1, it can be observed that the experimental removal is lower than the expected one. The adsorption process is then not independent in each layer, but increasing the thickness may change the mass transport regime compared to the single layer.

Fig. 2.8B shows that the lowest concentration achievable is then 6 ng L^{-1} , still higher compared to the proposed target water quality of 0.4 and 1 ng L^{-1} .

2.3.4 Comparison between PBSAC mat and packed-layer

The PBSAC mat is a commercial material; a "glue" is present within the mat because it helps the particles to stick together in the production process. The breakthrough of E2 in an ideal packed-layer was measured to assess the impact on the adsorption of this "glue". The packed-layer and the mat used are characterized by a similar thickness and mass of PBSAC (Table 2.5).

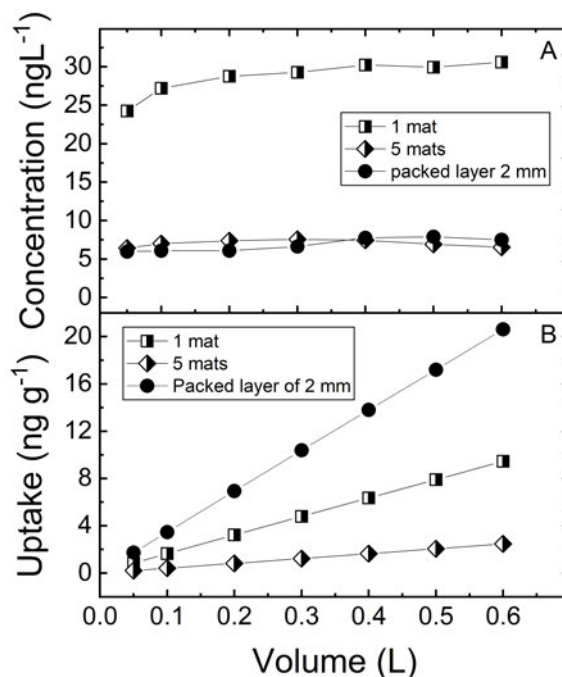


Figure 2.9: Comparison between the breakthrough curve (A) and the uptake (B) of E2 for the PBSAC mat and the PBSAC packed layer. Flux $125 \text{ L m}^{-2} \text{ h}^{-1}$. Feed concentration: 100 ng L^{-1} . Temperature: $25 \text{ }^\circ\text{C}$. Adapted from [80].

Fig. 2.9A shows that the shape of the breakthrough curve is the same in both cases. This shape is a characteristic of the early adsorption stage typical of this process, as already discussed. On the contrary, the permeate concentration of E2 is reduced from 30 ng L^{-1} for the one single PBSAC mat (thickness of 2.2 mm) to $6\text{-}7 \text{ ng L}^{-1}$ for the packed PBSAC layer (thickness of 2 mm). The adsorption process is significantly improved when spare PBSAC is packed in the layer, meaning that the "glue" within PBSAC particles in the mat has some negative effect on the adsorption process.

Two main possible reasons were considered to explain these results: (i) the presence of the "glue" reduces the contact time by filling the void volume within the particles; (ii) the "glue" blocks the pores hindering the access of E2 inside the PBSAC porosity (hence reducing the adsorption capacity). Anyway, considering that

the capacity in this early adsorption stage is not a limiting factor, the reduced contact time was identified as the strongest explanation for the results in Fig. 2.9. It is interesting to notice that a similar permeate concentration can be achieved using a 2 mm PBSAC packed layer and 5 PBSAC mats (Fig. 2.9A). In summary, the PBSAC packed layer offers the same performance of the PBSAC mat at a consistently lower thickness (hence lower EBCT).

The effect of the "glue" on the adsorption capacity of PBSAC within the mat was also investigated. Maximum adsorption capacity can not be achieved for E2 even in static adsorption experiments. For this reason, MB was used that has a very high solubility in water. As a first step, the amount of PBSAC (excluding the "glue") in the mat was estimated as shown in Appendix C.2. It was concluded that the PBSAC account for roughly 80 % of the total mass of the mat.

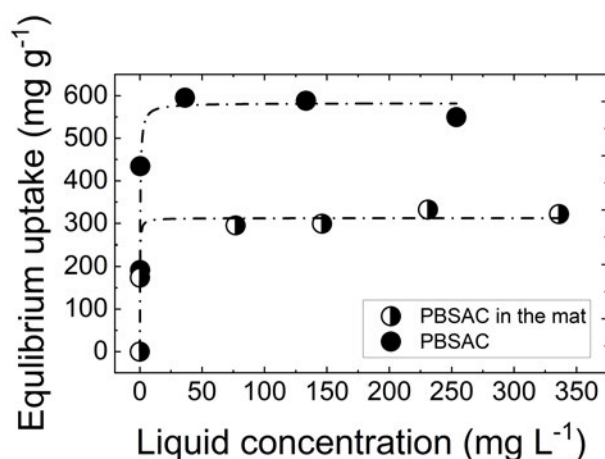


Figure 2.10: Comparison of the adsorption isotherm (obtained in static adsorption experiments) of MB for loose PBSAC and PBSAC embedded in the mat. Temperature 20 °C. Equilibrium time: 120 h.

Fig. 2.10 reports the adsorption isotherm of MB for spare PBSAC and PBSACs embedded in the mat. The maximum adsorption capacity for MB is reduced for the PBSAC within the mat, showing that the "glue" may block part of the PBSAC surface and internal porosity.

2.3.5 Considerations about the lifetime of the layer

As presented in the previous sections, the saturation of a PBSAC mat or packed-layer for E2 could not be achieved. Considering the maximum adsorption capacity of more than 500 mg g⁻¹ measured for MB, it is clear that saturation is far in the experimental conditions used for E2 dynamic adsorption experiments. The highest adsorption capacity (or uptake) experienced for E2 was 100 ng g⁻¹ (Fig. 2.6B).

Anyway, an estimation of the lifetime of a PBSAC layer can be performed to have an idea of the order of magnitude of the breakthrough time (corresponding to the lifetime of a PBSAC layer). This was based on the following assumption: (i) the maximum adsorption capacity of E2 is similar to the one of MB (≈ 500 mg

2.3. Results and discussion

Table 2.5: Comparison of the main characteristics of a 2 mm PBSAC packed-layer and a PBSAC mat.

| Parameter | Unit | PBSAC packed-layer | 1 PBSAC mat |
|--------------------------------|--------------|--------------------|-------------|
| PBSAC diameter | μm | 450 | 450 |
| Thickness | mm | 2 | 2.2 |
| Mass of PBSAC | g | 2.4 | 2.7 |
| EBCT | s | 60 | 66 |
| E2 removal | $\%$ | 94 | 70 |
| MB maximum adsorption capacity | $mg\ g^{-1}$ | 518 | 312 |

g^{-1}); (ii) infinitely fast mass transfer processes and missing dispersion (ideal breakthrough). Under these assumptions, the uptake would increase linearly until the maximum adsorption capacity is reached. At that moment, the permeate concentration would reach instantaneously the same value of the feed concentration (as shown in Fig. C.2, Appendix C.3). The procedure for determining the breakthrough volume under these assumptions is shown graphically in Fig. 2.11.

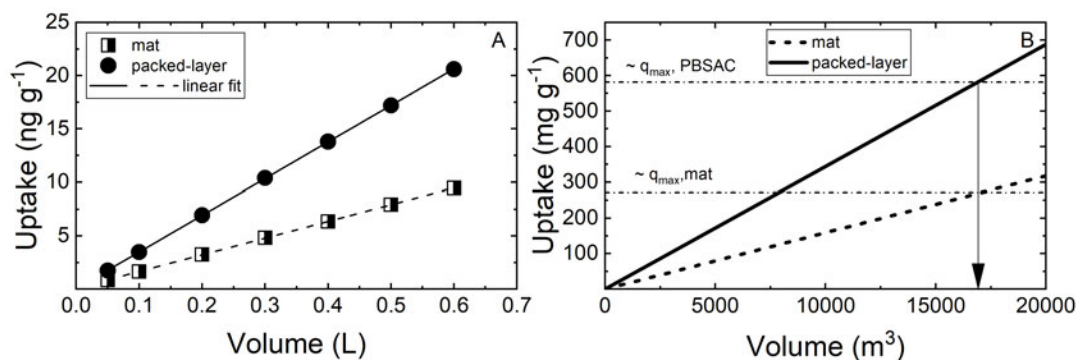


Figure 2.11: Estimation of the E2 treatable volume (breakthrough volume) based on the assumption that uptake increases linearly until reaching the value of the maximum adsorption capacity for MB.

Fig. 2.11B indicates that a volume in the order of 17000 m^3 is estimated to be processed before saturation both for the PBSAC mat and packed-layer. This corresponds to $\sim 500\ m^3$ per cm^2 of UF-PBSAC. Considering hypothetical volumetric flow rates in the range of 0.4 to 1 $L\ h^{-1}$, the UF-PBSAC would have an estimated lifetime from 15 to more than 100 years. These huge values are an apparent overestimation of the real lifetime of the filter because they were derived using assumptions that are not expected to be valid in a real process. The use of MB maximum uptake for hormones could be reasonable because MB and hormones present a similar size (and the charged MB would be expected to have even a lower affinity compared to the hydrophobic hormones for AC). On the other hand, the assumptions of infinite mass transport rate and missing dispersion are weak. Besides, in a real process, other compounds present in water may adsorb, reducing the surface area available

for hormones adsorption.

However, this estimation is helpful to make some general considerations about the process. The smaller maximum uptake (or saturation capacity) of a thin AC layer compared to a column may not be limiting if the target pollutant is present at trace concentration in water. Further, the saturation time of the PBSAC layer may be longer than the lifetime of the UF membrane (that can be assumed to be 5 years). The last consideration is important if we consider the regeneration of the PBSAC layer once it is saturated. Conventional thermally-based regeneration of AC is not compatible with the presence of a polymeric membrane in the filter. Nevertheless, if the lifetimes of the membrane and the PBSAC layer are of the same order of magnitude, then the carbon layer could be replaced and regenerated separately when the membrane is replaced.

2.3.6 Nanofiltration-PBSAC mat

The last section deals with the residual adsorption of E2 from the permeate of NF membranes. NF90 and NF270 can reject hormones, but the removal is incomplete based on the results reported in the literature [44].

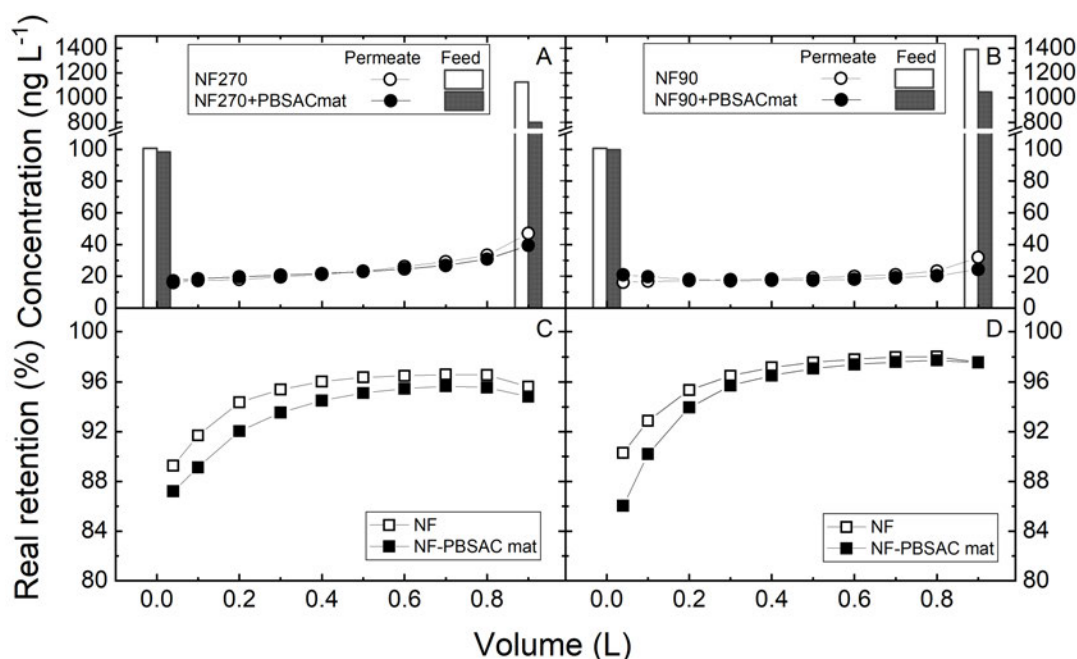


Figure 2.12: Permeate and initial/final feed concentration of E2 as a function of permeate volume for (A) NF270 and NF270-PBSAC mat and (B) NF90 and NF90-PBSAC mat. Real retention of E2 for (C) NF270 and NF270-PBSAC mat and (D) NF90 and NF90-PBSAC mat. Feed concentration: 100 ng L⁻¹. Temperature: 25 °C. Stirring 400 rpm. Adapted from [91].

Fig. 2.12A&B reports the breakthrough curves and the real retention (e.g., the removal considering the increase of E2 feed conc.) for the NF and the NF-PBSAC mat. For NF90, the real retention (98 %) is slightly higher compared to NF270 (96 %) (Fig. 2.12C&D), which is in accordance with the pore size of the membrane (≈ 0.5 and ≈ 0.7 nm respectively). Surprisingly, permeate concentrations (Fig. 2.12A&B)

are the same when the PBSAC mat is added compared to the case when only NF is used as the filtration medium. Thus, the addition of the PBSAC mat on the permeate side of NF is not effective. Focusing on the feed concentration inside the stirred cell in (Fig. 2.12A&B), it can be noticed that the final values are higher for NF compared to NF-PBSAC (1127 compared to 802 ng L⁻¹ for NF270 and 1390 compared to 1046 ng L⁻¹ for NF90). This suggests that the rejection of E2 by NF is deteriorated by the presence of the PBSAC mat on the permeate side.

The negative effect of the PBSAC mat on the rejection of E2 by NF was not fully understood. An hypothesis is that the adsorbing layer enhances the permeate side diffusion of E2 through the membrane, a phenomenon already reported as a possible reason for the lower rejection of hormones by NF membranes [44]. More likely, the PBSAC mat affects the rejection by influencing the solute flux (J_{E2}) through the membrane. The solution-diffusion theory states that (J_{E2}) is proportional to the difference between solute feed and the permeate concentration by means of solute permeability coefficient (B) [93], as shown in Eq. (2.11). Note the $c_{f,m}$ in Eq. (2.11) is the feed concentration at the membrane surface, which is higher compared to the one in the bulk solution due to concentration polarization.

$$J_{E2} = B(c_{f,m} - c_p) \quad (2.11)$$

E2 concentration in the water adjacent to the NF is lower when the PBSAC mat is present (see Fig. 2.13) due to adsorption. As a consequence, the gradient concentration across the NF is higher, bringing to an increased E2 permeate flux when an adsorbing layer is present on the permeate side of the membrane.

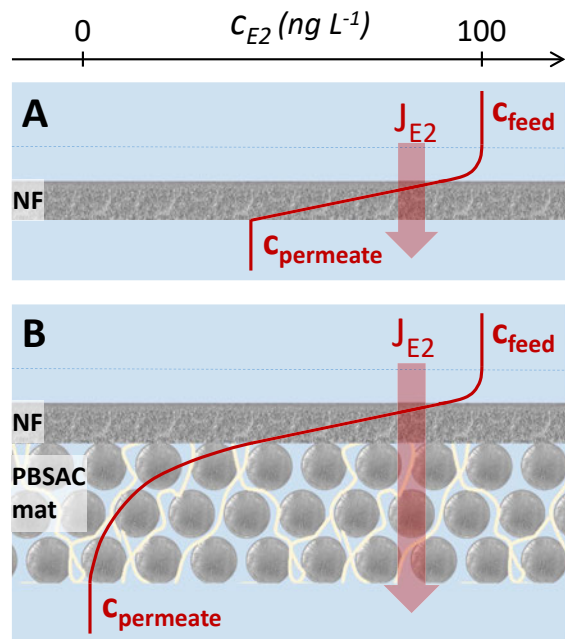


Figure 2.13: Qualitative representation of the concentration profile of E2 in the NF (A) and the NF-PBSAC mat (B).

In summary, the use of a UF was shown to be more advantageous compared to NF when coupled with a permeate side adsorbing layer. In fact, the higher pressure needed by NF are not balanced by better performances.

2.4 Conclusions

- The level of steroid hormones can be significantly reduced from 100 to 20-40 ng L⁻¹ by filtration through UF coupled with a thin PBSAC mat of 2.2 mm thickness.
- The adsorption process in the PBSAC mat is effective even at an EBCT of 1 min, remarkably shorter compared to typical AC filters (5-30 min [51]).
- The reduced maximum uptake (or adsorption capacity) of the thin layer (compared to a conventional column) was not limiting considering the environmentally relevant hormone concentrations used (in the ng L⁻¹ range).
- E2 removal increased up to 94 % (corresponding to 6 ng L⁻¹ remaining in the permeate) by increasing the number of PBSAC mats from 1 to 5.
- A packed-layer of PBSAC performs significantly better than the commercial filter mat. A 2 mm thick packed-layer can achieve the same removal (94 %) of 5 mats (thickness 11 mm).
- The UF-PBSAC is a promising approach to remove hormones from water at higher permeability compared to NF/RO and lower carbon consumption compared to the conventional AC column.
- The level of hormones in the permeate was not reduced enough to meet the current drinking and environmental quality standard proposed by WHO;
- The PBSAC mat was not effective in polishing the residual hormone concentration permeating the NF membrane. The permeate-side adsorption step deteriorates the rejection process by NF.

Chapter 3

Influence of PBSAC material characteristics on the adsorption of hormones in the thin packed-layer*

The use of a polymer-based spherical activated carbon (PBSAC) thin layer coupled with an ultrafiltration membrane was proven to be a promising approach in the previous chapter. In this chapter, the adsorption process was further advanced through a systematic investigation of the important material characteristics of PBSAC: the particle diameter, the internal porous morphology and the surface chemistry. The diameter of PBSAC in the layer was shown to be the most critical factor. E2 concentration of 100 ng L^{-1} in the feed could be reduced to $< 1 \text{ ng L}^{-1}$ in the permeate using a 2 mm layer packed with PBSAC of $80 \text{ }\mu\text{m}$ in diameter. Further, the E2 drinking water standard (1 ng L^{-1}) could be safely reached with a layer thickness of 2 and 4 mm for PBSAC diameter of 80 and $200 \text{ }\mu\text{m}$, respectively. Besides the particle diameter, the surface chemistry can be used to improve the adsorption process. Adsorption kinetics enhancement by increasing the oxygen content on the carbon was observed for OH-containing pollutants such as estradiol. The experimental evidence presented in this chapter confirms that UF-PBSAC is a competitive and promising technology. Removals comparable to high-pressure membranes and advanced oxidation processes are coupled with some advantages including the process permeability and no risk of dangerous byproducts' formation. However, a solid theoretical understanding of the adsorption mechanism was not thoroughly achieved. In addition, the impact of organic matter present in the water, together with estrogens, needs to be addressed to claim the applicability of this process in a real case.

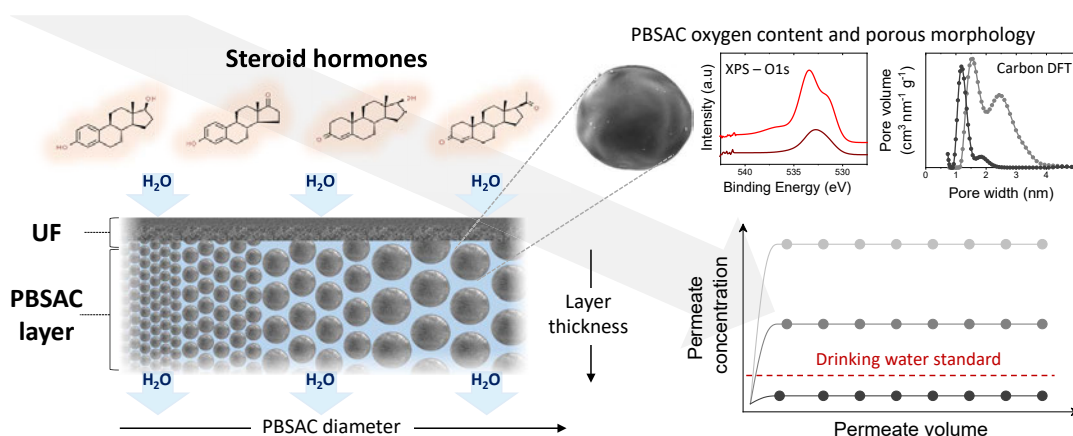


Figure 3.1: Graphical abstract of Chapter 3. Adapted from [80].

* This chapter is based on the following publication: "Polymer-based spherical activated carbon-ultrafiltration (UF-PBSAC) for the adsorption of steroid hormones from water: Material characteristics and process configuration", Water Research, 2020, 185, 116249. For this thesis chapter, part of the content has been rewritten and some of the graphs have been adapted by the author.

3.1 Introduction

In Chapter 2 the feasibility of using a thin polymer-based spherical activated carbon (PBSAC) layer on the permeate side of a membrane to remove estrogenic micropollutants (MPs) was demonstrated. The process is promising, especially when PBSAC is packed in a layer without the use of any "glue" (present in the commercial PBSAC filter mat). Estradiol (E2) removal higher than 90 % could be achieved in a layer of 2 mm. The goal of Chapter 3 is to seek room for improvement of the adsorption process to achieve even higher MP removal. This would make the UF-PBSAC approach competitive to other technologies such as high-pressure membranes and advanced oxidation processes.

For this purpose, a systematic investigation of the influence of some selected material characteristics of PBSAC will be carried out. The adsorption of MP onto activated carbon (AC) is known to depend on parameters like the structural morphology (surface area and pore size distribution) and surface chemistry, both of carbon and pollutant. Also, the size of the PBSAC packed in the layer will be considered. In packed-bed (fixed-bed), the size of the packing (PBSAC in this case) influences the mass transport regime. Smaller particles are characterized by larger external surface area, convectively exposed to the flow of the pollutant. A review of the relevance of the material characteristics in the adsorption of MP onto AC is first briefly discussed in the following paragraphs.

The size of the AC is related to the application technique. Typically, granular activated carbon (GAC, 0.4-5 mm) is arranged in a fixed bed in what is referred to as a "GAC filter" [81, 83, 84, 94, 95]. The typical height of GAC filters ranges between 2 and 4 m [51]. On the other side, the smaller powdered activated carbon (PAC, < 40 μm) is continuously fed as a slurry. In conventional processes, the separation of PAC from the treated water is achieved by coagulation-flocculation. Alternatively, PAC can be continuously removed using low pressure membrane in the so-called membrane-AC hybrid process [69].

Besides the application technique, the size of the AC has a strong influence on the adsorption kinetics of MPs. Smaller carbon adsorbents are characterized by a shorter diffusion path and a larger specific external surface area [49] that results in faster kinetics. This has pushed the researchers to use AC even smaller than PAC, namely superfine powdered activated carbon (SPAC, 1 μm -100 nm) and carbon nanoparticle (CNP, 20 μm - 1 nm). SPAC can be obtained preferentially by wet milling of conventional-sized PAC [50, 96–98]. Bonvin *et al.* [50] have observed further enhancement of the adsorption kinetics towards pharmaceuticals and pesticides of SPAC compared to PAC.

On the contrary, the adsorption capacity at equilibrium is not clearly correlated with the adsorbent size [97, 99]. Other factors, such as pollutant size and chemistry, have an influence on the equilibrium adsorption capacity. Matsui *et al.* have shown that the adsorption capacity increases with increasing AC size for large molecules

like natural organic matter (NOM) [97, 100]. Some authors [97, 101] have also observed a change of the AC surface chemistry (specifically the oxygen content) as a consequence of the milling process. CNP should be the best option in terms of the kinetics of adsorption due to high external specific surface area (hence, no diffusion limitation). However, it is challenging to obtain a proper dispersion of CNP. Aggregation can lead to particles larger than 1 μm , hindering the theoretical advantages compare to PAC and SPAC [66, 102, 103].

While many researchers have focused on the influence of adsorbent size in the PAC and SPAC range, systematic investigations of the size of the adsorbent in GAC filters are rare. In this sense, inspiration can be taken from other fields. The improved separation efficiency deriving from the use of smaller particles as packing is known and used in analytical and preparative chromatography, for example.

ACs were initially produced from raw materials such as coal, peat and lignin. Agricultural wastes (the most common being coconut-shell) are of great interest due to their abundance and low cost. Polymeric macromolecules can also be used as a precursor for the production of AC [104, 105]. The production process can be classified in: (i) physical activation, (ii) chemical activation and (iii) micro-waved assisted activation. The production process is divided into two steps (not clearly distinguishable for chemical activation): carbonization and activation [106, 107]. During carbonization, the elimination of non-carbon components is achieved via heat treatment in an inert atmosphere at temperatures ranging from 400 to 600 $^{\circ}\text{C}$. During physical activation, a gaseous oxidative agent (CO_2 , steam or air at 700 to 900 $^{\circ}\text{C}$) removes the more reactive carbon species and brings to the formation of the porous structure of the AC [106, 107]. The pores form in a three-stage process: (i) opening of previously inaccessible pores (removal of tars), (ii) creation of new pores and (iii) broadening of the existing pores [106, 108].

Characteristics such as the structural morphology and the surface chemistry of the AC depend both on the precursor material and the activation process (the type of process, temperature and activation degree). Longer activation leads to an increase in the specific surface area and pore volume. The pore size distribution is built in this stage with the formation of interconnected meso (2-50 nm) and micropores (<2nm) [108]. A high fraction of micropores is beneficial for the adsorption of small molecules like MPs [109]. However, the broadening of the pores can be advantageous for the adsorption of larger molecules. Li *et al.* [110] managed to increase the adsorption capacity (from 374 to 842 mg g^{-1}) of AC for Rhodamine B by physical activation with CO_2 and consequent pores broadening.

The surface chemistry is highly dependent on the precursor material. The presence on the AC surface of a vast range of heteroatoms (O, P, K, N) is reported in the literature (e.g., for oxygen from 2 to 20 %) [111–114]. The use of synthetic precursors (such as polymer fibers or spheres) with define and reproducible properties allows better control of the surface chemistry of the AC [104, 105].

Higher oxygen contents on the carbon surface are expected to decrease the adsorption capacity of MPs due to enhanced water adsorption (wetting) of the surface. Enhanced water adsorption has the consequence of reducing the hydrophobic interactions between the MP and the carbon. Indeed, several authors [101, 109, 115] reported a decrease in the adsorption capacity at equilibrium of hydrophobic pollutants such as 2-methylisoborneol and trichloroethylene at higher oxygen content. From the kinetics point of view, the influence of AC's oxygen species was never discussed in the literature. It is worth mentioning that typical AC-filters are designed mainly based on the equilibrium adsorption capacity because, typically, a large contact time is offered to the adsorption process. In the thin-layer adsorption approach, the short contact time may not be sufficient to reach equilibrium. Hence, pure adsorption kinetics may also play a role.

PBSAC is produced by means of carbonization and physical activation of polystyrene spherical precursors [116]. Thus, PBSAC can be produced in various sizes simply starting with precursors with the desired size. On the other hand, conventional AC (e.g., coconut shell-based) is characterized by random and irregular shape. It is challenging to control on the final size that depends on the crushing and grinding process. In addition, the use of polymeric precursor allows better control of the surface chemistry. In this chapter, the diameter, the porous structure and the surface chemistry of PBSAC packed in a millimetric layer are systematically investigated. The influence of these characteristics on the adsorption of hormones is assessed, followed by a critical discussion on what are the implications on estrogens removal by a thin AC layer. Thus, the final goal is to clarify which characteristics the AC should exhibit in order to reduce the estrogen concentration below the current water quality standard.

3.2 Materials and methods

3.2.1 Membrane

In this chapter, the UF membrane (Merck-Millipore, PLHGC) is used in all experiments. In the previous chapter, it was shown that this membrane is characterized by negligible adsorption and rejection of hormones. In this way, the breakthrough curve of hormones is determined only by the PBSAC layer on the permeate side. Thus, the material characteristics of PBSAC can be investigated without interference from the membrane.

3.2.2 Polymer-based spherical activated carbon

The material was already presented in Chapter 2. In this chapter, PBSAC with different material characteristics are used. Some material characteristics are selected because they are expected to affect and possibly improve the adsorption process. PBSAC with different activation degree at a constant diameter of 200 μm is used.

3.2. Materials and methods

The activation degree influences the specific pore volume inside the particle. For this reason, the specific surface area increases at increasing activation. On the other side, the tapped density of the particle decreases at increasing activation degree as a consequence of the formation of pores inside the carbon.

Further, PBSAC with different diameters (80 to 640 μm) is produced by Blücher using polymeric precursors with different sizes. These samples have an intermediate activation level. Finally, two further samples are investigated, characterized by an increased and decreased content of oxygen on the surface. The properties of all the samples used in this chapter provided by the manufacturer are reported in Table 3.1.

Table 3.1: List of the PBSAC samples and the properties provided by the manufacturer [80].

| Sample label | Particle diameter μm | Tap density g L^{-1} | BET specific surface area $\text{m}^2 \text{g}^{-1}$ | Mass of PBSAC per layer (2 mm) g |
|--|------------------------------------|----------------------------------|---|-------------------------------------|
| <i>Samples with increasing activation time</i> | | | | |
| A1 | 200 | 794 | 813 | 5.32 |
| A2 | 200 | 735 | 1024 | 4.87 |
| A3 | 200 | 685 | 1167 | 4.54 |
| A4 | 200 | 625 | 1365 | 4.16 |
| A5 | 200 | 495 | 1766 | 3.29 |
| <i>Samples with increasing particle diameter</i> | | | | |
| P80 | 80 | 617 | 1421 | 4.09 |
| P200 | 200 | 602 | 1436 | 3.99 |
| P380 | 380 | 588 | 1445 | 3.60 |
| P470 | 470 | 570 | 1445 | 3.78 |
| P580 | 580 | 540 | 1509 | 3.58 |
| P640 | 640 | 598 | 1380 | 3.97 |
| <i>Samples with increased and decreased oxygen content</i> | | | | |
| O+ | 200 | 602 ^a | 1436 ^a | 3.98 |
| O- | 200 | 602 ^a | 1436 ^a | 3.92 |

^a Assuming that the tap density and BET specific surface area does not change compared to the pristine sample (P200)

3.2.3 Chemicals and analytical methods

The feed solution used in this chapter is composed always of 100 ng L^{-1} of hormone in the background buffer (1 mM NaHCO_3 and 10 mM NaCl) and it is prepared in a similar way as previously described in Chapter 2. However, the background solution is not prepared before each experiment, but a stock solution (0.1 M NaHCO_3 and 1 M NaCl) is prepared for each set of experiments and then diluted with MilliQ

water. This procedure is faster but it revealed to be problematic in terms of pH. In fact, the pH of the stock solution becomes more alkaline within 1 week after preparation (because bicarbonate can react with H^+ , forming first carbonic acid and then dissociating in H_2O and CO_2 , released in the air). For this reason, background solution pH is in the range 8 to 9 for the results reported in this chapter. Nevertheless, this is not affecting the results as it was shown that the hormones adsorption is not influenced by pH in the range 2-12 [54].

The hormones used in this chapter have a specific activity of 91, 90, 93 and 89 Ci $mmol^{-1}$ for estradiol (E2), estrone (E1), progesterone (P) and testosterone (T), respectively.

The hormones concentration is again measured with a Liquid Scintillation Counter (LSC). The calibration curves using three standards (1, 10 and 100 ng L^{-1}) for E1, P and T are reported in Appendix A (Fig. A.3). Considering that, in this chapter, the goal is to reduce E2 concentration below the drinking water quality standard of 1 ng L^{-1} , the calibration curve for E2 was performed using standards down to 0.05 ng L^{-1} . The error of the triplicates was calculated based on the maximum and minimum values detected Eq. (3.1) for each concentration. Assuming the value of 5 % as the threshold value for reliable detection, the limit of quantification results in 0.5 ng L^{-1} , as shown in Fig. 3.2.

$$\%error = \frac{CONC.max - CONC.min}{CONC.average} 100 \quad (3.1)$$

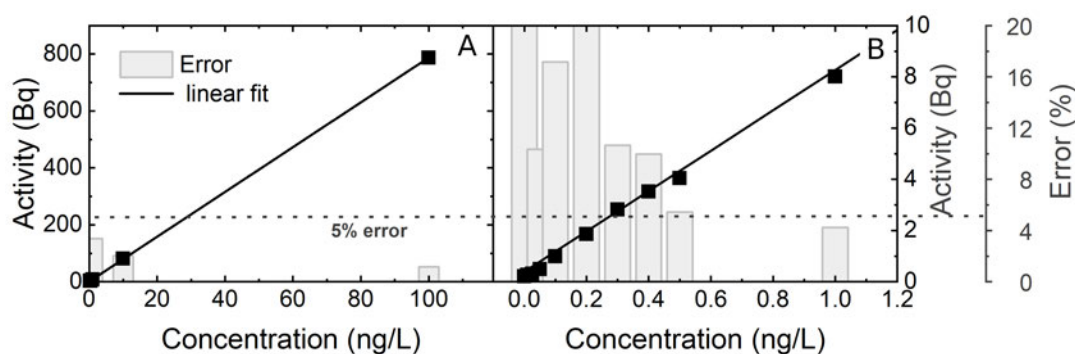


Figure 3.2: A) Calibration curve of E2 in the range 1-100 ng L^{-1} . B) Calibration curve for concentrations lower than 1 ng L^{-1} and estimation of the limit of detection (error < 5 %).

Methylene blue (MB) solution preparation and detection with the UV-vis follow the same protocol already reported in Chapter 2.

3.2.4 Dynamic adsorption experiments

Dynamic adsorption experiments in the UF-PBSAC packed-layer are carried out using the same set-up, layer preparation and filtration protocol reported in Chapter 2 and Appendix B. However, the PBSAC samples used in this chapter are characterized by different values of tap density. For this reason, the mass of PBSAC present

in the layer can be different depending on the sample used. In Table 3.1, the tap densities and the weights of PBSAC for a 2 mm thick layer are reported.

3.2.5 Static adsorption experiments

In some cases, static adsorption experiments are carried out to clarify the results obtained in dynamic adsorption experiments. In particular, the static adsorption kinetics is measured for the four hormones on PBSAC with increased and reduced oxygen content. For every experiment, one single hormone is used (thus not in a mixture of the four). The feed solution (0.25 L) of each hormone (initial concentration of 100 ng L^{-1}) is poured inside a conical flask (Duran Group, Germany). The desired amount of PBSAC particles to reach a concentration of 0.1 g L^{-1} is added. The flask is placed into the incubator shaker, stirring and temperature are set to 260 rpm and $20 \text{ }^\circ\text{C}$, respectively. Samples are collected at different time intervals (0.25, 0.5, 1, 3, 7, 24 and 26 h) and the concentration of hormones measured with the LSC.

In addition, adsorption isotherms of MB for PBSAC samples with increasing activation are measured. The same protocol is used already reported in Chapter 2.

3.2.6 Material characterization

The porous morphology of the PBSAC is characterized via Argon adsorption/desorption data are collected at 87 K (Autosorb1-MP, Quantachrome, USA). The measurements are performed by Dr. Peter Weidler from the Institute of Functional Interfaces (IFG, KIT). Before analysis, PBSAC samples are degassed at $300 \text{ }^\circ\text{C}$ in vacuum for 24 h. Non-local density functional theory model (DFT) model is used to fit experimental data and estimate the pore volume and specific surface area distribution of PBSAC. Two pore models for carbon were compared, namely slit-like and a mixture of spherical and cylindrical pore shapes.

To characterize the surface chemistry of PBSAC, X-ray photoelectron spectroscopy (XPS) is performed by Dr. Christian Njel and Dr. Julia Maibach from the Institute for Applied Materials (IAM, KIT) using a Thermo Scientific K-alpha+ spectrometer. The monochromatic $\text{AlK}\alpha$ line is used as X-ray excitation (1486.6 eV) with pass energy of 50 eV to obtain high resolution spectra. The samples were analyzed using a micro-focused, monochromated $\text{Al K}\alpha$ X-ray source ($40 \text{ }\mu\text{m}$ spot size). Voigt profiles were applied to fit XPS spectra and Scofield sensitivity factors for quantification [117]. C 1s peak (C-C) at 284.50 eV binding energy [118] were used as reference spectra. The Carbon (C1s) spectra were done at the beginning and end of each resolution analysis, to check the absence of any sample degradation under irradiation.

3.2.7 Data analysis

Similarly to Chapter 1, the performance parameters used to characterize the adsorption process at varying PBSAC characteristics are the hormone removal Eq. (3.4) and the hormone uptake Eq. (3.6).

Table 3.2: Summary of the parameters used in Chapter 3 together with the units and the formulae for their calculation.

| Parameter | Unit | Formula | |
|------------------------|--------------------|--|-------|
| Empty bed contact time | s | $EBCT = \frac{V_{PBSAC}}{\dot{V}_P}$ | (3.2) |
| Relative concentration | – | $Relative\ conc. = \frac{c_P}{c_F}$ | (3.3) |
| Removal | % | $R = (1 - \frac{c_P}{c_F}) 100$ | (3.4) |
| Mass of MP adsorbed | ng | $m_{ads} = V_F c_F - \sum_{i=1}^{n.samples} V_{P,i} c_{P,i} - V_R c_R$ | (3.5) |
| Uptake | ng g ⁻¹ | $q_{ads} = \frac{m_{ads}}{m_{PBSAC}}$ | (3.6) |

| | |
|--|---|
| V_{PBSAC} : volume of the PBSAC layer | V_F : volume of the feed |
| \dot{V}_P : volumetric flow rate of the permeate | c_F : MP concentration in the feed |
| V_P : volume of the permeate collected | V_R : volume of the retentate |
| c_P : MP concentration in the permeate | c_R : MP concentration in the retentate |

3.3 Results and discussion

3.3.1 External surface area in a PBSAC layer

The surface area of the adsorbent is a crucial parameter in the adsorption process. The goal in this chapter is to investigate the external surface area, directly exposed to the flow, and the internal surface area deriving from the porosity inside the adsorbent. The first one depends on the size of PBSAC packed in the layer, the second one on the activation degree.

At first, the external surface area of PBSAC particles in a 2 mm packed layer is estimated, multiplying the number of particles for the surface area of a single one. To calculate the number of particles in the layer, Eq. (3.7) was used:

$$\begin{aligned}
 \text{Number of PBSACs} &= \frac{\text{volume of PBSACs in the layer}}{\text{Volume of 1 PBSAC}} = \\
 &= \frac{\text{volume of the layer} \cdot \text{PBSAC fraction}}{\text{Volume of 1 PBSAC}} \quad (3.7)
 \end{aligned}$$

The PBSAC fraction is the opposite of the so-called bed porosity and it is assumed to be 60 %, hence assuming to be close to the densest possible random packing for spheres of equal size [119]. The results of these calculations are shown in Table 3.3. Decreasing the diameters of PBSAC from 640 to 80 μm corresponds to an increase in

3.3. Results and discussion

the external surface area from 0.037 to 0.306 m² for a 2 mm layer. These samples with different particle sizes have the same degree of activation, so they are characterized by a really similar internal surface area.

Table 3.3: External surface area of one single PBSAC and of a 2 mm PBSAC layer (6.6 mL in volume) for different PBSAC diameters.

| Diameter | 1 single PBSAC | | 2 mm PBSAC layer | |
|---------------|-----------------------|-------------|------------------|-----------------------|
| | External surface area | Volume | Number of PBSAC | External surface area |
| μm | mm^2 | mL | – | m^2 |
| 80 | 0.019 | 2.5E-07 | 1.6E+07 | 0.306 |
| 200 | 0.126 | 4.2E-06 | 9.5E+05 | 0.119 |
| 375 | 0.442 | 2.8E-05 | 1.4E+05 | 0.064 |
| 470 | 0.694 | 5.4E-05 | 7.3E+04 | 0.051 |
| 580 | 1.057 | 1.0E-04 | 3.9E+04 | 0.041 |
| 640 | 1.287 | 1.4E-04 | 2.9E+04 | 0.037 |

3.3.2 Influence of PBSAC diameter on the dynamic adsorption of E2

The first materials characteristic investigated is the diameter of PBSAC in the layer and, as a consequence, the external surface area. For this purpose, dynamic adsorption experiments were carried for decreasing PBSAC size at two fluxes (100 and 400 L m⁻² h⁻¹) and a layer thickness of 2 mm. The removal, uptake and permeate concentration of E2 are plotted as a function of PBSAC size in Fig. 3.3(AB&C) and correspondent external surface area in Fig. 3.3DE&F).

Fig. 3.3A shows that decreasing the diameter of PBSAC increases the removal of E2. Removal increases from 89 to 99 % at 100 L m⁻² h⁻¹ and 71 to 97 % at 400 L m⁻² h⁻¹ with decreasing particle diameter from 640 to 80 μm . The influence of diameter (and external surface area) is more pronounced at the high flux. This is likely a consequence of the shorter residence time occurring at the higher flux (EBCT of only 18 s). In these conditions, the overall adsorption kinetics is more limited and the improvement brought by using smaller PBSAC is more evident.

The uptake (Fig. 3.3B) follows a similar trend compared to the removal. However, the maximum uptake is observed for a PBSAC diameter of 200 μm and not for the smallest diameter of 80 μm . This is related to the fact that the mass of PBSAC in the layer is lower for P200 compared to P80 (Table 3.1). Focusing on the permeate concentration (Fig. 3.3C), it can be observed that the E2 can be reduced to a value close to the drinking water standard (1 ng L⁻¹) when the smallest PBSAC is used at a flux of 100 L m⁻² h⁻¹.

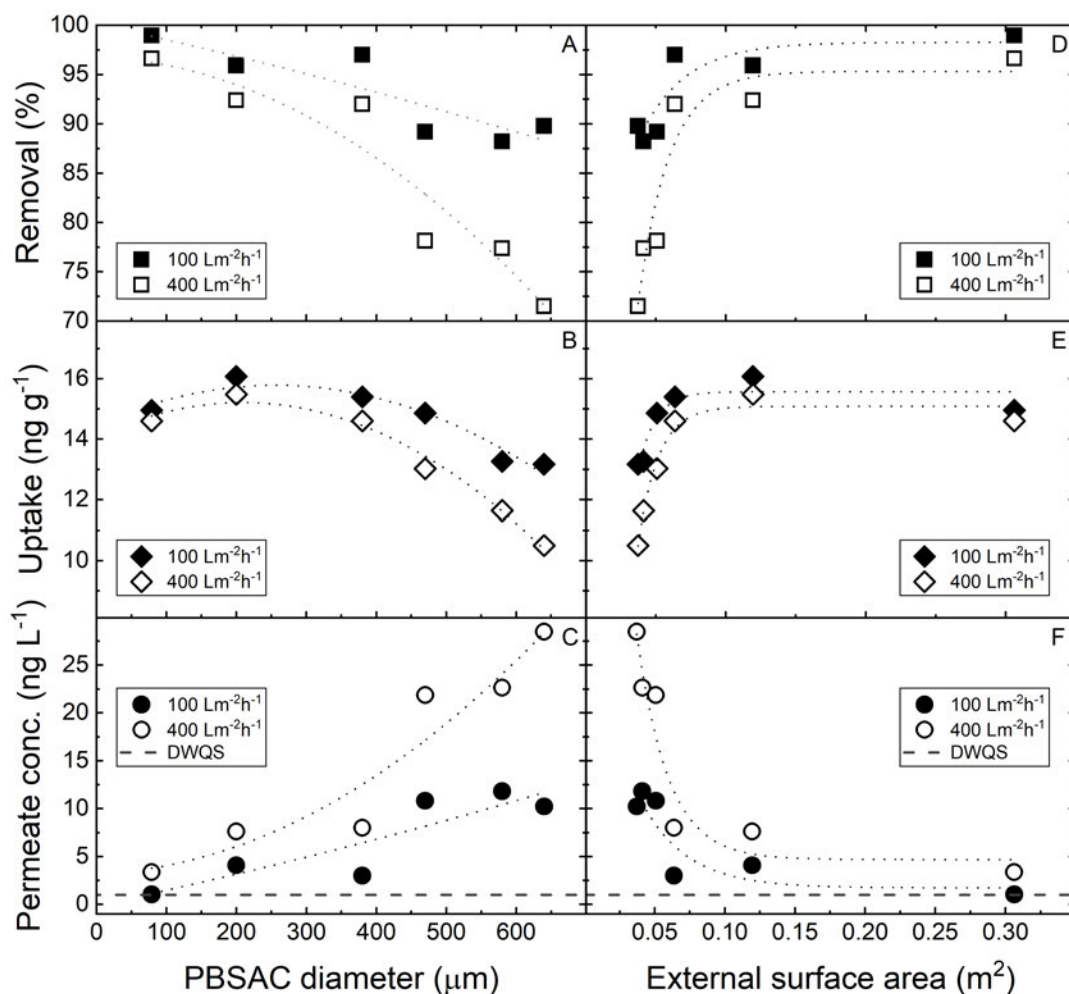


Figure 3.3: Removal, uptake and permeated concentration of E2 as a function of PBSAC size (A, B and C) and external surface area (D, E and F). Flux 100 and 400 L m⁻² h⁻¹. Feed concentration 100 ng L⁻¹. Temperature: 25 °C. Layer thickness: 2 mm. Mass of PBSAC in the layer reported in Table 3.1. The dashed line (C and F) represents the drinking water quality standard (DWQS). Adapted from [80].

3.3.3 Implication of PBSAC diameter on the required layer thickness

The main goal of the work is to achieve effective adsorption of hormones in a carbon layer as thin as possible. Thus, the required layer thickness to reach the drinking water (DW) standard was compared for three PBSAC diameters (80, 200 and 640 μm) as shown in Fig. 3.4.

E2 concentration can be reduced below the drinking water standard of 1 ng L⁻¹ for PBSAC diameters of 80 and 200 μm. The minimum thickness to meet the guideline is 4 mm and 6 mm for PBSAC diameter of 80 and 200 μm, respectively. In contrast, the guideline value cannot be reached with the large PBSAC particles (640 μm) even for a 6 mm layer. These results are extremely interesting and highlight the potential of the process presented in this work to address the issue of the estrogens in water. It is also worth to mention that the feed concentration of 100 ng L⁻¹ is an overestimation of the actual average concentration found in water (see Chapter 1).

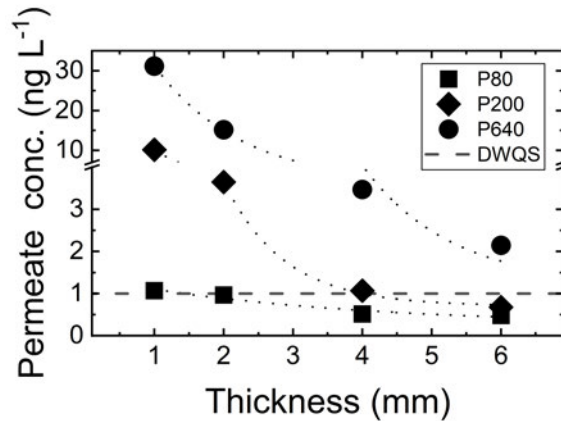


Figure 3.4: Permeate E2 concentration as a function of the layer thickness for different PBSAC diameters. Flux: $200 \text{ L m}^{-2} \text{ h}^{-1}$. The dashed line represents the drinking water quality standard (DWQS) for E2. Adapted from [80].

Thus, even lower PBSAC layer thickness should be enough to meet the DWQS at lower E2 concentrations in the feed.

In the following sections, the internal porous morphology of PBSAC and its influence on the adsorption of E2 is considered by varying the activation degree of PBSAC.

3.3.4 Considerations about the pressure drop in the UF-PBSAC

Decreasing the adsorbent size improves the adsorption kinetics, but it also has the drawback of increasing the pressure drop across the adsorbent bed. However, in the UF-PBSAC this drawback has no consequence for the overall process. As it was experimentally shown in Chapter 2, the overall process permeability in the UF-PBSAC is controlled by the UF membrane. In Appendix C.4 this issue is discussed in more details. The pressure drop in low pressure membranes is estimated from the membrane water permeability, while the one in a millimetric PBSAC layer is estimated using Carman-Kozeny relation. In this way, it can be shown that the PBSAC layer pressure drop is at least four orders of magnitude lower compared to low pressure membranes.

Focusing on the adsorbent layer only, it is worth underlying that the pressure drop increases also with the thickness of the packed-bed. Thus, a thin layer has a smaller pressure drop compared to a column. In particular, a layer of 10 mm thickness packed with the smallest PBSAC used ($80 \mu\text{m}$) is characterized by a pressure drop similar to a column packed with adsorbent with a size in the range 0.6-1 mm (Appendix C.4).

3.3.5 Characterization of the porous morphology of PBSAC at different activation

During the activation process, the porous structure inside the PBSAC particles is developed. Increasing the activation degree, the pore volume and specific surface area

increase as shown by the BET surface area provided by the manufacturer (Table 3.1). However, BET theory lacks of scientific basis to characterize microporous materials even if it is still largely used in the industry. For this reason, Argon adsorption data were measured and interpreted using a DFT-based model for carbon adsorbent rather than the BET model. Fig. 3.5 reports the pore volume and specific surface area of PBSAC predicted by the carbon DFT model using two different pore geometries: slit-like and a mixture of spherical and cylindrical pores.

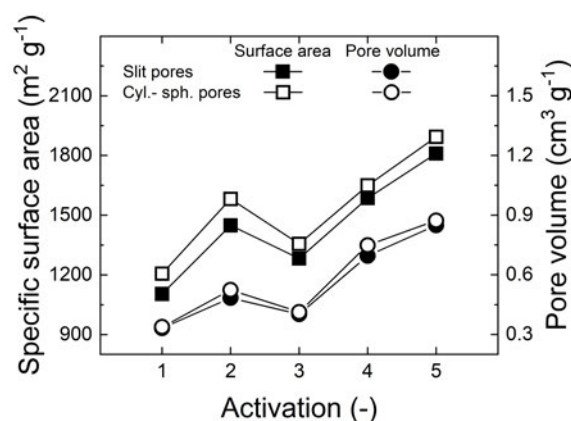


Figure 3.5: Specific surface area and pore volume of PBSAC predicted by the carbon DFT model (slit-like and a mixture of spherical and cylindrical pore shapes) as a function of activation degree. Adapted from [80].

Both pore geometry models predict an increase of the pore volume and surface area at increasing activation degree. The model based on slit pores predicts an increase of the specific surface area and the pore volume from $1103 \text{ m}^2 \text{ g}^{-1}$ and $0.331 \text{ cm}^3 \text{ g}^{-1}$ (A1) to $1810 \text{ m}^2 \text{ g}^{-1}$ and $0.849 \text{ cm}^3 \text{ g}^{-1}$ (A5), respectively. Using cylindrical pores geometry, the model predicts a specific surface increase from 1205 to $1893 \text{ m}^2 \text{ g}^{-1}$ and pore volume from 0.337 to $0.873 \text{ cm}^3 \text{ g}^{-1}$.

Considering that adsorption of MP occurs more efficiently in the smaller pores (micropores, $< 2 \text{ nm}$), the pore volume distribution is a factor that needs to be also taken into account. Fig. 3.6 reports the pore volume distribution of PBSAC samples at different activation.

The slit pores-based model performs better (see the fitting errors in Table 3.4) and predicts smaller pore width compared to the spherical/cylindrical pores one as shown in Fig. 3.6. In both cases, it can be noticed that increasing the activation, the pore volume distribution shifts to larger pores. The micropores volume and fraction of micropores compared to total pore volume was determined from Fig. 3.6 using the gadget function "integrate" in Origin Pro 2018b. The comparison is reported for both pore geometries in Table 3.4, which highlight that, at increasing activation (especially A4 and A5), the micropores fraction decreases. This is a sign that part of the micropores is broadened, creating pores larger than 2 nm for longer activation time. However, the predicted absolute micropores volume still increases at increasing activation from 0.331 to $0.789 \text{ cm}^3 \text{ g}^{-1}$ (slit-like pores model) and from 0.327 to $0.585 \text{ cm}^3 \text{ g}^{-1}$ (spherical-cylindrical pores model).

3.3. Results and discussion

Table 3.4: Predicted micropores volume and micropores fraction compared to the total pore volume for PBSAC samples with increasing activation. Fitting errors of the carbon DFT model and the two selected pore geometries are also reported. Adapted from [80].

| Sample | Slit-like pores | | | Spherical/Cylindrical pores | | |
|--------|-----------------------------------|--------------------------|--------------------|-----------------------------------|--------------------------|--------------------|
| | Micropore volume $cm^3 g^{-1}$ | Micropores fraction % | Fitting error % | Micropore volume $cm^3 g^{-1}$ | Micropores fraction % | Fitting error % |
| A1 | 0.331 | 100 | 0.14 | 0.327 | 97 | 0.51 |
| A2 | 0.464 | 96 | 0.08 | 0.502 | 96 | 0.40 |
| A3 | 0.393 | 98 | 0.07 | 0.400 | 97 | 0.39 |
| A4 | 0.605 | 87 | 0.26 | 0.628 | 84 | 0.40 |
| A5 | 0.798 | 94 | 0.23 | 0.585 | 67 | 0.64 |

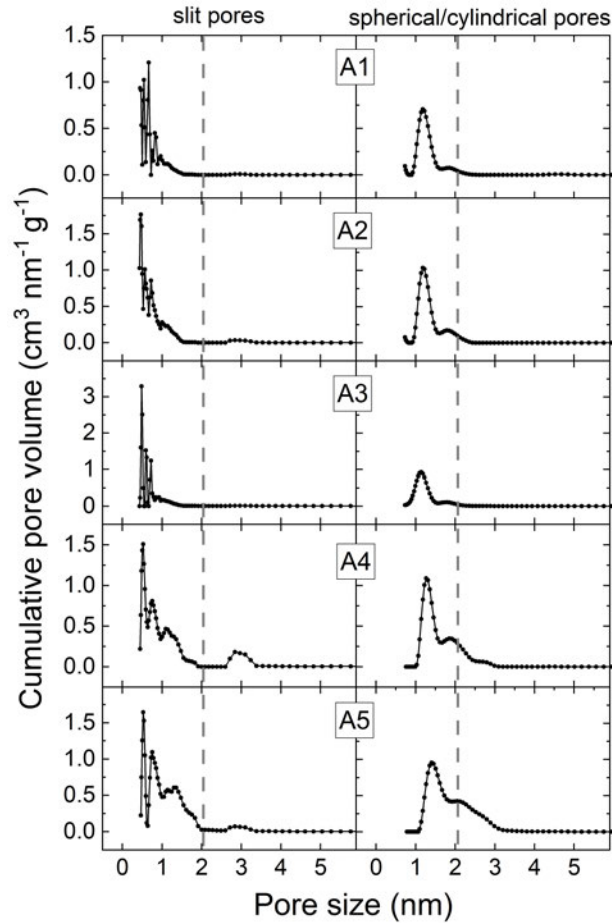


Figure 3.6: Pore size distributions for the PBSAC sample with different activation using two pore geometries for the carbon DFT model. The dashed line represents the threshold between micro (< 2 nm) and mesopores (2-50 nm).

In the next section, the influence of activation degree (thus the porous morphology of PBSAC) on the dynamic adsorption of E2 is investigated for a 2 mm thick PBSAC packed-layer. Considering the mass of PBSAC in the layer (Table 3.1) and the micropores volume of each sample (Table 3.4), it can be calculated (Eq. (3.8)) that

increasing the activation degree translates in an increase of the micropores volume in the layer from 1.7 to 2.6 cm³.

Micropore volume in 2 mm layer =

$$\text{Specific micropore volume} \cdot \text{Mass of PBSAC in the layer} \quad (3.8)$$

3.3.6 Influence of the activation degree on the dynamic adsorption of E2

The removal, uptake and permeate concentration of E2 are plotted as a function of activation degree in Fig. 3.7A&B&C and correspondent micropores volume in the layer in Fig. 3.7D&E&F.

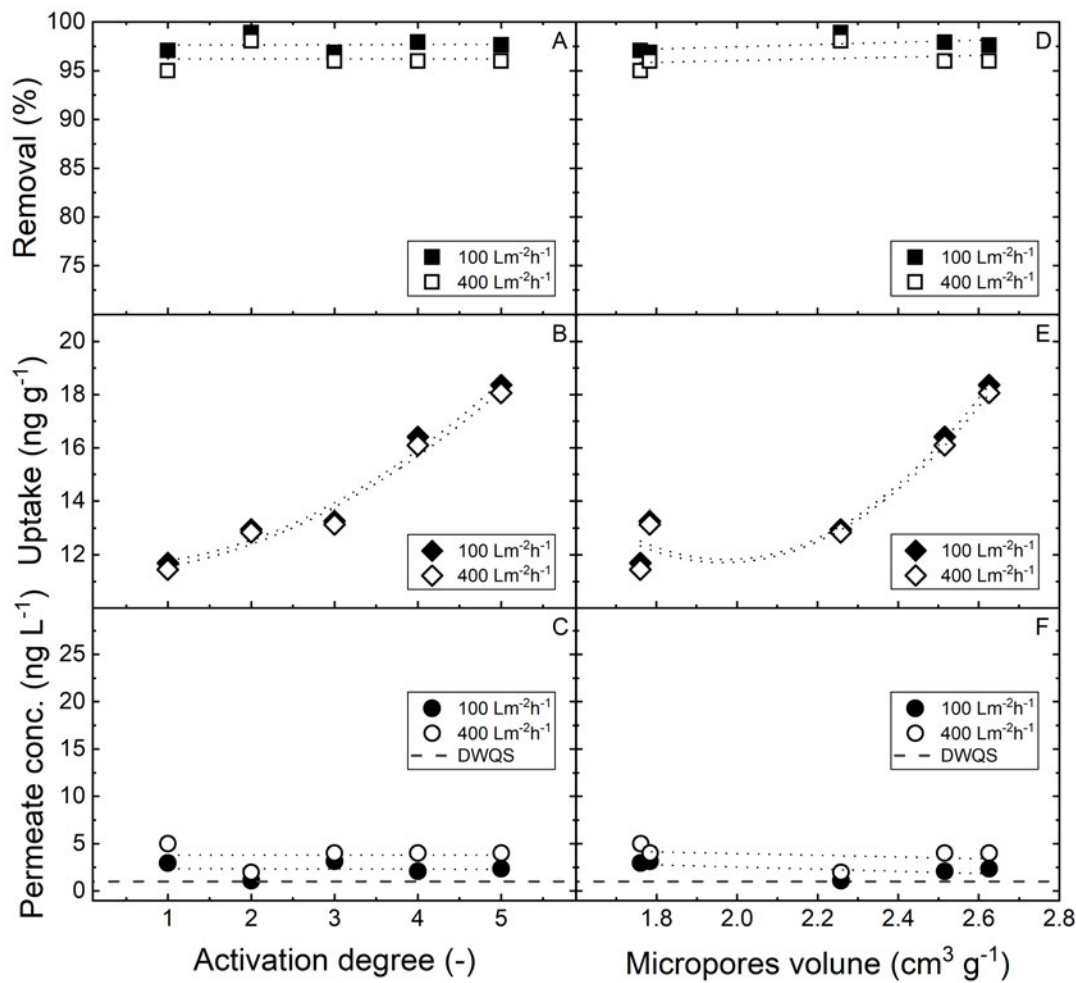


Figure 3.7: Removal, uptake and permeated concentration of E2 as a function of PBSAC activation (A, B and C) and total volume of micropores in the layer (D, E and F). Flux 100 and 400 L m⁻² h⁻¹. Feed concentration: 100 ng L⁻¹. Temperature: 25 °C. Layer thickness: 2 mm. Mass of PBSAC in the layer reported in Table 3.1. The dashed line (C and F) represents the drinking water quality standard (DWQS). Adapted from [80].

The permeate concentration and, as a consequence, the removal are not affected by the activation degree at both fluxes (Fig. 3.7A&C). On the other hand, the uptake increases with the activation degree. This is related to the lower mass of PBSAC

present in the layer at increasing activation degree. Indeed, the mass of PBSAC in the layer decreases from 5.32 g for activation 1 to 3.29 g for activation 5 as previously reported in Table 3.1. Considering that the mass of E2 adsorbed depends only on the removal and is really similar for the different activation levels, the specific mass adsorbed (uptake) increases at decreasing mass of PBSAC in the layer (Eq. (3.5)).

The porous morphology and the surface area are usually critical parameters in AC adsorption. The lack of an influence shown in Fig. 3.7 is interesting. It is likely related to the experimental conditions used in this work. First, the concentration of pollutants is low, and, second, the dynamic adsorption experiments are carried out for a relatively short time. These conditions result in the constant permeate concentration profile (or breakthrough curve) already shown in Chapter 2 (e.g., Fig. 2.9A). As a preliminary conclusion, the results about the influence of PBSAC size (or external surface area) and PBSAC activation (internal surface area) suggest that the initial breakthrough curve is completely determined by the size of the adsorbent and not by its internal porous morphology.

A more rigorous understanding of the mass transport regime in the layer will be the goal of Chapter 4. However, these results allow anticipating some considerations about the relevance of the different mass transport mechanisms in the dynamic adsorption of MP in the thin layer. The models to describe adsorption in a packed-bed typically consider the following mechanisms: convection (and possibly dispersion) in the bulk phase, film diffusion through the boundary layer around the adsorbent and pore diffusion inside the adsorbent. The adsorbent characteristics that determine film diffusion is the size, while the porous morphology determines pore diffusion. Thus, the experimental evidence that the PBSAC size is more important than its activation degree (Fig. 3.3 and Fig. 3.7) suggests that the film diffusion mechanism controls the overall adsorption kinetics of E2 in a thin PBSAC layer. This confirms the findings reported many years ago by some authors (Cornell and Fetting), who stated that the initial part of the breakthrough in an AC-MP process is determined by film diffusion only [49].

While the activation of PBSAC did not influence the initial E2 removal, it is expected to play a role in a hypothetical real process where the filtration process is carried on for a much longer time. For this reason, the next section deals with the expected influence of PBSAC activation on the lifetime (or breakthrough time) of the layer, which was estimated based on MB maximum uptake.

3.3.7 Implication of PBSAC activation on the expected lifetime of the layer

As in Chapter 2, MB was used as an indicator of the maximum uptake achievable on PBSAC with different activation. The adsorption isotherms of MB for increasing PBSAC activation are reported in Fig. 3.8.

Fig. 3.8 shows that the adsorption isotherm, and, as a consequence, the maximum uptake of MB is significantly affected by the activation degree of PBSAC. Maximum

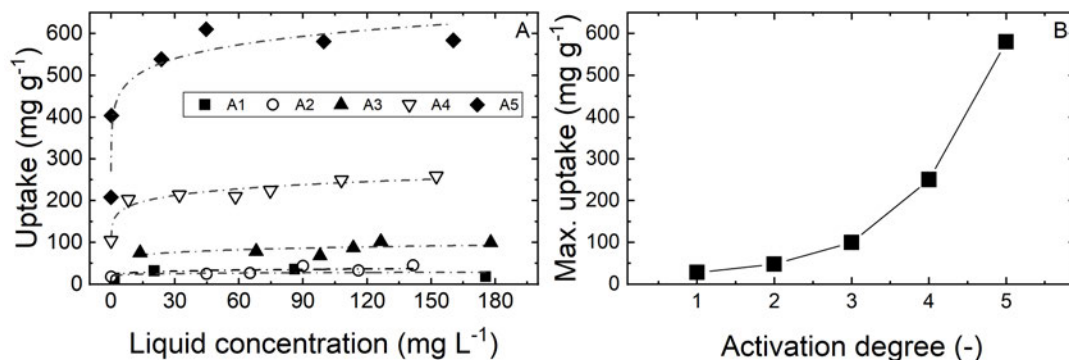


Figure 3.8: (A) Adsorption isotherms (obtained in static adsorption experiments) of MB for PBSAC with different activation degrees; (B) Maximum experimental uptake achieved as a function of activation degree. Temperature 20 °C. Equilibrium time: 120 h.

MB uptake achievable increases from around 30 mg g⁻¹ for activation 1 to more than 500 mg g⁻¹ for activation 5.

The implication of the significant different maximum uptake for different activation degree is that PBSAC layers composed of low-activation particles are expected to have a lower lifetime (saturation time). The volume of contaminated water that could be treated before saturation occurs was estimated at different activation following the same procedure reported in 2 (2.3.5). In Table 3.5, the estimated treatable volumes for a layer with different PBSAC activation are reported. The volume decreases from ~ 500 to ~ 40 m³ cm⁻². Again, these values represent a rough estimation due to the many and, in some cases, weak assumptions needed.

Table 3.5: Estimated volumes that can be treated by a layer made of PBSAC with different activation.

| Activation | — | 1 | 2 | 3 | 4 | 5 |
|---|---------------------------------|----|----|-----|-----|-----|
| Treatable volume | m ³ cm ⁻² | 40 | 70 | 140 | 300 | 500 |
| Percentage compared to the highest activation | % | 8 | 14 | 28 | 60 | 100 |

The last characteristic of PBSAC studied in this chapter is the surface chemistry. It was first characterized with XPS and the oxygen content of all samples quantified. The influence of the oxygen content was then assessed on the adsorption of the four hormones: E1, E2, P and T.

3.3.8 Characterization of PBSAC surface chemistry

The results from XPS indicate that PBSAC samples are exclusively composed of carbon (C 1s) and oxygen (O 1s) (Fig. 3.9Aa). The amount of oxygen was quantified in all the samples used in this work (Table 3.6). The atomic% ranges from 2.9 % to 8 % with an average of 5.2 %. The PBSAC samples where the oxygen was intentionally increased and decreased have an oxygen content of 9.1 % and 1.5 %, respectively.

3.3. Results and discussion

Table 3.6: Summary of the oxygen content of PBSAC samples used in this work.

| Sample | Oxygen content | Sample | Oxygen content | Sample | Oxygen content |
|--------|----------------|--------|----------------|---------------------|----------------|
| | % | | % | | % |
| P80 | 8 | A1 | 2.9 | P200 O ₊ | 9.1 |
| P200 | 5.7 | A2 | 3.7 | P200 O ₋ | 1.5 |
| P380 | 5.2 | A3 | 7.9 | | |
| P470 | 4.1 | A4 | 5.5 | | |
| P580 | 4.8 | A5 | 5.3 | | |
| P640 | 5.3 | | | | |

Survey XPS, oxygen (O1s) and carbon (C1s) spectra for "standard", increased and decreased oxygen content are reported in Fig. 3.9.

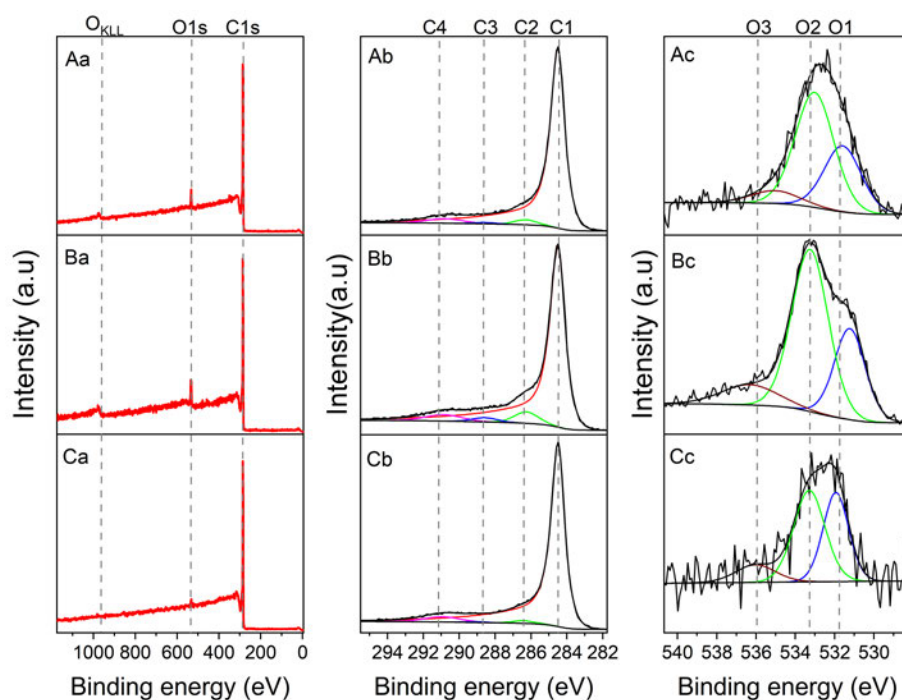


Figure 3.9: XPS spectra of carbon and oxygen for PBSAC with "standard" (A a-c), increased (B a-c) and decreased oxygen content (C a-c). Adapted from [80].

The carbon spectra are characterized by four distinct peaks that mainly correspond carbon from PBSAC. C1 peak with asymmetry shape and satellite (C4 peak) are the signature of the carbon structure of PBSAC whereas C2 and C3 are characteristic of the carbon bound to oxygen (e.g., carboxylic or hydroxyl groups). The asymmetric shape of C1 peak at 284.5 eV corresponds to the C-C environment with sp² hybridization, showing a graphitic character [120]. The other peak at 291 eV (C4) is attributed to π - π^* shake-up from unsaturated carbon of the C=C double bond

[121]. The C2 peak at 286.5 eV is assigned to the C-O environment and the peak C3 at 288.6 eV corresponds to O-C=O environment. O 1s spectra (Fig. 3.9c) show three peaks from all oxygenated species present at the surface. A characteristic O 1s peak is observed at 531.6 eV, which corresponds to the C=O environment of oxygen. The two others peaks, one at 533.2 eV, is attributed to the C-O-C environment of oxygen and another one at 535.8 eV, indicating the presence of water molecules adsorbed (narrow component) [122].

In summary, oxygen is the only heteroatom (apart from carbon) detected on PBSAC confirming a previous work [54]. The dynamic adsorption of E1, E2, T, P is now investigated for three oxygen level: 4.1 % ("standard" PBSAC), 9.1 % (oxygen rich PBSAC) and 1.5 % (oxygen poor PBSAC).

3.3.9 Influence of oxygen content of the adsorption of hormones

The removal and the permeate concentration of E1, E2, T and P in dynamic adsorption experiments are shown in Fig. 3.10 as a function of oxygen content. The error bars shown in the graph were derived from a triplicate in one selected experimental condition (using oxygen rich PBSAC and E2, reported in Appendix B.2, Fig. B.2). These are the conditions that results in the lowest permeate concentration. Thus, the error is expected to be the highest because of the highest contribution of analytical error (at the lowest concentration, see Fig. 3.2).

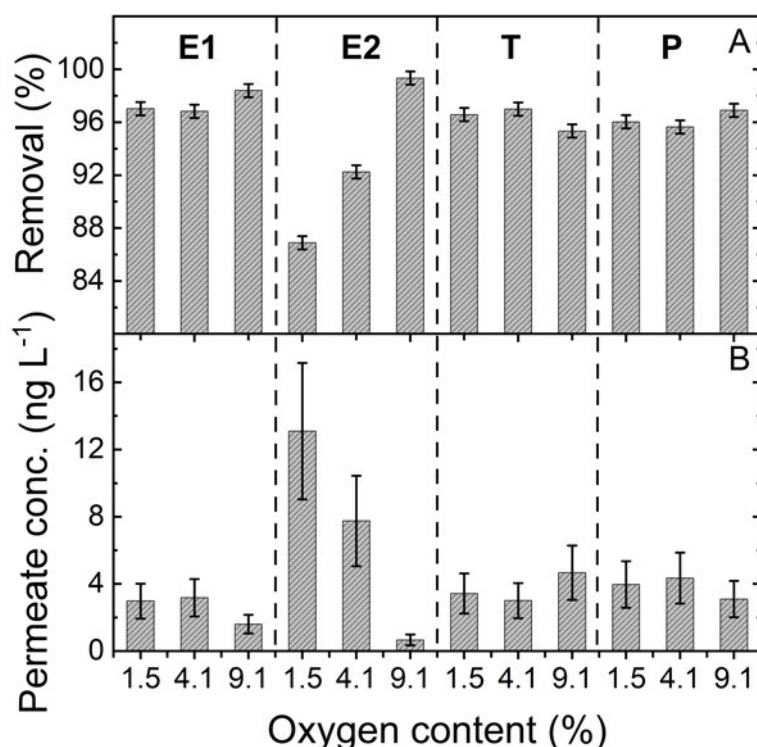


Figure 3.10: Removal (A) and permeate concentration (B) of E1, E2, P, T (for a permeate volume of 600 mL) for three PBSAC oxygen content. Filtration at a flux of $400 \text{ L m}^{-2} \text{ h}^{-1}$ (EBCT: 18 s). Temperature: $26 \text{ }^\circ\text{C}$. Feed hormone concentration: 100 ng L^{-1} . Adapted from [80].

3.3. Results and discussion

Fig. 3.10 shows that a significant influence of oxygen is observed only for E2. The removal decreases from 99 % (for an O content of 9.1 %) to 86 % (for an O content of 1.5 %). Also, it can be noticed that the removal of E1, T and P is higher compared to E2 at a "standard" O content of 4.1 %. No clear trend on the influence of oxygen is observable for E1, T and P. This may be because the removal is higher than 96 % and hence so high that oxygen influence cannot be observed even at a flux of $400 \text{ L m}^{-2} \text{ h}^{-1}$.

Further, static adsorption kinetics experiments were carried out for the four hormones and the two extreme oxygen contents (1.5 % and 9.1 %) to clarify its influence. The decrease in relative concentration and the corresponding increase in the uptake of hormones as a function of time are shown in Fig. 3.11. The pseudo-first order model was applied to quantify the increase or decrease in the adsorption kinetics.

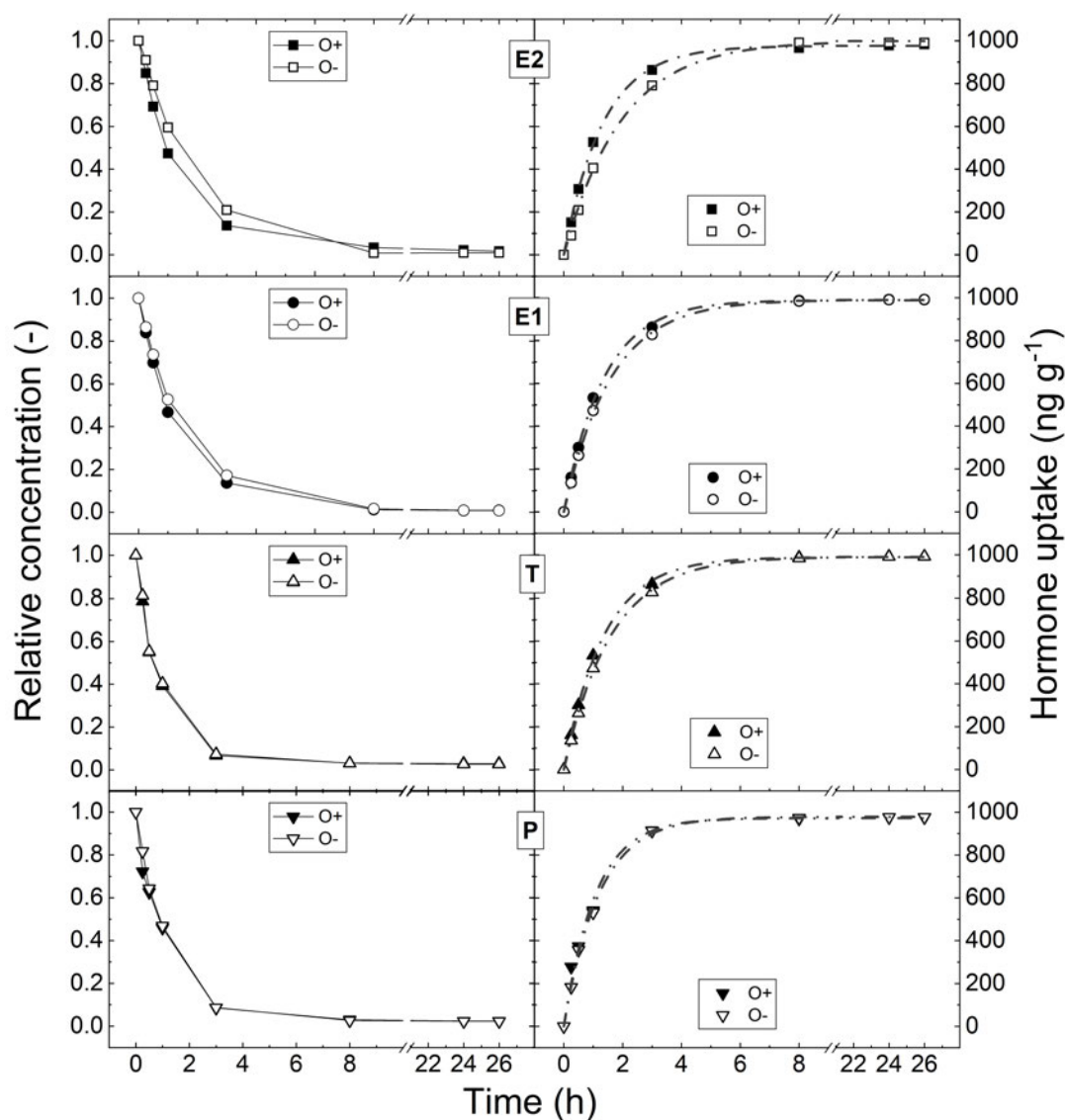
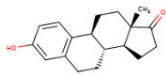
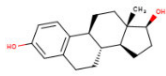
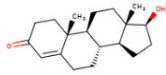
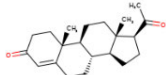


Figure 3.11: Relative concentration and uptake by PBSAC of steroid MPs during static adsorption experiments. PBSAC concentration 0.1 g L^{-1} . MP feed concentration: 100 ng L^{-1} . Pseudo-first order model (dash dot lines) was applied to have quantitative value for the kinetics rate

For all the four hormones, the removal at equilibrium (contact time of 26 h) is not significantly affected by O content (Fig. 3.11). On the contrary, in some cases, the rate of concentration decrease is affected by the oxygen content. This effect can be more clearly noticed by looking at the pseudo-first order kinetics constant (Table 3.7). Focusing on the difference in the adsorption kinetics constant between high and low oxygen content, the difference follows the trend $E2 > E1 \sim T > P$. This trend is in accordance with the OH bonding potential of the four hormones ($E2 > E1 = T > P$) also reported in Table 3.7. The formation of H bonds between the hydroxyl groups of the hormones and the oxygen species on the PBSAC surface may lead to an adsorption kinetics enhancement for E2 (and moderately for E1 and T). This hypothesis would be consistent also with the results of dynamic adsorption experiments in Fig. 3.10.

Table 3.7: Steroid hormones structure, H-bond forming potential and pseudo-first order adsorption kinetics constant at high and low PBSAC oxygen content (estimated in the static adsorption experiments reported in Fig. 3.11. Adapted from [80].

| Hormone | Structure | H bond acceptor donor counts | Kinetics constant (h^{-1}) | |
|---------|---|------------------------------------|--------------------------------|------------|
| | | | %O = 9.1 % | %O = 1.5 % |
| E1 |  | 1 / 2 | 0.73 | 0.62 |
| E2 |  | 2 / 2 | 0.75 | 0.50 |
| T |  | 1 / 2 | 0.94 | 0.84 |
| P |  | 0 / 2 | 1.07 | 1.03 |

In summary, the surface chemistry revealed to be a parameter that can affect the adsorption kinetics, although never reported in previous studies. In the thin layer adsorption approach, increased oxygen could be exploited to improve the adsorption process for some specific compounds (containing OH groups). Similarly to the PBSAC diameter, an improved adsorption process translates into the possibility to achieve the target pollutant permeate concentration at a reduced PBSAC layer thickness (Fig. 3.12).

The hypothesis proposed is that the adsorption rate (rather than the mass transport rate) was improved due to hydrogen bonding interactions between the carbon surface and the hydroxyl group present on E2. However, a conclusive statement on this hypothesis can not be drawn due to the limited experimental evidence obtained. Target studies of the surface chemistry influence on the adsorption of different micropollutants are needed to elucidate the potential of the surface chemistry modification.

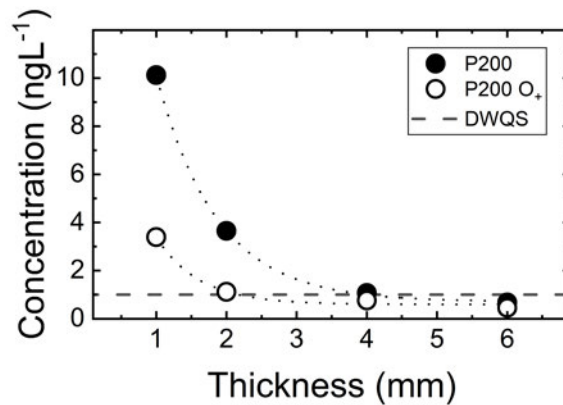


Figure 3.12: Permeate E2 concentration as a function of the layer thickness for different PBSAC diameters. Flux: $200 \text{ L m}^{-2} \text{ h}^{-1}$. The dashed line represents the drinking water quality standard (DWQS) for E2. Adapted from [80].

3.4 Conclusions

- The systematic investigation of the material characteristics has been successfully carried out, bringing to a significant improvement of the adsorption process in the thin layer.
- Smaller PBSAC translates into a larger external surface area available for immediate adsorption. E2 removal increases from 89 to 99 % at $100 \text{ L m}^{-2} \text{ h}^{-1}$ and from 71 to 97 % at $400 \text{ L m}^{-2} \text{ h}^{-1}$ by decreasing the diameter of PBSAC from 640 to 80 μm .
- The use of smaller PBSAC has significant implications on the required PBSAC layer thickness to meet the proposed drinking water level for E2. Indeed, this target can be safely achieved with a layer of 2 and 4 mm for PBSAC diameters of 80 and 200 μm , respectively.
- PBSAC with a higher activation degree is characterized by larger surface areas and pore volumes in the microporous range. However, the removal of E2 was not affected by the activation degree.
- The primary role of PBSAC compared to activation in determining the adsorption efficiency of E2 brings some highlights on the adsorption mechanism. The overall adsorption kinetics appears to be entirely controlled by the film diffusion mass transport (related to the external surface area) and not by the diffusion inside PBSAC (related to the porous morphology, thus the activation).
- The oxygen content of PBSAC also influenced the adsorption, in particular for E2 whose removal increased from 93 to 99 %, increasing the oxygen content from 4.1 to 9.1 atomic%.
- In summary, the performance of a millimetric PBSAC layer was significantly enhanced compared to Chapter 1. The UF-PBSAC was thus demonstrated to

be a technology that can compete in terms of estrogenic MP removal with high-pressure membranes and advanced oxidation processes.

Chapter 4

Modeling the adsorption of estradiol in the UF-PBSAC packed-layer

In the previous chapter, the size of PBSAC appeared to be the most critical factor determining the adsorption efficiency of estrogens, suggesting that the film (or external) mass transport is the dominant adsorption mechanism. The goal of this chapter is to clarify the adsorption mechanism of estrogens in the UF-PBSAC. A breakthrough model that can describe the transport and adsorption first in the UF and then in the PBSAC packed-layer was formulated. The UF, with negligible adsorption towards estrogens, had no effect on the breakthrough curve in the UF-PBSAC. The mechanisms considered for the PBSAC layer are convection, axial dispersion and film mass transport, while diffusion inside the adsorbent can be neglected for the initial (constant permeate concentration) breakthrough. Axial dispersion in the PBSAC layer has been shown to be an important transport mechanism that can not be neglected when modeling the adsorption in a thin adsorbent layer. The empirical correlations available for estimating the axial dispersion coefficient (developed for packed-columns) are not applicable for a millimetric packed layer. The axial dispersion coefficient estimated via fitting of the experimental data resulted in being dependent on the ratio between packed-layer thickness and particle diameter (L/d_p). The values of this coefficient ranged from 0 (for a L/d_p lower than 3) up to $40 \text{ mm}^2\text{s}^{-1}$ (for a L/d_p of 75). These results help to clarify the adsorption mechanism, but further investigation is advised to clarify the role of dispersion and, ideally, to provide a way for calculating it a priori. This model can be useful to predict the minimum PBSAC layer thickness to meet a certain target level at varying feed concentrations.

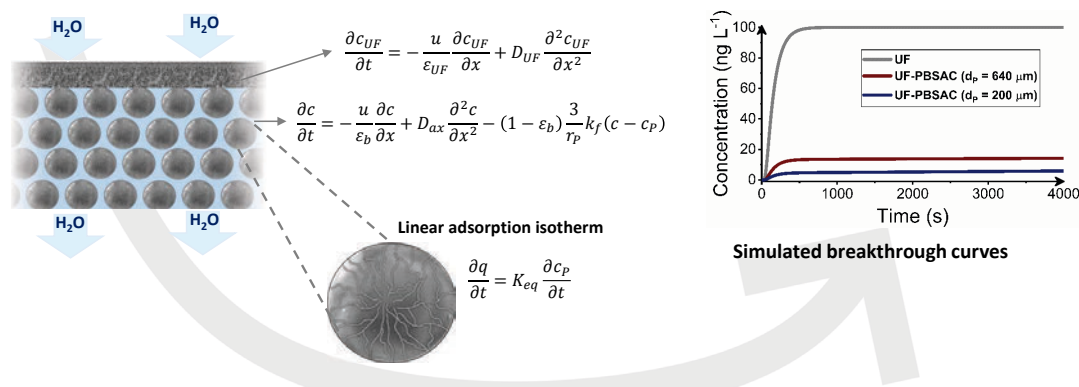


Figure 4.1: Graphical abstract of Chapter 5.

4.1 Introduction

Mathematical tools to predict the breakthrough of pollutants in a fixed-bed adsorber can be divided into scale-up methods and breakthrough curve (BTC) models. The most common scale-up method is the mass transfer zone (MTZ) model. Parameters obtained from the full breakthrough curves measured in the lab are used to design the full-scale adsorber [51]. This is not applicable in this case because no complete breakthrough could be measured in the laboratory, as discussed in the previous two chapters. On the other hand, complete breakthrough models allow a deeper insight into the mechanisms of the adsorption process. They consider both adsorption equilibrium (e.g. isotherm) and kinetics (mass transfer) [51, 123]. Complete BTC models consist of a material balance, an adsorption equilibrium and a set of equations that describe external (film diffusion) and eventually internal (pore diffusion) mass transport [123].

Typically, models to describe adsorption in a fixed-bed divide the volume of the adsorbent in bed (or inter-particle) porosity and adsorbent (intra-particle) porosity. In the bed porosity, the pollutant is transported by convection and axial dispersion. Further, the rate of pollutant transfer from the bed porosity to the adsorbent porosity is described by the film transport theory. Finally, diffusion of the pollutant inside the adsorbent can occur in the pore and/or on the solid surface. For activated carbon (AC) processes, the most used model is the homogeneous surface diffusion model (HSDM) [123–125]. In the HSDM, the adsorbent is considered a homogeneous medium (e.g., does not consider the adsorbent porosity) and transport of pollutants from the external surface to the center of the adsorbent occurs by surface diffusion. The other assumptions that need to be valid for this model are: (i) isothermal process; (ii) no concentration gradient in the radial direction (of the bed); (iii) constant superficial velocity of the water.

When modeling the BTC of a fixed-bed adsorption process, the so-called "system dispersion" needs to be taken into account [126]. Typically, system dispersion is related to the dead-volume present in the filtration system (e.g., pump, tubing, fittings). In the case of PBSAC, the membrane is also present before the PBSAC packed-layer. Considering that some UF membranes can adsorb estrogens, they may also influence the overall BTC in the UF-PBSAC. Some examples of modeling adsorptive membranes can be found in the literature [126, 127]. Typically, film transport is neglected and the main transport mechanisms involved are convection and dispersion in the porous fraction of the membrane. Similarly to fixed-bed, the transport equations need to be completed with an equilibrium relationship that relates the liquid concentration of the pollutant in the bulk phase to the adsorbed one (e.g. an adsorption isotherm).

Beyond giving insight into the mechanism, a validated model could be relevant

for practical application in that it can assist the design of a treatment unit for hormone removal. Selection of the PBSAC size and thickness be made without laborious experimental optimization depending on the quality of the water to treat and the target concentration to achieve in the permeate.

In summary, this chapter aims to develop a model that can describe the transport-adsorption of estradiol (E2) in a millimetric PBSAC layer coupled with ultrafiltration (UF). Validation of this model is carried out using PBSAC of different sizes and a non-adsorbing UF. Since saturation of PBSAC could not be achieved experimentally, model validation will focus on the initial (constant permeate concentration) BTCs obtained in the previous chapter. In the next section, the mechanisms that might be relevant in the transport-adsorption of E2 in the PBSAC layer will be critically discussed. In particular, the goal of the next section is (i) understand which transport mechanisms can be neglected for the case under investigation (adsorption of trace pollutants in a millimetric packed-bed) and (ii) understand which of the transport mechanisms are likely to be affected by the use of a millimetric packed-bed rather than a conventional column.

4.2 Analysis of transport/adsorption mechanisms in the UF-PBSAC

In the layer (or interparticle porosity), the relevant transport mechanisms are convection and axial dispersion. At the PBSAC particle boundary, the pollutant is transported inside PBSAC by film diffusion. Finally, the diffusion in the solid adsorbent is taking place. As introduced, the most common model for AC adsorption (HSDM) considers the solid phase as homogeneous, and the surface (rather than pore) diffusion is assumed to be the dominant mechanism. A summary of the relevant transport mechanisms and the parameters associated is reported in Fig. 4.2.

The different transport mechanisms and, eventually, the empirical correlations proposed in the literature to determine the parameters associated are discussed in the following sections. In order to predict the BTC, the mass transport parameters involved needs to be estimated a priori. Accordingly, the empirical correlations available in the literature to estimate such parameters are presented. The main focus is on understanding if such correlations (developed for packed-bed columns) are applicable in a millimetric packed-layer case.

4.2.1 Film diffusion

The film diffusion mechanism describes the transfer of pollutants from the bulk phase to the external surface of the particle. The rate of transport is proportional to the concentration gradient between the bulk phase and particle surface concentration by means of a mass transport coefficient, k_f [51]. The coefficient k_f depends on the thickness of the boundary layer (σ) surrounding the particles, which, in turn,

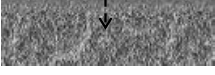
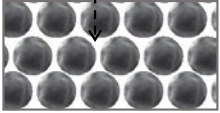
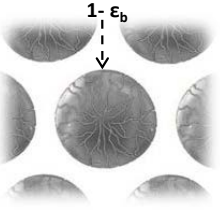
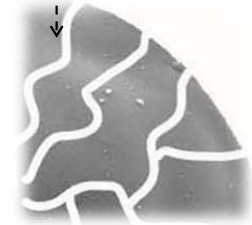
| Scale | Mechanisms | Parameters |
|--|--|--|
| <p>UF membrane</p> <p>c_{UF} : liquid concentration q_{UF} : adsorbed concentration ϵ_{UF} : UF porosity</p>  | <p><i>Convection</i></p> <p><i>Axial dispersion</i></p> <p><i>Adsorption</i></p> | <p>L_{UF} : thickness (mm)</p> <p>u : superficial velocity (mm s^{-1})</p> <p>D_{UF} : axial dispersion coefficient (mm^2s^{-1})</p> |
| <p>PBSAC layer</p> <p>c : concentration in the layer ϵ_b : layer (bed) porosity</p>  | <p><i>Convection</i></p> <p><i>Axial dispersion</i></p> | <p>L : thickness (mm)</p> <p>u : superficial velocity (mm s^{-1})</p> <p>D_{ax} : axial dispersion coefficient (mm^2s^{-1})</p> |
| <p>PBSAC-liquid interface</p>  | <p><i>Film (external) mass transfer</i></p> | <p>r_p : radius of PBSAC (mm)</p> <p>k_f : film mass transfer coefficient (mms^{-1})</p> |
| <p>PBSAC phase</p> <p>q : adsorbed concentration</p>  | <p><i>Adsorption</i></p> <p><i>Diffusion inside PBSAC</i></p> | <p>ρ_{app} : apparent PBSAC density</p> <p>D_s : surface diffusion coefficient (mm^2s^{-1})</p> <p>K_{eq} : linear distribution coefficient (-)</p> |

Figure 4.2: Main transport mechanisms and parameters relevant in modeling the adsorption process through the UF-PBSAC packed layer.

depends on the velocity of the bulk phase and the size of the adsorbent (PBSAC in this case) [51]. The boundary layer thickness is reduced at a higher flow rate and for smaller particle sizes. It results that film transport is faster for smaller particle diameter. In contrast, k_f does not depend on the thickness of the adsorbent bed and should not be affected by the peculiar thin layer investigated in this work. Besides, k_f also depends on the molecular diffusion coefficient (D_m) of the pollutant in water. Thus, it is a pollutant-specific parameter. k_f does not depend on the length of the packed-bed; thus, it should not be affected by the peculiar thin layer considered in this work.

Several correlations were proposed [128–130] to estimate k_f . A common procedure is to estimate the Sherwood number (Sh , Eq. (4.1)), which is related to k_f , as a function of Reynolds number (Re , Eq. (4.2)) and Schmidt number (Sc , Eq. (4.3)):

$$Sh = \frac{k_f d_p}{D_m} \quad (4.1)$$

$$Re = \frac{u d_p}{\varepsilon_b \nu} \quad (4.2)$$

$$Sc = \frac{\nu}{D_m} \quad (4.3)$$

where d_p is the diameter of the adsorbent particle, ε_b is the bed (e.g., inter-particle) porosity and ν is the kinematic viscosity. Units selection is arbitrary provided that Sh , Re and Sc results are dimensionless numbers.

Two correlations were selected because they were derived in a Re range applicable to this work Table 4.1.

Table 4.1: Selected correlations for the estimation of the film mass transfer coefficient and conditions of applicability.

| Correlation | Condition for validity | Validity in this work |
|--|---|---|
| $Sh = 1.85 \left(\frac{\varepsilon_b}{1 - \varepsilon_b} \right) Re^{1/3} Sc^{1/3} \quad (4.4)$ | [128] $Re \left(\frac{\varepsilon_b}{1 - \varepsilon_b} \right) < 100$ | $Re \left(\frac{\varepsilon_b}{1 - \varepsilon_b} \right) = 0.1 \text{ to } 0.7$ |
| $Sh = 2 + 1.85 Re^{0.4} Sc^{1/3} \quad (4.5)$ | [129] $0.001 < Re < 5.8$ | $Re = 0.01 \text{ to } 0.1$ |

4.2.2 Diffusion inside PBSAC

PBSAC diffusion represents the transport of the target pollutant from the external surface to the inside of the particle. In the HSDM, the adsorbed concentration is assumed to be in equilibrium with the one in the liquid phase at the external surface of the adsorbent. A surface diffusion, D_s , is employed to describe the rate of surface diffusion along the internal surface of the particle. D_s depends on factors like temperature and molecular weight of the pollutant. Typical values of the diffusion coefficient range from $10^{-5} \text{ mm}^2 \text{ s}^{-1}$ for small molecules (e.g., MP) to $10^{-9} \text{ mm}^2 \text{ s}^{-1}$ for large molecules such as humic substances [51]. There are not reasons for which this diffusion mechanism should depend on the length of the adsorbent bed.

4.2.3 Relative importance of film transport and PBSAC diffusion

Film diffusion and diffusion inside the adsorbent are mechanisms occurring in series. If one of the two is at least one order of magnitude faster, it follows it can be neglected in the formulation of the model [51]. For the traditional process of adsorption of MP on activated carbon, pore diffusion cannot be neglected a priori [131]. Nevertheless, at the early stage of adsorption, when the permeate concentration is constant (as in the case of hormones-PBSAC), the breakthrough appears to be determined by film diffusion only [49] (see Fig. 4.3). This is because the adsorbed concentration of pollutants inside the particles is still really low. Further evidence about this hypothesis (that diffusion inside PBSAC is negligible) comes from the experimental results of Chapter 3. The breakthrough curves were shown to depend on the PBSAC size but not on the activation level (Fig. 3.3 and Fig. 3.7). At different activation, the PBSAC porous morphology (e.g., the particle porosity and the pore size distribution) changes but this was shown to have no effect on the BTC of E2. This behavior confirms that the initial adsorption of hormones is controlled by film transport and not by PBSAC diffusion.

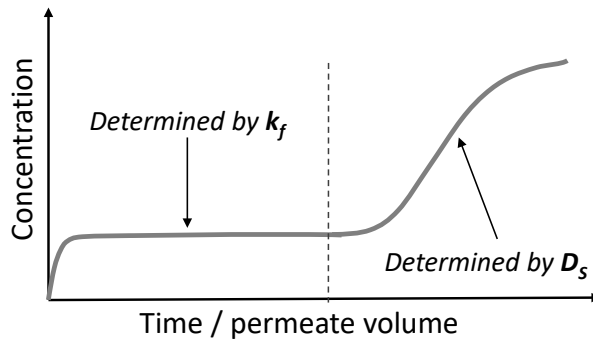


Figure 4.3: Example of the breakthrough curve shape for short-bed studies where the part determined by k_f and by D_s are highlighted.

4.2.4 Axial dispersion

Dispersion in packed-bed occurs due to "combined effects of molecular diffusion and convection in the spaces between particles" [132]. For activated carbon process, dispersion can sometimes be neglected [123], while it is typically included in other fixed-bed adsorption processes such as protein chromatography [133]. Empirical correlations for calculating the Peclet particle number (Pe_p , Eq. (4.6)) are available in the literature and allow to determine the axial dispersion coefficient (D_{ax}) [134].

$$Pe_p = \frac{u d_p}{D_{ax}} \quad (4.6)$$

These empirical correlations were developed measuring the dispersion of a tracer under the assumption of semi-infinite bed length [132, 134]. The correlation from

Gunn (Eq. (4.7)) [135] is the most used. The semi-infinite bed length assumption has been quantitatively formalized in different ways, as shown in Table 4.2 [132].

$$\frac{1}{Pe_p} = \frac{\varepsilon_b}{1.4 Re Sc} + \frac{Re Sc}{4 \alpha_1^2 (1 - \varepsilon_b)} (1 - p)^2 + \frac{Re^2 Sc^2}{16 \alpha_1^4 (1 - \varepsilon_b)^2} p (1 - p)^3 \left\{ \exp \left[-\frac{4 \alpha_1^2 (1 - \varepsilon_b)}{p (1 - p) Re Sc} \right] - 1 \right\} \quad (4.7)$$

where p and α_1 are constants.

Table 4.2: Conditions proposed in the literature for the validity of the axial dispersion coefficient estimated through empirical correlations.

| Condition for validity | Validity in this work |
|---|--|
| $\frac{L}{d_p} > 20$ (4.8) | $\frac{L}{d_p} = 2 \text{ to } 75$ |
| $\frac{L}{d_p} \gg Pe_p \left(\frac{\varepsilon_b}{1 - \varepsilon_b} \right)$ (4.9) | $Pe_p \left(\frac{\varepsilon_b}{1 - \varepsilon_b} \right) = 4 \text{ to } 38$ |

Thus, unlike film and PBSAC diffusion, the dispersion mechanism could be affected by the use of a thin absorbent layer. Carberry and Breton [136] investigating axial dispersion in fixed-bed concluded that: *"short-bed studies revealed unusually high dispersion coefficients, reflecting short-circuiting, that is, poor cell-mixing efficiencies in these shallow beds, presumably owing to entrance effects"*. The hypothesis was that this anomalously high dispersion might be related to the rapid acceleration of fluid upon entering a system restricting flow (packed bed). For a ration between bed thickness and particle diameter (L/d_p) of 50, dispersion coefficients up to $900 \text{ mm}^2 \text{ s}^{-1}$ were measured by these authors. In this chapter, the BTCs to be modeled are characterized by a L/d_p that varies from 1.5 to 75. As a consequence, the dispersive behavior of hormones in the PBSAC layer is expected to deviate compared to a conventional packed-bed column.

To understand the relevance of axial dispersion, model validation will be first carried out neglecting axial dispersion. Later the model including axial dispersion will be considered and D_{ax} will be determined by fitting the experimental BTCs with the theoretical model.

4.2.5 System dispersion

The BTCs measured using a certain filtration system maybe affected by the so-called "system dispersion". The presence of pumps, tubes and valves in any filtration system introduce dead volumes which can affect the actual BTC. Since the stirred-cell set-up (Section 2.2.5) has no pump, the main components that can cause system dispersion were assumed to be the permeate tube and porous stainless steel support layer. As discussed in more details in the Appendix D.1, system dispersion in the stirred-cell has a minor effect on the BTC and it will simply modeled as a delayed injection (to mimic the delay time caused by the permeate tube).

4.3 Model formulation

4.3.1 Mass balance in the UF membrane

The first step in the model formulation is to consider the transport and, eventually, adsorption of E2 in the UF membrane. A non-retaining membrane can be modeled as a dispersive porous medium characterized by a porosity ε_{UF} and a dispersion coefficient D_{UF} [126, 127]. A differential balance considering convection, dispersion and adsorption can be expressed as follows:

$$\varepsilon_{UF} \frac{\partial c_{UF}}{\partial t} = -\varepsilon_{UF} \frac{u}{\varepsilon_{UF}} \frac{\partial c_{UF}}{\partial x} + \varepsilon_{UF} D_{UF} \frac{\partial^2 c_{UF}}{\partial x^2} - (1 - \varepsilon_{UF}) \frac{\partial q_{UF}}{\partial t} \quad (4.10)$$

where c_{UF} and q_{UF} are the E2 concentration in liquid and adsorbed to the membrane, respectively.

The UF membrane used in the previous chapters had negligible adsorption for E2. Thus, the last term in Eq. (4.10) can be removed, and the balance in the UF reduces to:

$$\varepsilon_{UF} \frac{\partial c_{UF}}{\partial t} = -\varepsilon_{UF} \frac{u}{\varepsilon_{UF}} \frac{\partial c_{UF}}{\partial x} + \varepsilon_{UF} D_{UF} \frac{\partial^2 c_{UF}}{\partial x^2} \quad (4.11)$$

4.3.2 Mass balance in the PBSAC layer

The differential mass balance in the PBSAC layer bulk phase (ε_b) is obtained by considering that the accumulation term ($\partial c / \partial t$) is equal to the E2 transported by convection and axial dispersion, minus the solute entering the PBSAC phase ($1 - \varepsilon_b$) through film diffusion:

$$\varepsilon_b \frac{\partial c}{\partial t} = -\varepsilon_b \frac{u}{\varepsilon_b} \frac{\partial c}{\partial x} + \varepsilon_b D_{ax} \frac{\partial^2 c}{\partial x^2} - (1 - \varepsilon_b) \frac{6}{d_p} k_f (c - c_p) \quad (4.12)$$

where c and c_p are the concentration of E2 in bulk and inside the particle (see Fig. 4.2). The factor $6/d_p$ represents the external surface area per volume of a spherical particle.

The differential mass balance in the bulk phase needs to be completed with boundary conditions. In the case of negligible dispersion in the PBSAC layer, the Dirichlet boundary condition at the inlet can be used. It simply states that the concentration at $x = 0$ (inlet of the layer) is equal to the feed concentration entering the layer (in this case, it corresponds to the outlet of the UF membrane):

$$c(t, 0) = c_{UF} \quad (4.13)$$

On the other hand, for a dispersive packed-bed, Danckwerts [137] proposed that, as soon as the feed enters the bed, it will be diluted by axial mixing. So, it requires that the flow upstream the bed (no dispersion) needs to be equal to the flow at the entrance (determined both by convection and dispersion):

$$\frac{u}{\varepsilon_b} c_{UF} = \frac{u}{\varepsilon_b} c(t, 0) - D_{ax} \frac{\partial c}{\partial x} \quad (4.14)$$

In both cases, the outlet boundary condition requires that the concentration stops changing at the point where the flow leaves the bed:

$$\frac{\partial c(t, L)}{\partial x} = 0 \quad (4.15)$$

4.3.3 Mass balance in the PBSAC phase

An additional mass balance is performed in the PBSAC phase ($1 - \varepsilon_b$) assuming that diffusion in the PBSAC phase can be neglected. The accumulation ($\partial c_P / \partial t$) of the pollutant in the PBSAC phase ($1 - \varepsilon_b$) is equal to the flux entering the PBSAC phase through film diffusion and the pollutant adsorbed to the solid phase:

$$(1 - \varepsilon_b) \frac{dc_P}{dt} = (1 - \varepsilon_b) \frac{6}{d_p} k_f (c - c_P) - (1 - \varepsilon_b) \rho_{app} \frac{dq}{dt} \quad (4.16)$$

where ρ_{app} is the so-called apparent density, which is the density of PBSAC, including its intrinsic porosity. This equation (Eq. (4.16)) contains only derivatives with respect to time. So boundary conditions are not needed.

Finally, the adsorbed pollutant concentration is coupled with the adsorption isotherm. It was shown to be linear for the system E2-PBSAC in the experimental conditions used to obtain the breakthrough curves in Chapter 2 and Chapter 3:

$$\frac{\partial q}{\partial t} = K_{eq} \frac{\partial c_P}{\partial t} \quad (4.17)$$

To account for the delay time caused by the permeate tube (see Appendix D.1), a delay step injection will be implemented.

4.3.4 Solution of the model

The resulting models (neglecting and including axial dispersion in the PBSAC layer) are systems of partial differential equations (PDE) and an ordinary differential equation (ODE) (summarized in Eq. (4.18) and Eq. (4.19)). To solve such models, the procedure reported by Hahn [138] based on linear finite elements space discretization is used. The procedure is adapted to solve the models formulated. In particular, the UF dispersion step is introduced and the inlet concentration to the PBSAC layer is set to the outlet concentration of the UF membrane. Further, a linear adsorption isotherm is implemented in the balance in the solid phase (PBSAC here). More details are reported in Appendix D.2.

$$\left\{ \begin{array}{l}
 \text{Convection – film transport – adsorption} \\
 \frac{\partial c_{UF}}{\partial t} = -\frac{u}{\varepsilon_{UF}} \frac{\partial c_{UF}}{\partial x} + \frac{D_{UF}}{\varepsilon_{UF}} \frac{\partial^2 c_{UF}}{\partial x^2} \\
 \frac{\partial c}{\partial t} = -\frac{u}{\varepsilon_b} \frac{\partial c}{\partial x} + -\frac{(1-\varepsilon_b)}{\varepsilon_b} \frac{6}{d_p} k_f (c - c_P) \\
 \frac{\partial c_P}{\partial t} = \frac{6}{d_p} k_f (c - c_P) - \rho_{app} \frac{\partial q}{\partial t} \\
 \\
 \text{Initial condition} \\
 c_{UF} = c = c_P = 0 \quad \text{for } t = 0 \\
 \\
 \text{Boundary conditions} \\
 \frac{\partial c_{UF}}{\partial x} = \frac{u}{\varepsilon_{UF} D_{UF}} (c_{UF} - c_{feed}) \quad \text{for } x = 0 \\
 \frac{\partial c_{UF}}{\partial x} = 0 \quad \text{for } x = L_{UF} \\
 c = c_{UF} \quad \text{for } x = L_{UF} \\
 \frac{\partial c}{\partial x} = 0 \quad \text{for } x = L
 \end{array} \right. \quad (4.18)$$

$$\left. \begin{aligned}
 & \text{Convection – dispersion - film transport – adsorption} \\
 & \frac{\partial c_{UF}}{\partial t} = -\frac{u}{\varepsilon_{UF}} \frac{\partial c_{UF}}{\partial x} + \frac{D_{UF}}{\varepsilon_{UF}} \frac{\partial^2 c_{UF}}{\partial x^2} \\
 & \frac{\partial c}{\partial t} = -\frac{u}{\varepsilon_b} \frac{\partial c}{\partial x} + D_{ax} \frac{\partial^2 c}{\partial x^2} - \frac{(1 - \varepsilon_b)}{\varepsilon_b} \frac{6}{d_p} k_f (c - c_p) \\
 & \frac{\partial c_p}{\partial t} = \frac{6}{d_p} k_f (c - c_p) - \rho_{app} \frac{\partial q}{\partial t} \\
 \\
 & \text{Initial condition} \\
 & c_{UF} = c = c_p = 0 \quad \text{for } t = 0 \\
 \\
 & \text{Boundary conditions} \\
 & \frac{\partial c_{UF}}{\partial x} = \frac{u}{\varepsilon_{UF} D_{UF}} (c_{UF} - c_{feed}) \quad \text{for } x = 0 \\
 & \frac{\partial c_{UF}}{\partial x} = 0 \quad \text{for } x = L_{UF} \\
 & \frac{\partial c}{\partial x} = \frac{u}{\varepsilon_b D_{ax}} (c - c_{feed}) \quad \text{for } x = L_{UF} \\
 & \frac{\partial c}{\partial x} = 0 \quad \text{for } x = L
 \end{aligned} \right\} \quad (4.19)$$

4.4 Experimental methodology

The experimental BTCs used to validate the proposed model were obtained in the previous chapter using the stirred-cell filtration set-up and the filtration protocol previously described (Section 2.2.5 and Section 2.2.7, respectively). In particular, the BTCs for three PBSAC sizes (80, 200 and 640 μm), a flux of 200 $\text{L m}^{-2} \text{h}^{-1}$ and a PBSAC layer thickness from 1 to 6 mm are considered in this chapter (note the the final permeate concentration of these BTCs are reported in Fig. 3.4).

The adsorption isotherms of E2 on PBSAC samples with different PBSAC diameters (80, 200 and 640 μm) are obtained in batch conditions. For one PBSAC diameter (200 μm), two PBSAC concentrations (0.5 and 1 g L^{-1}) are used. For PBSAC with diameter of 80 and 640 μm , only one PBSAC concentration is used (1 g L^{-1}). The protocol to obtain the adsorption isotherms is the following: for each PBSAC diameter (i) five E2 concentrations (10, 30, 60, 100 and 150 ng L^{-1}) are prepared; (ii) the amount of PBSAC to reach the desired concentration is poured inside the flask; (iii) the concentration of E2 in each flask is measured before addition of PBSAC and after a contact time of 26 h. Finally, the E2 uptake is calculated in the same way as described for methylene blue in Chapter 2 (Eq. (2.2)).

4.5 Parameters determination

The parameters in the model presented that are fixed or measured are the thickness of the layer (L : 1 to 6 mm), the PBSAC diameter (d_p : 80, 200 and 640 μm), the superficial velocity (u : 0.056 mm s⁻¹) and the feed concentration ($c_{feed} \approx 100 \text{ ng L}^{-1}$). The remaining input parameters need to be assumed or estimated from the empirical correlations. These parameters are the porosity of the layer (ε_b), the apparent density of PBSAC (ρ_{app}), the mass transfer parameters (k_f , and D_{ax}). Finally, the adsorption equilibrium parameters can be determined from static adsorption experiments.

4.5.1 Layer porosity and apparent PBSAC density

PBSAC particles are packed in the layer in the same way as it occurs when the tap density (ρ_{tap}) is measured (in practice, the layer porosity is assumed to be the same achieved in the tapping process to measure ρ_{tap}). The layer porosity (ε_b) is assumed to be 0.4. This value is close to the maximum random packing density achievable for a constant radius sphere [139].

The apparent PBSAC density (e.g., including the intrinsic porosity) can be related to ρ_{tap} through a mass balance on the volume of a PBSAC layer, as shown in Fig. 4.4 and Eq. (4.21):

$$\rho_{tap} = (1 - \varepsilon_b) \rho_{app} = (1 - \varepsilon_b) \varepsilon_{PBSAC} \rho_{carbon} \quad (4.20)$$

$$\rho_{app} = \frac{\rho_{tap}}{(1 - \varepsilon_b)} \quad (4.21)$$

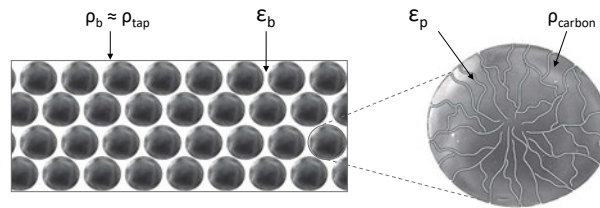


Figure 4.4: Relation between the density of the PBSAC bed and the apparent density of PBSAC.

Three PBSAC samples of different diameters (80, 200 and 640 μm) are used for the validation of the model on the experimental BTCs. These samples are characterized by an activation level of 4, corresponding to a tap density in the range 598-617 g L⁻¹ (see Table 3.1 in Chapter 3). The apparent density is 1028, 1003 and 997 g L⁻¹ for PBSAC of diameter 80, 200 and 640 μm .

4.5.2 E2 adsorption isotherms

The linear distribution coefficient (also called Henry constant), K_{eq} , is determined from adsorption isotherms of E2 on the three PBSAC samples in static adsorption experiments at 25°C. The adsorption isotherms of E2 on PBSAC with a diameter of 200 μm at two different adsorbent concentrations are shown in Fig. 4.5A. It can be noticed that the slope of the linear isotherm is different at the two PBSAC concentrations. In addition, this slope has the dimension of $(\text{ng g}^{-1})(\text{ng L}^{-1})^{-1}$.

The linear distribution coefficient to use as input for the model should be independent of the PBSAC concentration and dimensionless [140, 141]. In contrast, when the mass of E2 in the solid as a function of the one remaining in the liquid phase at equilibrium is considered, the adsorption isotherm is independent of the adsorbent concentration (Fig. 4.6B). In this way, a dimensionless linear distribution coefficient can be obtained [142].

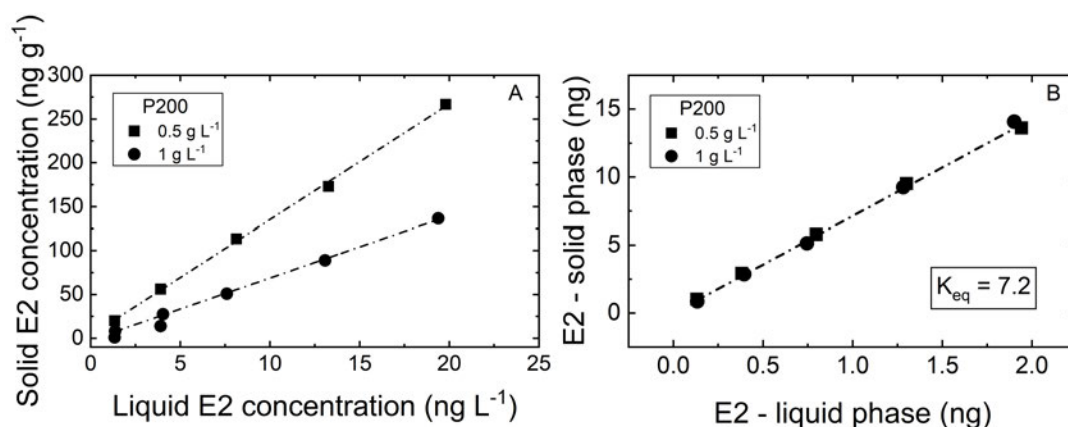


Figure 4.5: Concentration (A) and mass (B) of E2 in the solid phase (PBSAC) as a function of concentration (A) and mass (B) in the liquid phase at equilibrium. Temperature: 25 °C. PBSAC diameter: 200 μm .

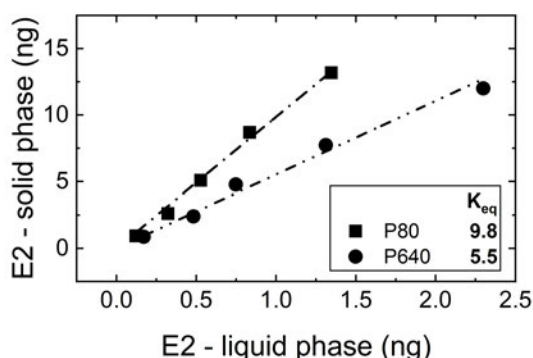


Figure 4.6: Mass of E2 in the solid phase (PBSAC) as a function of mass of E2 remaining the liquid phase at equilibrium for PBSAC with diameters 80 and 640 μm . Temperature: 25 °C. PBSAC conc. of 0.5 g L⁻¹.

4.5.3 Mass transport parameters

The mass transport parameters involved, namely k_f and D_{ax} , were initially estimated using empirical correlations. For the film transport coefficient, the correlation proposed by Ohashi *et al.* [129] was used. The particles Reynolds and Schmidt number are first determined from Eq. (4.11) and Eq. (4.12), then the film coefficient, k_f , is calculated from Eq. (4.10) (reported in Table 4.3). A least-square based fitting procedure is also applied to determine the value of k_f that best fits the experimental BTCs for the three PBSAC diameters using a model that neglects the axial dispersion through the layer.

Table 4.3: Reynolds number, Schmidt number and film mass transport coefficient (k_f) for the three PBSAC diameters considered in this chapter and a flux of $200 \text{ L m}^{-2} \text{ h}^{-1}$ (0.056 mm s^{-1}).

| PBSAC diameter μm | Reynolds nr. - | Schmidt nr. - | k_f mm s^{-1} |
|---------------------------------|-------------------|------------------|-----------------------------|
| 80 | 0.013 | 1438 | 0.039 |
| 200 | 0.031 | 1438 | 0.020 |
| 640 | 0.100 | 1438 | 0.009 |

As it was previously discussed, the empirical correlations available for the axial dispersion coefficients are likely to be inconsistent with describing the dispersion phenomena in a millimetric packed-layer. For this reason, the dispersion coefficients were mainly determined using the least-squares fitting procedure. The values obtained in this way were then compared with the ones calculated using the well-known empirical correlation form Gunn, as shown in the next section.

4.6 Model validation

In this section, the simulated BTCs of E2 in the UF-PBSAC are compared to the experimental data obtained in the previous chapter. A least-squares-based fitting procedure is also used to determine the mass transport coefficient values that provide the best fitting with experimental data. Initially, the dispersion in the bed is neglected, and the best-fitting procedure is focused on the film mass transport coefficient. Later, the model including dispersion is used, and the fitting procedure is employed to derive the axial dispersion coefficient. The conceptual flow diagram followed to validate the model is reported in Appendix D, Fig. D.4.

In both cases, the transport of E2 in the UF membrane is also considered. Due to the negligible adsorption of the membrane, the UF step has little influence on the BTCs of E2 in the UF-PBSAC, as shown in Appendix D). However, in other cases, where the UF membrane is characterized by significant adsorption, the effect of the UF on the final BTC should be considered in detail.

4.6.1 Convection – film transport – adsorption

The simulated breakthrough curves for the three PBSAC diameter neglecting dispersion and using the value of k_f from an empirical correlation are reported in Fig. 4.7A. It can be noticed the model provides good agreement with experimental data for the larger PBSAC (diameter of 640 μm), while it significantly underestimates the permeate concentration for the smaller PBSAC (for both diameters, the model predict a concentration really low, and thus they can not be distinguished).

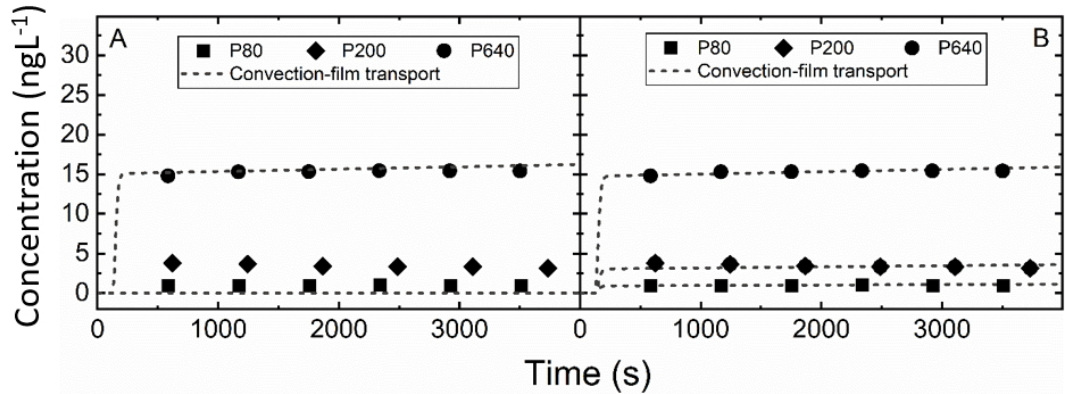


Figure 4.7: Comparison of simulated BTCs and experimental data for the convection-film transport-adsorption model with k_f determined by empirical correlation (A) and by the best-fitting procedure (B). PBSAC layer of 2 mm.

The fitting procedure allows having an agreement between simulated BTCs and experimental data for all PBSAC diameters Fig. 4.7B. The film transport coefficients that provide the best fitting (reported in Table 4.4 for the three PBSAC diameter) increases at increasing particle diameter. However, k_f is expected to follow the opposite trend, decreasing at increasing particle diameter as discussed in a previous section. In conclusion, the model neglecting axial dispersion can describe the experimental data only if k_f is forced to assume values that compromise its physical meaning.

Table 4.4: Comparison between film transport coefficients estimated from an empirical correlation and the ones providing the best-fitting to the experimental data.

| PBSAC diameter μm | k_f mm s^{-1} | |
|---------------------------------|-----------------------------|----------|
| | Correlation [129] | Best-fit |
| 80 | 0.039 | 0.003 |
| 200 | 0.020 | 0.005 |
| 640 | 0.009 | 0.009 |

4.6.2 Convection – dispersion - film transport – adsorption

Axial dispersion is also considered in this section. The film transport coefficient was fixed to the value obtained from the empirical correlation. In contrast, the values D_{ax} from Gunn correlation were compared to the ones providing the best fitting to the experimental data.

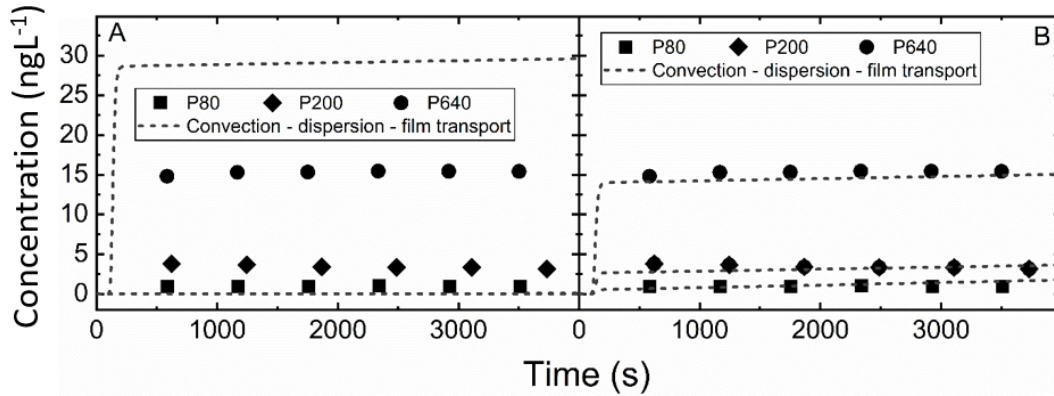


Figure 4.8: Comparison of simulated BTCs and experimental data for the convection-dispersion-film transport-adsorption model with k_f determined from an empirical correlation and D_{ax} determined either from empirical correlation (A) and by the best-fitting procedure (B). PBSAC layer of 2 mm.

The simulated BTCs using Gunn correlation for D_{ax} are reported in Fig. 4.8A. Similarly to the model neglecting dispersion (previous section), the simulated BTCs underestimate the concentration for PBSAC diameter of 80 and 200 μm . However, simulated and experimental BTCs are not in agreement even for the larger PBSAC, where the concentration of E2 is overestimated in the model compared to the experiment. It follows that, when D_{ax} is let vary to provide the best fit (Fig. 4.8B), the resulting dispersion coefficient is higher for the small PBSAC and lower for the larger one (compared to the value estimated from empirical correlation) (Table 4.5).

Table 4.5: Comparison between axial dispersion coefficients estimated from an empirical correlation and the ones providing the best-fitting to the experimental data.

| PBSAC diameter μm | D_{ax} $\text{mm}^2 \text{s}^{-1}$ | |
|---------------------------------|---|----------|
| | Correlation [135] | Best-fit |
| 80 | 0.005 | 2.350 |
| 200 | 0.026 | 0.547 |
| 640 | 0.320 | 0.002 |

4.6.3 Axial dispersion at different layer thicknesses

Further, the D_{ax} -focused fitting procedure was applied to the experimental BTCs at different thicknesses of the PBSAC layer (from 1 to 6 mm) for the three PBSAC

diameters. The values of D_{ax} determined are shown in Fig. 4.9. For all PBSAC diameters, the axial dispersion coefficient increases as a function of thickness. In practice, it means that the adsorption process becomes less efficient by increasing the thickness of the adsorbing layer due to enhanced dispersive transport of the pollutant. Interestingly, a similar behavior was already noticed in Chapter 2 (Fig. 2.8), where, by increasing the number of PBSAC mats, the removal of E2 did not increase as expected in the ideal case (e.g., as if each PBSAC mat acted as a separate layer, see Fig. C.1 in Appendix C).

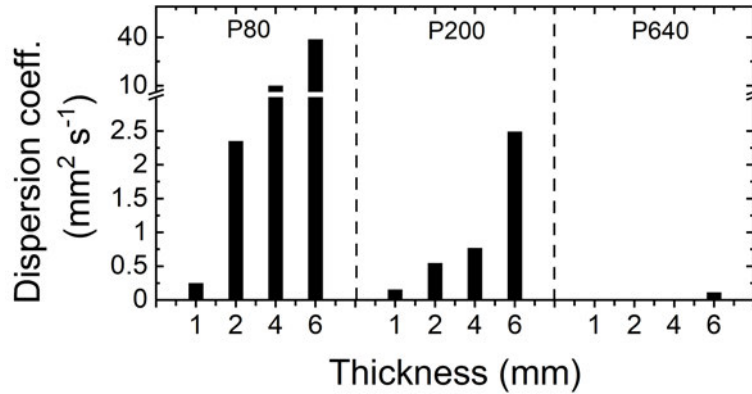


Figure 4.9: Axial dispersion coefficient estimated by best-fit procedure at increasing PBSAC layer thickness.

For PBSAC of diameter 80 and 200 µm, these results would suggest the dispersion in a millimetric layer is higher compared to a column (where the empirical correlation for D_{ax} was developed and validated). This consideration is in agreement with previous results reported by Carberry and Breton [136], which noticed anomalous high dispersion in short packed-bed. In that case, higher axial dispersion was correlated to entrance effect due to the rapid acceleration of the fluid entering a system restricting flow (the packed-bed).

On the contrary, the results for the layer packed with PBSAC of 640 µm shows a different behavior in that the dispersion coefficient is actually lower compared to the one estimated with correlation (thus valid for packed columns). However, it can be highlighted how the "characteristic length of the pores" of a layer packed with PBSAC of 640 µm (calculated from Eq. (4.22) [143]) is 0.43 mm, close to the thickness of the layer itself (1-6 mm). Thus, it is not surprising that the packed-layer of large PBSAC does not behave, in terms of dispersion, as packed-bed but rather as porous materials with pores that are in the same order of magnitude as the thickness.

$$l_{\beta} = d_p \frac{\varepsilon_b}{1 - \varepsilon_b} \quad (4.22)$$

In summary, axial dispersion appears to depend not on the adsorbent size but on the ratio between layer thickness and particle size (L/d_p). Indeed, a correlation can be observed between D_{ax} and L/d_p regardless of the particle size, as shown in Fig. 4.10. However, these results are difficult to interpret and a conclusive statement

would be possible only with further investigations. In particular, the BTCs of a solute that does not adsorb and enter the pores could be really helpful. In this way, the other transport mechanisms (adsorption and film transport) could be neglected, together with the uncertainty related to their parameters (equilibrium adsorption constant and film transport coefficient).

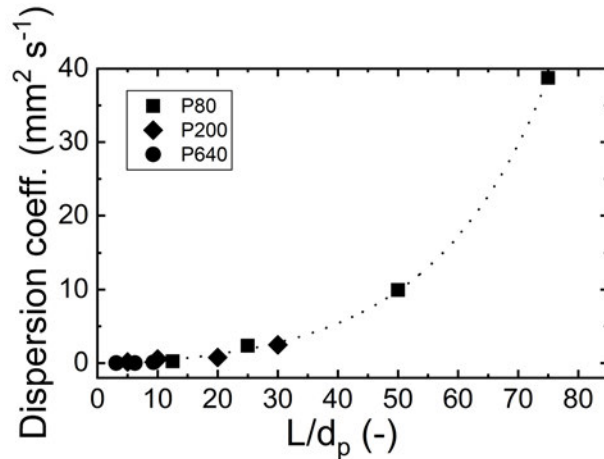


Figure 4.10: Axial dispersion coefficient estimated by the best-fit procedure as a function of the ratio between layer thickness and PBSAC diameter.

The final section of this chapter presents an example of how the model formulated and validated could be applied to support the design of a real UF-PBSAC treatment unit.

4.7 Example of model application

As discussed in Chapter 1, E2 concentration in European surface water ranges from few ng L^{-1} to over 200 ng L^{-1} . It follows that the required PBSAC layer thickness depends on the actual E2 concentration in the water to treat. In this section, the required PBSAC layer thickness to meet the target value of 1 ng L^{-1} at varying feed concentration is predicted. For BTC prediction, k_f from empirical correlation and D_{ax} previously obtained by fitting the experimental data will be employed. Note that, since a correlation to estimate a-priori D_{ax} is not available, the BTC of E2 can be simulated only in the conditions (thickness/PBSAC diameter) for which D_{ax} was estimated by the fitting procedure, thus 1 to 6 mm of thickness and 80, 200 and 640 μm of adsorbent diameter.

Fig. 4.11 shows the required layer thickness as a function of feed concentration for the three different PBSAC diameters. The maximum E2 feed concentration for which the target value can be met (in a layer of 6 mm, PBSAC 80 μm) is 200 ng L^{-1} . Until 50 ng L^{-1} of E2 feed concentration, a PBSAC 80 μm layer of only 1 mm is enough to reduce the concentration below the target value. The maximum feed concentration for which the target value can be met using a PBSAC layer packed with PBSAC with a diameter of 640 μm is 50 ng L^{-1} .

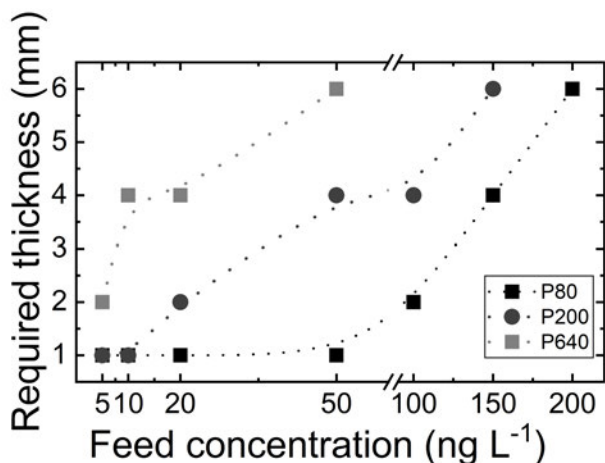


Figure 4.11: Required layer thickness to reach 1 ng L^{-1} in the permeate as a function of feed concentration for different PBSAC diameters obtained from simulated BTCs.

4.8 Conclusions

- For a UF membrane with negligible adsorption, the transport of estradiol in the UF has little influence on the final breakthrough of the UF-PBSAC layer and could be neglected.
- The model considering only convection and film mass transport (thus neglecting axial dispersion) can not describe the experimental breakthrough curve unless the film transport coefficient is forced to assume values that compromise its physical meaning.
- The axial dispersion mechanism in a thin packed-layer behaves significantly different compared to conventional packed-columns. It follows that empirical correlations reported in the literature to estimate the dispersion coefficient are not applicable in the case of a thin layer.
- Axial dispersion depends on the ratio between the thickness of the packed-layer and the particle diameter (L/d_p). The dispersion coefficient ranges from negligible for a small ratio L/d_p to almost $40 \text{ mm}^2 \text{ s}^{-1}$ for a higher L/d_p of 75 (which is still a much lower value compared to conventional packed-column).
- The model developed is a useful tool to predict the required PBSAC layer thickness to meet the proposed target value of 1 ng L^{-1} at varying feed concentration.

Chapter 5

Impact of dissolved organic matter on the removal of estradiol by the UF-PBSAC*

The UF-PBSAC approach was shown to be a promising approach to remove steroid hormones from water. However, the presence of background dissolved organic carbon (DOC) is known to be a factor that can compromise the adsorption of micropollutants on activated carbon. In this chapter, the impact of two types of DOC was assessed with a focus on the possible competition mechanisms. Environmentally relevant concentrations of DOC and E2 were used: 10 mgC L^{-1} and 100 ng L^{-1} , respectively. The adsorption of E2 was shown to be effective even in DOC-containing water. No early breakthrough, which would be caused by a strong competitive behavior of DOC, was observed. Preferential adsorption of estradiol even in the presence of DOC (present in much higher concentration) was attributed to its faster adsorption kinetics. Indeed, DOC molecules are likely to be excluded by the major part of PBSAC internal porosity due to their large size. DOC interacting with E2 can marginally interfere with the adsorption process (indirect competition) despite not entering the porous system. A reduction of the mass of estradiol adsorbed of about 10 % was observed when the large DOC fractions interacting with estradiol could access the PBSAC layer. However, this interference can be simply controlled by using a UF with a MWCO less than or equal to 10 kDa. These results confirm that UF-PBSAC is an effective approach to remove estrogens from real water. The permeate side adsorption layout is particularly interesting in that it can reduce the interference of DOC. Pilot-scale investigations are the natural progression to further develop the process in more realistic conditions.

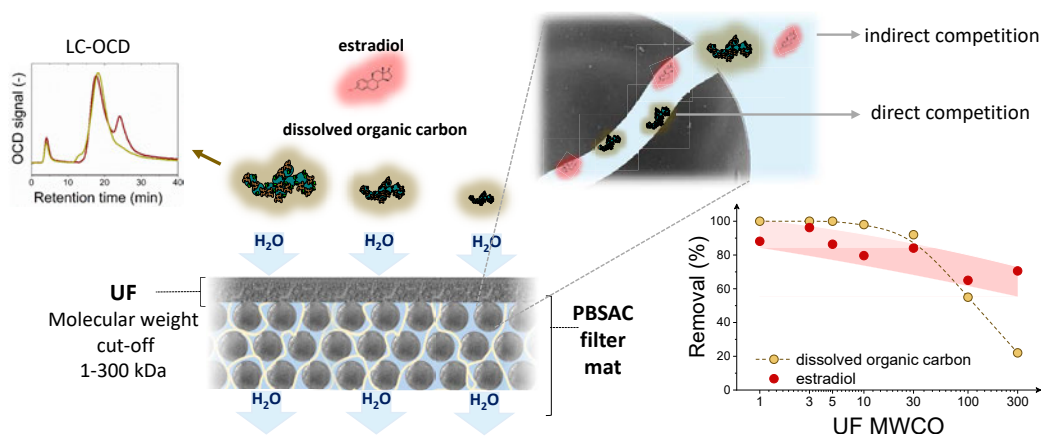


Figure 5.1: Graphical abstract of Chapter 5. Adapted from [144].

* This chapter is based on the following publication: "Removal of steroid hormone micropollutants by UF-PBSAC composite in presence of organic matter", Journal of Membrane Science, 2019, 592, 117315. For this thesis chapter, part of the content has been rewritten and some of the graphs have been adapted by the author.

5.1 Introduction

In a real process, dissolved organic carbon (DOC) is also present in the water, together with micropollutants (MPs). The goal of this chapter is thus to assess the impact of DOC on the removal of the estrogenic estradiol (E2) by UF-PBSAC. The main focus is on the expected interference of DOC on the adsorption step in the PBSAC layer. The largely different concentration levels of DOC ($\sim \text{mgC L}^{-1}$) and MP ($\sim \text{ng L}^{-1}$) may strengthen the interference effect [51]. In practice, the effect of DOC on activated carbon (AC) adsorption is typically to reduce the volume of MPs that can be treated (early breakthrough) and thus the lifetime. The interference of DOC on activated carbon (AC) adsorption is generally regarded as "competition". However, competition can occur mainly in two ways, very different from each other. Direct competition is caused by DOC molecules that adsorb to the same adsorption sites of MPs on the AC surface. On the other hand, indirect competition (or better interference) occurs when DOC hinders the MPs from entering the pore system of the AC. The latter mechanism is also called pore blocking or AC fouling.

The size of DOC is the most critical factor in defining which interference mechanism occurs in AC-MP systems. Direct competition is mostly related to small DOC fractions. Larger molecules are either hindered from entering the pore system or slower in diffusion and weaker in adsorption. Besides, the chemistry of DOC plays a role. Less charged fractions adsorb more effectively due to enhanced hydrophobic interaction [145, 146]. Zietzschmann *et al.* [147] identified direct competition of low molecular weight (MW) DOC fractions as the main competition mechanism, which reduced the adsorption capacity for MP onto powdered activated carbon (PAC). Matsui *et al.* [148] investigated competition in superfine PAC, confirming that the organic matter competing most has a similar MW to the target MP. Other authors [149, 150] observed a reduction of PAC and AC fibers adsorption capacity in the presence of both low and high MW DOC fractions, a sign that both competitive mechanisms were simultaneously occurring.

DOC competition was also investigated in GAC filters. Kennedy and Summers [82] investigated the effect of DOC size on the adsorption of MPs. Again, the strongest reduction in MP adsorption capacity was observed for water containing only low MW DOC. However, the adsorption capacity was also reduced when only high MW DOC was present, indicating indirect competition. Other researchers [83] have also concluded that indirect competition is relevant in GAC filters by grinding apparently exhausted GAC and observing a residual adsorption capacity.

DOC has an impact also on the rejection of MPs by membranes. In the presence of organic matter, literature reports increased steroid hormones rejection both for nanofiltration (NF) [151] and ultrafiltration (UF) [152]. This increase in the rejection was attributed to the interactions between hormones and DOC and the consequent rejection. Shen *et al.* [151] also noticed a decrease of the estrone adsorbed to the nanofiltration membrane in the presence of DOC.

In conclusion, DOC could affect the removal of hormones in the UF-PBSAC in different ways (Figure 5.2). Rejection of E2 by the UF is expected to become a relevant factor if E2 interacts with the DOC used in this work. Further, the adsorption process of E2 in the adsorbing layer may be deteriorated by competition effects with DOC. The impact of DOC on the UF-PBSAC process will be assessed by comparing the breakthrough curves of E2 in the presence and absence of DOC. Two types of DOC will be used: commercial humic acid and natural surface water.

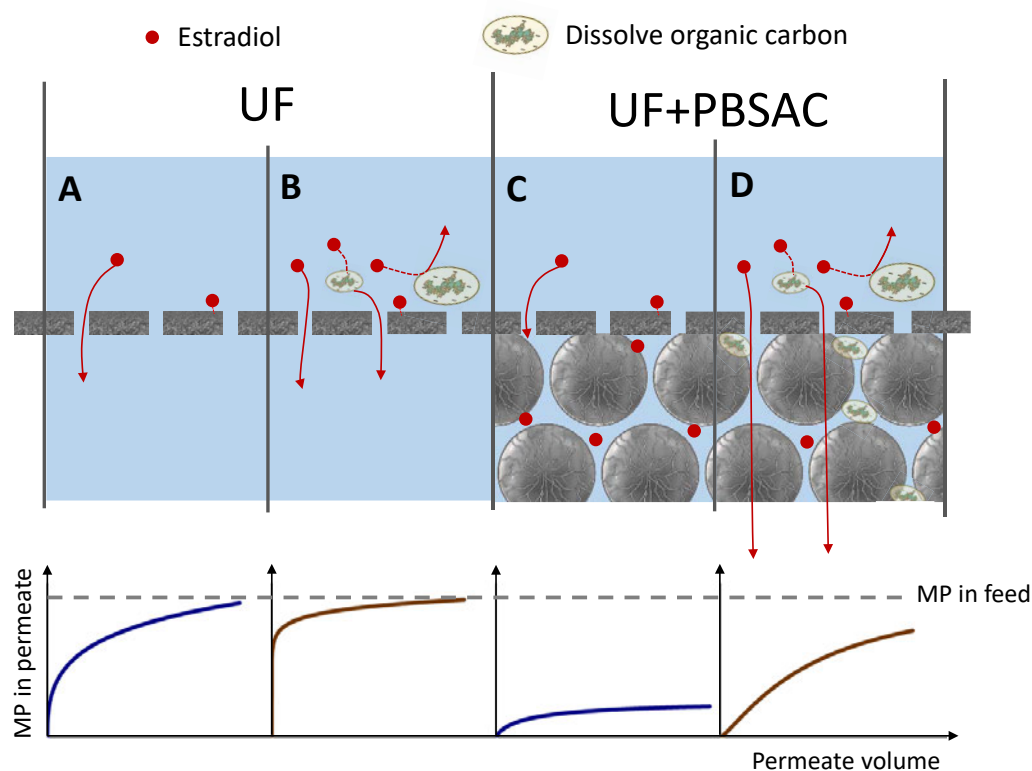


Figure 5.2: Schematic representation of the possible retention and transport mechanism of MP in water (A and C) and in water containing DOC (B and D) for UF (A and B) and UF-PBSAC (C and D) and expected permeate concentration profile for the different scenarios. Adapted from [144].

5.2 Materials and methods

5.2.1 Membranes

In this chapter, seven UF membranes provided by Millipore (Bedford, USA) as PLH and PLC type of Ultracel series are used. The molecular weight cut-off (MWCO) of these ranges from 1 to 300 kDa that corresponds to estimated membrane pore sizes in the range 1.6 to 32.6 nm (Table 5.1). The active layer for both PLH and PLC is made of regenerated cellulose. The main difference is the substrate on which the regenerated cellulose layer is cast; the PLH series is cast on polypropylene nonwoven substrate and the PLC series is on a microporous ultra-high MW polyethylene

membrane support. Also, PL membranes are thicker (230 μm) compared to PLC membranes (130 μm) [153].

Considering the wide range of permeability of the membranes, they were divided into two groups (see Fig. 5.3). Membranes of higher permeability (10, 30, 100 and 300 kDa) are operated at lower pressures (0.1-1.5 bar corresponding to a flux of $125 \text{ L m}^{-2} \text{ h}^{-1}$) and are called "low-pressure UF". Membranes of lower permeability (1, 3 and 5 kDa) are operated at higher pressures (4-10 bar corresponding to a flux of $40 \text{ L m}^{-2} \text{ h}^{-1}$) and are called "high-pressure UF" in this chapter. A list of the membranes used, including information provided by the manufacturer, is reported in Table 5.1.

Table 5.1: List of the membranes used in this chapter and the properties reported by the manufacturer (n.a., not available). Adapted from [144].

| Supplier code | MWCO kDa | Pore diameter ^a nm | Permeability $\text{L m}^{-2} \text{ h}^{-1}$ bar^{-1} | Thickness μm |
|-------------------------|-------------|-------------------------------------|---|----------------------------|
| <i>High-pressure UF</i> | | | | |
| PLH AC | 1 | 1.59 | 7 | 230 |
| PLC BC | 3 | 2.84 | n.a. | 130 |
| PLH CC | 5 | 3.72 | 22 | 230 |
| <i>Low-pressure UF</i> | | | | |
| PLH GC | 10 | 5.37 | 108 | 230 |
| PLC TK | 30 | 9.62 | 312 | 130 |
| PLC HK | 100 | 18.20 | 1270 | 130 |
| PLC MK | 300 | 32.58 | 3900 | 130 |

^a Calculated using equation [154]: $d = 2 \cdot 2.0374 \cdot 10^{-11} \text{ MW}^{0.53}$

5.2.2 Polymer-based activated carbon mat and particles

In this chapter, the PBSAC filter mat is mainly employed. It was already introduced in Chapter 1. For comparison, loose PBSAC is also used in static adsorption experiments. The two PBSAC sample used in this chapter has a diameter of 450 μm (same as in the mat) and 200 μm . They are characterized by a high activation degree (see Chapter 2 for the definition of activation degree).

5.2.3 Dissolved organic matter feed solution

Two types of DOC (10 mgC L^{-1}) are used in the feed solution, also containing hormones: commercial humic acid (HA, Sigma Aldrich, Germany, technical grade) and natural organic matter (NOM) from a Tanzanian blackwater. For what concerns HA, a stock solution of 1000 mgC L^{-1} is prepared by dissolving 4 g of HA in 2 L of 0.1 M

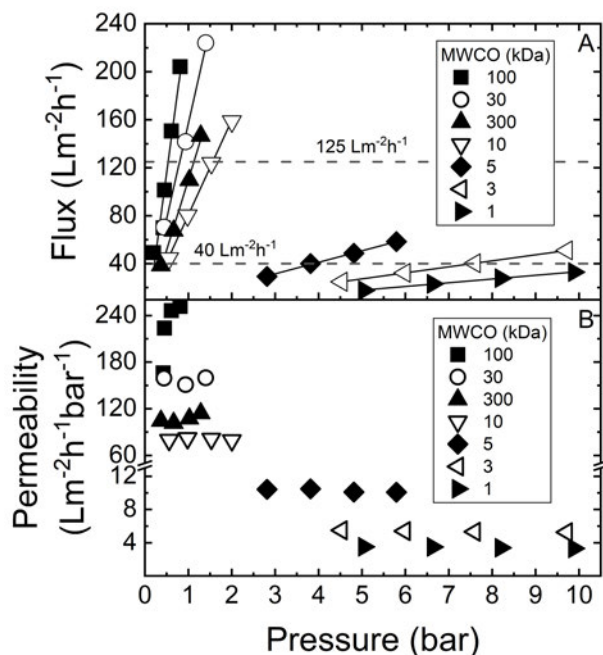


Figure 5.3: Flux and permeability as a function of applied pressures of all membranes used in this chapter. Adapted from [144].

NaOH (EMD Millipore, Germany, 99 % purity). The addition of NaOH is needed to increase the pH to 13 in order to increase the solubility of HA. The solution is stirred for 24 h and stored in a fridge in a glass bottle protected from light to avoid degradation. To prepare 0.7 L of HA feed solution with a concentration of 10 mgC L^{-1} , 7 mL of the stock solution is diluted with the background solution (1 mM NaHCO_3 , 10 mM NaCl). Before diluting with the background solution, the HA stock solution is filtered using a Minisart syringe filter ($0.45 \mu\text{m}$, cellulose acetate, Sartorius, Germany). Tanzanian NOM water has an organic matter concentration of 70 mgC L^{-1} . It was filtered using a Minisart syringe filter and diluted with the background solution to achieve a final concentration of 10 mgC L^{-1} . For both type of DOC, pH was adjusted to 8 by adding 1 M HCl (VWR Chemicals, Germany, analytical grade). A pH meter (WTW InoLab pH720, Germany) is used to determine the pH of HA stock solution and of all feed solutions.

5.2.4 Analytical methodology for DOC

DOC in water samples can be typically quantified by Total organic carbon (TOC) analyzers. In this case, TOC measurement is challenged by the presence of ethanol in the solution containing hormones and DOC. As described in Chapter 2 and Appendix A, hormones are dissolved in ethanol in the native solutions purchased from Perkin Elmer. After dilution to the "standard" hormones feed solution (100 ng L^{-1}), ethanol is present in relevant concentration (0.03 %vol corresponding to $\approx 13 \text{ mgC L}^{-1}$). Thus, the residual ethanol compromises the use of the TOC analyzer.

As a substitute for DOC quantification, a UV-Vis spectrophotometer can be used to measure the absorbance of organic matter. A correlation between absorbance detected by UV-vis and DOC detected by the TOC analyzer (Sievers M9, GE Analytical Instruments, USA) is performed using a DOC solution without hormones (thus without ethanol). After that, DOC concentration in the samples can be estimated from the absorbance values. The TOC/UV-vis correlation is reported in Fig. 5.4. Absorbance increases with aromaticity and molecular weight [155–157], leading to an error in the determination of concentration when DOC is fractionated by membranes. The retention will be overestimated, as explained by Schäfer [158].

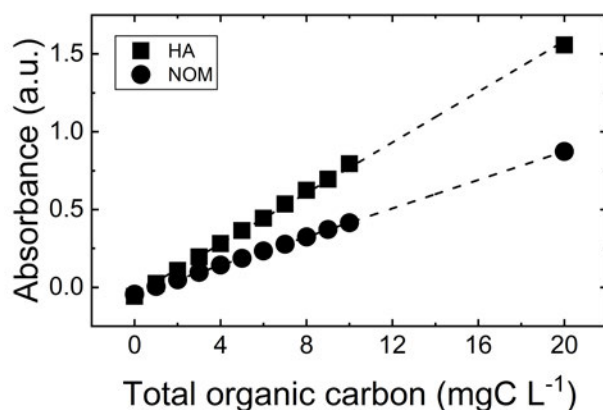


Figure 5.4: UV-vis absorbance as a function of DOC concentration for HA and NOM.

In addition, some selected HA and NOM samples are fractionated and analyzed with liquid chromatography – organic carbon detection (LC-OCD, Model 9, DOC-Labor Dr. Huber, Germany). LC-OCD allows separating based on the size and detect the different fractions of DOC, namely biopolymers, humic substances (HS), building blocks (BB), low molecular weight (LMW) acids and neutral. In this system, size exclusion-based fractionation is performed in a TSK HW 50S gel column and the fractionated DOC is detected by the organic carbon detector (OCD). Also, two additional detectors are present in the system: a UV-detector set to 254 nm (UVD) and an organic nitrogen detector (OND) [159]. For data acquisition and processing, ChromLOG and ChromCALC (LabView based software) are used, and for figures and tables, ChromFIG and ChromRES software are used. Peak integration is performed following Huber *et al.* [159]. The mobile phase solution is 2 g L⁻¹ KH₂PO₄ and 1.2 g L⁻¹ Na₂HPO₄ (2 H₂O) dissolved in Milli-Q. The flow rate is set to 2 mL min⁻¹, and the sample injection volume is 1 mL.

Like the TOC analyzer, the presence of ethanol together with hormones and DOC is problematic. The interference of ethanol on the LC-OCD is hence checked and is reported in Appendix B. Ethanol is a small molecule (46 Da) and presents a long residence time in the size exclusion column. However, the quantification of the smaller DOC fractions (BB and LMW) is compromised by the ethanol peak. The only fraction that can be reliably detected in the presence of ethanol is HS.

5.2.5 Chemicals and analytical method

As micropollutant, only E2 is used in this chapter. The E2 feed solution preparation is similar to the one reported in Chapter 2. However, the E2 stock solution of $10 \mu\text{g L}^{-1}$ is diluted with the DOC solution prepared as shown in the previous section. The E2 native solution used in this chapter has a specific activity of 94 Ci mmol^{-1} . The calibration is reported in Appendix A.

E2 concentration is again measured with the Liquid Scintillation counter (LSC). In this case the sample containing E2 also contains DOC (either HA or NOM) in the concentration range $0\text{-}10 \text{ mgC L}^{-1}$. DOC can interfere (quenching) with the activity detected by LSC. Fig. 5.5 shows that diluting the sample 10 times is enough to reduce DOC to a level where quenching does not occur. For this reason, all samples were diluted 10 times before measurement with LSC.

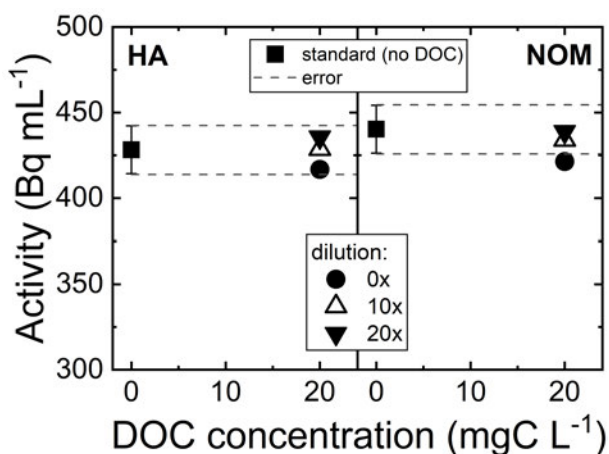


Figure 5.5: E2 activity detected by LSC in presence of DOC and effect of sample dilution.

In this chapter, six textile dyes of different sizes are used. These are methylene blue (MB), methyl orange (MO), malachite green (MG), rhodamine B (RB), titan yellow (TY) and red direct 80 (RD). The MW of these compounds ranges from 317 Da (for MB) to 1373 Da (for RD). Dye absorbance is measured with a UV-vis spectrophotometer and their concentration quantified through a calibration curve.

5.2.6 Dynamic adsorption of E2 in the presence of DOC for the UF-PBSAC mat

The impact of DOC on E2 adsorption is tested using only the PBSAC mat (and not the packed-layer). The protocol of the experiments is the same reported in Chapter 2 and Appendix B and it will only be briefly recalled. The PBSAC mat and the membrane are placed in the bottom part of the stirred cell. MilliQ water is filtered for 90 min. After that, the feed solution containing E2 and DOC is poured inside the cell. Depending on the permeability of the membrane, the pressure is set to 0.1-1.5 bar (flux of $125 \text{ L m}^{-2} \text{ h}^{-1}$) and 4-10 bar (flux of $40 \text{ L m}^{-2} \text{ h}^{-1}$) for low and high-pressure UF, respectively. Stirring is set to 400 rpm. The filtration of the DOC-E2

solution is carried out until 0.6 L of permeated is collected. Six samples of 0.1 L are collected as a function of volume (or time) filtered.

5.2.7 Static adsorption experiments

Static adsorption experiments are performed to study the adsorbability of the different DOC fractions on PBSAC. The feed solution (0.25 L) of each DOC type (initial concentration of 8 and 10 mgC L⁻¹ for HA and NOM, respectively) is poured inside a conical flask (Duran Group, Germany). The desired amount of PBSAC particles to reach a concentration of 1 g L⁻¹ is added. The flask is immediately placed into the incubator shaker (Innova 43 R, New Brunswick Scientific, USA); stirring and temperature are set to 260 rpm and 20 °C, respectively. Samples are collected at different time intervals (1, 3, 7, 24 and 26 h). The concentration of the different DOC fractions is finally measured with LC-OCD.

In addition, adsorption isotherms of six dyes with increasing MW are measured in static adsorption. The same protocol previously used for MB is used (see Chapter 2). The dyes solution (0.1 L at initial concentrations from 10 mg L⁻¹ to 500 mg L⁻¹) is placed inside the flask with 50 mg of PBSAC particles (final PBSAC concentration of 0.5 g L⁻¹).

Table 5.2: Summary of the parameters used in Chapter 5 together with the units and the formulae for their calculation. Adapted from [144].

| Parameter | Unit | Formula | |
|---|--------------------|--|-------|
| Relative concentration | – | $Relative\ conc. = \frac{c_P}{c_F}$ | (5.1) |
| Real retention | % | $R = (1 - \frac{c_P}{c_F}) 100$ | (5.2) |
| Mass of E2 adsorbed | ng | $m_{ads} = V_F c_F - \sum_{i=1}^{n.samples} V_{P,i} c_{P,i} - V_R c_R$ | (5.3) |
| Mass available for PBSAC adsorption | ng g ⁻¹ | $m_{avail.,PBSAC} = m_F - m_{ads,UF} - m_R$ | (5.4) |
| % mass adsorbed to PBSAC | % | $\%m_{ads,PBSAC} = \frac{m_{ads} - m_{ads,UF}}{m_{avail.,PBSAC}}$ | (5.5) |
| c_P : MP concentration in the permeate | | V_R : volume of the retentate | |
| V_P : volume of the permeate collected | | m_F : mass of E2 in the feed | |
| c_F : MP concentration in the feed | | m_R : mass of E2 in the retentate | |
| V_F : volume of the feed | | $m_{ads,UF}$: mass of E2 adsorbed to the UF | |
| c_R : MP concentration in the retentate | | | |

5.2.8 Data analysis

Besides the overall E2 adsorbed in the UF-PBSAC, E2 adsorbed to the PBSAC mat compared to the available for adsorption, calculated from Eq. (5.5). The goal is to obtain the adsorption efficiency in the PBSAC mat, excluding the effect of adsorption and rejection by the membrane. The mass available for adsorption is obtained by subtracting the E2 rejected and/or adsorbed to the UF to the mass fed to the system (Eq. (5.4)).

5.3 Results and discussion

5.3.1 Feed water characteristics

Considering that the different fractions of DOC are expected to interfere in different ways with the adsorption of E2, the two types of DOC (HA and NOM) were first characterized with LC-OCD. LC-OCD chromatograms of each feed water type are plotted in Fig. 5.6.

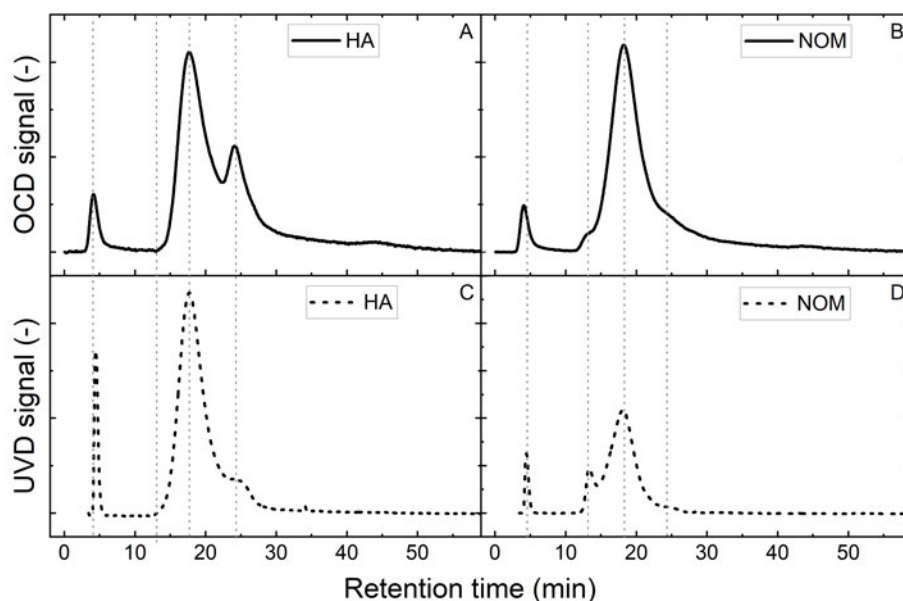


Figure 5.6: Signal detected by the OCD (A and B) and UVD (C and D) detector as a function of retention time for HA (left, A and C) and NOM (right and BD). Adapted from [144].

The first peak present in all chromatograms in Fig. 5.6 at ≈ 4 min corresponds to the total organic carbon (for the OCD signal) and the total absorbance (for the UVD signal). Part of the injected volume bypasses the column, and it is sent directly to detectors without being fractionated. A characteristic peak for the largest DOC fraction (biopolymers) can be seen at ≈ 13 min for NOM (Fig. 5.6B) but not for HA (Fig. 5.6A). Later on, the major fraction of DOC (HS) elutes at a retention time of ≈ 16 min. Breakdown products of HS (BB) do not present a clear peak, but they are related to the right-side slope of the HS peak. The LMW acids elute at a retention time of ≈ 24 min; this peak is clearly visible for the HA (Fig. 5.6A) but not for NOM

(Fig. 5.6B). Finally, the smallest and most hydrophobic fraction of DOC (LMW neutrals) elutes, it is not made by a distinct peak but rather by the tailing of the whole chromatograph.

The integration results showing the relative amount of the different fractions are reported in Table 5.3, while the characteristics of the major DOC fraction (HS) are detailed in Table 5.4. In summary, NOM contains a small fraction of biopolymers, a higher fraction of HS, and a slightly higher BB fraction compared to HA. LMW neutrals are present in a similar concentration in both waters, while the presence of LMW acids could only be found in HA. In addition, the characteristics of HS are different between HA and NOM. HS from HA presents a slightly higher MW and, especially, a significantly higher specific UV absorbance at 254 nm (SUVA) compared to HS from NOM as it can be seen also from the chromatographs detected by UVD (Fig. 5.6C&D). The values stated in Table 5.3 and Table 5.4 are the average of triplicate measurements each.

Table 5.3: Amount of the different fractions of DOC relative to total organic carbon in HA and NOM feed solution. Adapted from [144].

| DOC fraction | | HA | NOM |
|------------------------|---|-----|-----|
| Organic matter | % | 100 | 100 |
| Biopolymers | % | 0 | 4 |
| HS | % | 53 | 68 |
| Building Blocks | % | 19 | 14 |
| LMW neutrals | % | 17 | 14 |
| LMW acids | % | 6 | 0 |

Table 5.4: Specific UV absorbance and MW of the HS fraction from HA and NOM.

| Parameter | | HA | NOM |
|------------------|----------------------|------|-----|
| SUVA - HS | $L\ mg^{-1}\ m^{-1}$ | 13.7 | 6.0 |
| MW - HS | $g\ mol^{-1}$ | 876 | 805 |

Once that the DOC in the feed water was characterized, dynamic adsorption experiments were carried to obtain the breakthrough in the presence and absence of DOC. The breakthrough curves were obtained both for the UF membranes only and for the UF-PBSAC mat. They are shown in Fig. 5.7 for the high-pressure UF and in Fig. 5.8 for the low-pressure UF.

5.3.2 Breakthrough curves of E2 for the UF membranes

Removal of E2 in a UF membrane can occur because of sorption into the polymeric matrix. Regardless of the MWCO, rejection by size exclusion does not occur because the pore size of the membrane is too large compared to the size of E2. However,

the E2 breakthrough curves for the UF (hollow circle in Fig. 5.7 and Fig. 5.8) shows that the removal is highly variable depending on the UF used. In some cases, E2 immediately breaks through the UF and reaches the feed concentration after 100 mL of permeate volume (for example, Fig. 5.7C and Fig. 5.8A). In other cases, significant removal of E2 can be observed, and E2 concentration does not reach the feed value even at the end of the experiment (for example, Fig. 5.7B and Fig. 5.7B and D).

This different behavior does not depend on the MWCO of the membrane but is determined by the membrane series (PLH or PLC). In general, PLC membranes remove significant amount E2 due to adsorption while the removal in PL membranes is negligible. The different adsorption in the two membrane series is likely to be caused by a difference in the material, although both membrane series are regenerated cellulose membranes. To support this hypothesis, the electrokinetic potential is measured for all the membranes. The electrokinetic potential for PL membranes (-38 to -48 mV) is more negative compared to PLC (-20 to -28 mV), as shown in Appendix C.3.

Further, the presence of DOC appears to decrease the adsorption of E2 in the PLC membranes where adsorption is relevant. This reduction of E2 adsorption may result from membrane modification caused by DOC. DOC deposits on the membrane, making it more hydrophilic (negatively charged). The reduction of MP adsorption is observed in particular for open membranes (30, 100 and 300 kDa).

5.3.3 Breakthrough curves of E2 for the UF-PBSAC mat

The comparison of the breakthrough curves of E2 in the presence and absence of DOC is reported in Fig. 5.7 for the high-pressure UF and in Fig. 5.8 for the low-pressure UF.

For high-pressure UF, E2 concentration is reduced down to 10-20 ng L⁻¹ regardless of the presence of DOC. Thus, no strong competition leading to early breakthrough is observed. The concentration in the presence of organic matter is only a few ng L⁻¹ higher. This variation appears to be insignificant, considering the experimental error reported in Appendix B.2. In addition, when the E2 concentration relative to the feed is considered, almost no influence of DOC can be observed (Appendix C.6). Compared to the absolute E2 concentration in the permeate, the relative concentration accounts for the increase in feed concentration due to the rejection of E2 bound to DOC (that will be discussed in detail later). Due to the very high adsorption by the 3 kDa UF membrane, no interference determination is possible for the UF-PBSAC mat (Fig. 5.7B&E).

Similar considerations can be drawn for low-pressure UF (Fig. 5.8), where again no early breakthrough was observed. However, when HA is present in the feed, E2 permeate concentrations are higher for UF with MWCO > 10 kDa (full circles compared to full squares in Fig. 5.8BC&D). The difference in E2 concentration at the end of the experiment is 8, 18 and 16 ng L⁻¹ for UF MWCO of 30, 100 and 300

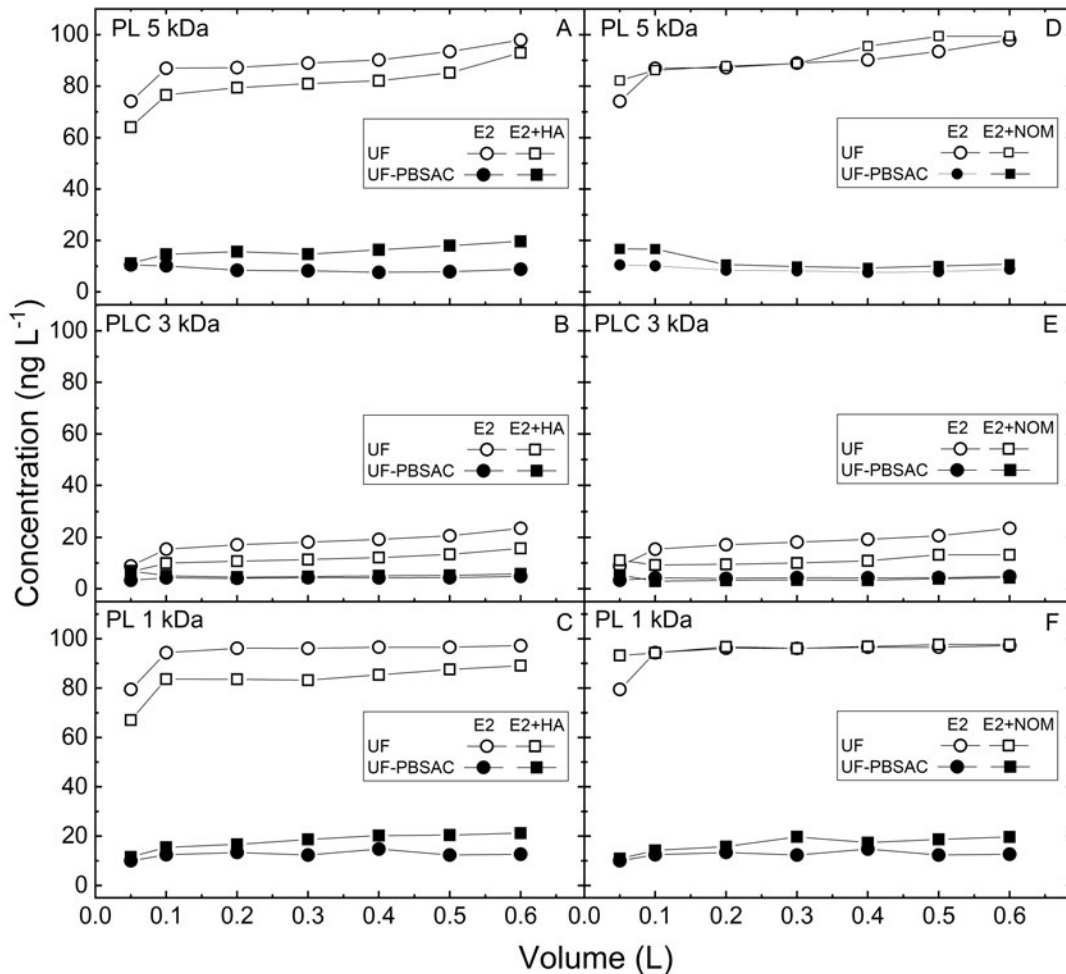


Figure 5.7: E2 breakthrough curves of filtration with high-pressure UF (MWCO 1-5 kDa) and UF-PBSAC. E2 feed conc. 100 ng L^{-1} . DOC feed conc. 10 mgC L^{-1} . Flux: $40 \text{ L m}^{-2} \text{ h}^{-1}$. Stirring 400 rpm. Temperature $23 \text{ }^\circ\text{C}$. Adapted from [144].

kDa respectively. The same effect is not observed when NOM is present in the feed. These results suggest the type of DOC may have different competitive behavior.

From the breakthrough curves, it is difficult to clarify if DOC interferes with the adsorption (although strong interference leading to an early breakthrough can be already excluded). For this reason, in the next section, the influence of DOC on the mass of E2 that adsorbs in the PBSAC mat is investigated.

5.3.4 Analysis of the mass adsorbed in the PBSAC mat

The mass of E2 adsorbed in the PBSAC mat as compared to the one available is determined to investigate the actual adsorption efficiency of the PBSAC mat in the presence of DOC. The mass of E2 adsorbed to each membrane is first calculated from the experiments without the PBSAC mat. Further, the mass of E2 that remained in the cell (retentate) is determined for each experiment. The mass of E2 available for adsorption in the mat is obtained subtracting, to the initial mass in the feed, E2 adsorbed to the membrane and the one remaining in the cell (Eq. (5.4)). Finally, the

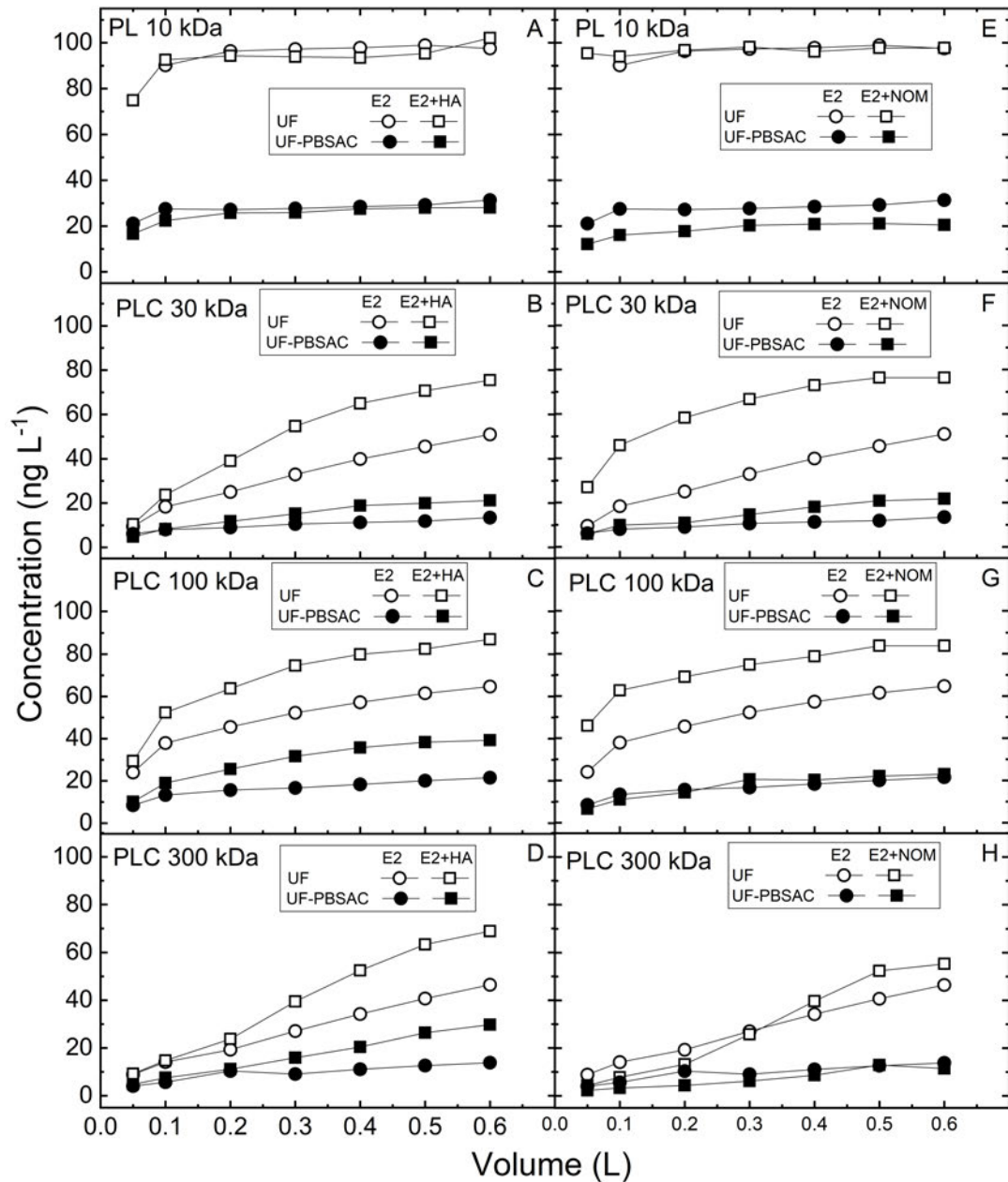


Figure 5.8: E2 breakthrough curves of filtration with high-pressure UF (MWCO 10-300 kDa) and UF-PBSAC. E2 feed conc. 100 ng L^{-1} . DOC feed conc. 10 mg C L^{-1} . Flux: $125 \text{ L m}^{-2} \text{ h}^{-1}$. Stirring 400 rpm. Temperature $23 \text{ }^\circ\text{C}$. Adapted from [144].

mass adsorbed to the PBSAC mat (again subtracting the contribution of the membrane) is compared to the one available for adsorption (Eq. (5.5)) and is plotted in Fig. 5.9 for both type of DOC. An error of 10 % on the mass adsorbed is assumed based on triplicates experiments reported in Appendix B.2.

From Fig. 5.9, it can be confirmed that DOC does not compromise the adsorption process in the whole MWCO range. At least 60 % of the E2 mass available adsorbs in the PBSAC mat. However, a minor interference of HA (5-15 %) can be noticed when MWCO of the UF is larger than 10 kDa (in particular for 100 and 300 kDa) in Figure Fig. 5.9A. On the contrary, no clear trend is visible for NOM (Fig. 5.9B).

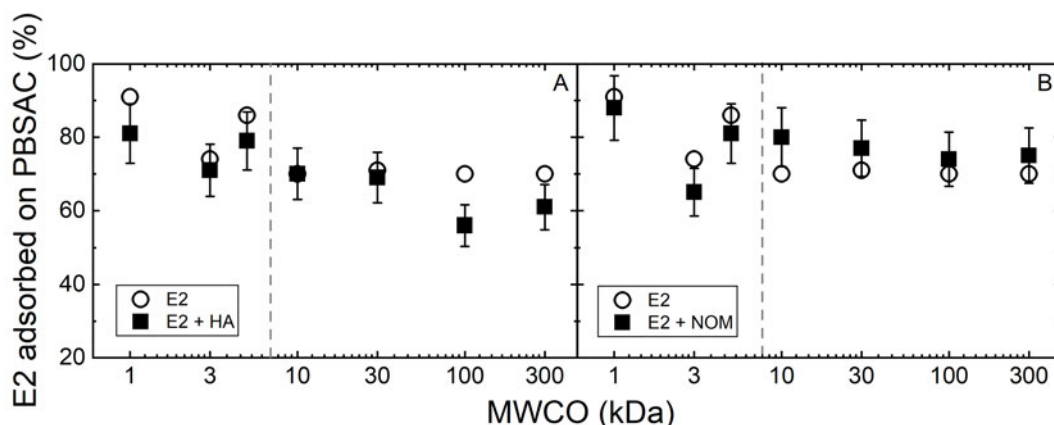


Figure 5.9: Adsorbed E2 (relative to the E2 available for PBSAC, hence subtracting the contribution of membrane adsorption and retention) in pure water and water containing HA (A) and NOM (B). Dashed lines separate membranes operated at $40 \text{ L m}^{-2} \text{ h}^{-1}$ (1-5 kDa) to the ones operated at $125 \text{ L m}^{-2} \text{ h}^{-1}$ (10-300 kDa). Adapted from [144].

These results suggest that the minor interference observed for HA is related to the presence of the larger DOC fractions (HS) in the permeate. Indeed, the interference is not observed for MWCO lower than 10 kDa, where the humic substances are rejected by the membrane.

To further clarify the impact of the DOC type on the process, the concentration of E2 in the feed at the end of the experiment (retentate) was considered.

5.3.5 Impact of the DOC type on the rejection of E2

E2 retentate concentrations in the presence and absence of DOC are plotted in Fig. 5.10A&B, while DOC retentate concentrations in Fig. 5.10C&D.

When only E2 is present in the feed, the retentate concentration of E2 is significantly higher compared to the feed only for a MWCO of 1 kDa (Fig. 5.10A&B). On the other hand, the presence of HA in the feed increases the retention of E2 by UF in the whole MWCO range, as shown in Fig. 5.10A. The increase of E2 concentration in the retentate correlates with the amount of HA retained by the UF (Fig. 5.10C) and hence its MWCO. As discussed in the introduction to this chapter, this effect was already reported in the literature. It is caused by the binding of E2 to DOC; as the membrane rejects the DOC, the E2 bound to DOC is also rejected.

For NOM, this increase in the rejection of E2 is not observed (Fig. 5.10B), although the rejection of DOC itself follows a similar trend for HA and NOM (Fig. 5.10C&D). This difference highlights that the two types of DOC have a different affinity to E2. In short, E2 does not significantly bind to NOM. This is probably related to the characteristics of the organic matter. HA has a higher value of SUVA compared to NOM (Table 5.4), which has been reported to increase the interaction with hormones [160]. This consideration can help to understand better the previous results on the interference of DOC on E2 adsorption. Apparently, the minor interference observed for HA (and not for NOM) is related to the binding of E2 to HA. E2 bound to HA flows

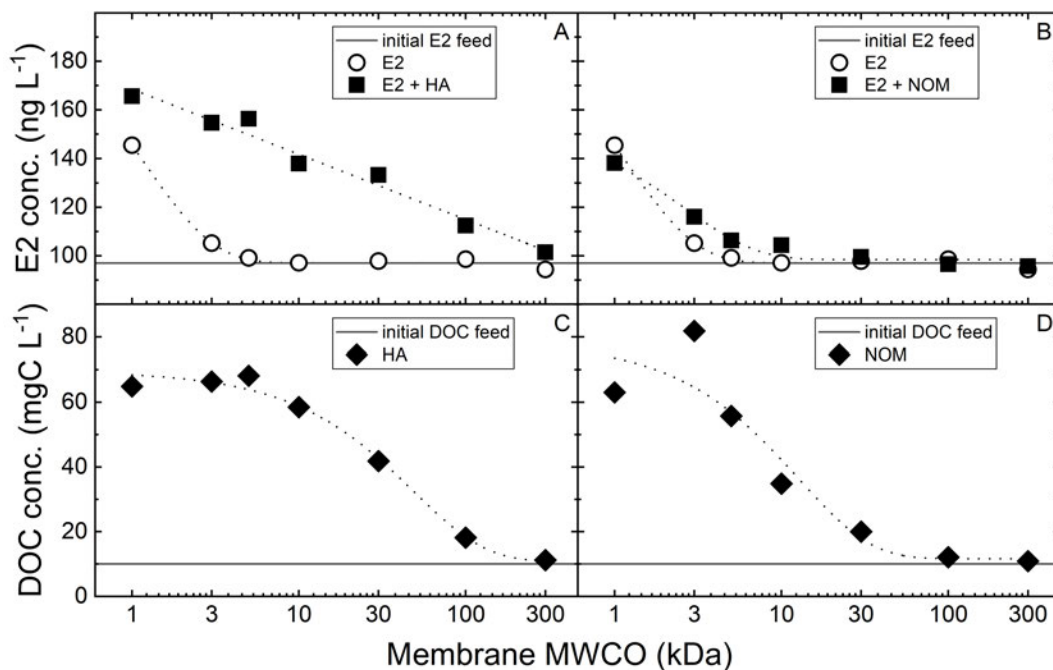


Figure 5.10: Retentate concentrations of E2 (A and B) and DOC (C and D) as a function of the MWCO of the membrane for HA (A and C) and NOM (B and D). Adapted from [144].

through the PBSAC mat without being adsorbed. Thus, an indirect competition of HA is observed while it is not occurring for NOM.

Although direct competition for the adsorption sites was not evident, it could be related to the fact that the volume filtered in this work is not enough. At higher volume filtrated, the adsorption of DOC on PBSAC could reduce the adsorption capacity for E2 (thus, having an impact on the process). Direct competition can occur only if some fractions of DOC effectively adsorb on PBSAC. For this reason, the adsorbability of the different fractions of DOC is considered in the next section.

5.3.6 Adsorbability of DOC on PBSAC

Static adsorption experiments were carried to clarify if DOC adsorbs to PBSAC. The meaningful DOC fractions were quantified with LC-OCD as a function of time during static adsorption experiments (Fig. 5.11).

Fig. 5.11 shows that all three fractions both from HA and NOM can, at least marginally, adsorb on PBSAC. HS and BB from NOM appear to adsorb more effectively compared to the ones from HA. For HA, the removal of HS and BB at the end of the experiment is 25 % and 12 %, respectively, compared to 55 % and 50 % for NOM. The fraction more likely competing with E2 is LMW neutral, but they are also only marginally adsorbing to PBSAC (Fig. 5.11C&F). Indeed, it can be observed that LMW neutrals adsorb faster compared to HS and BB. After 8 h, the concentration of LMW neutrals is already reduced to the final (equilibrium) value, while it keeps decreasing after 8 h for HS and BB (within the experimental error).

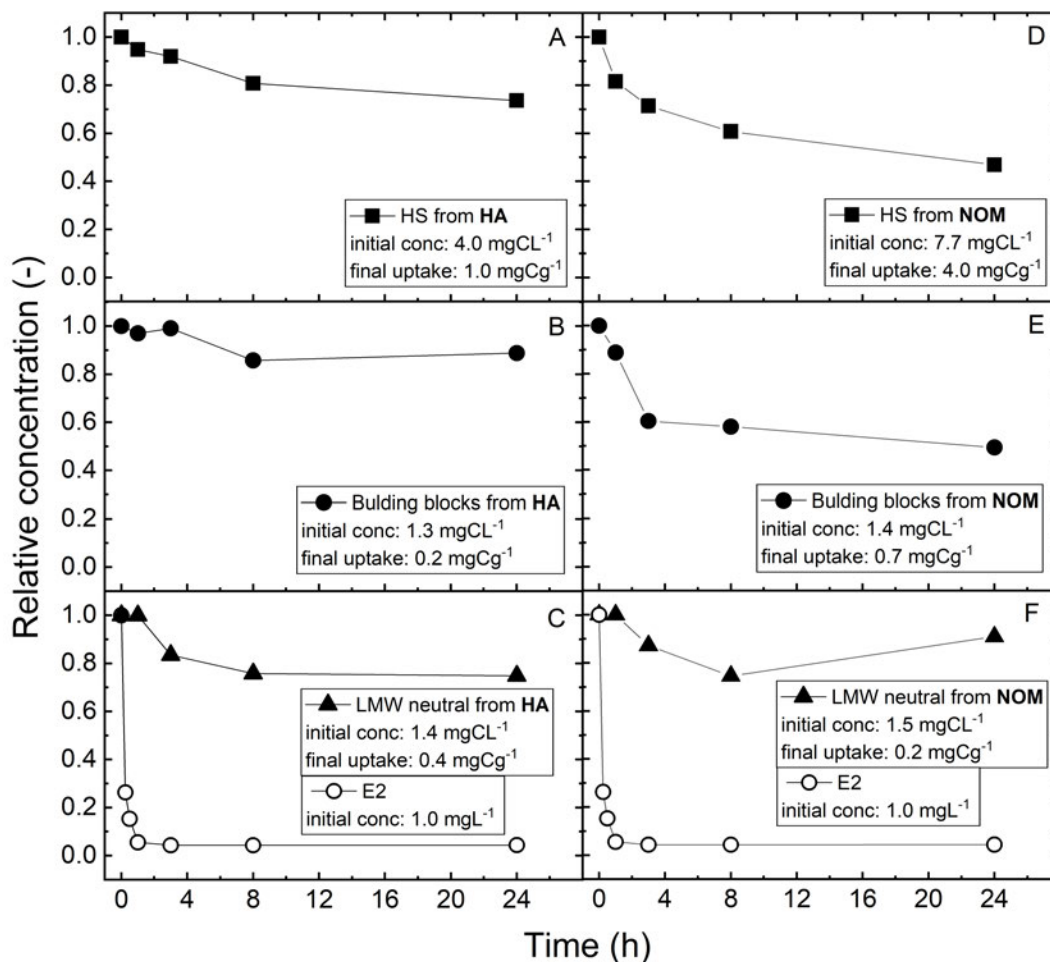


Figure 5.11: Relative concentration of HS, BB and LMW neutrals from HA and NOM as a function time during static adsorption experiments. The initial concentration and the final uptake by PBSAC are reported in the legend for each fraction. PBSAC concentration 1 g L⁻¹.

In Fig. 5.11C&F, the adsorption kinetics of LMW neutrals is compared to the one of E2 in the same range of initial concentration (1 mgC L⁻¹ for E2 and 1.4-1.5 mgC L⁻¹ for LMW neutrals). It is clear that E2 not only is characterized by a substantial higher removal, but also by faster kinetics in that the adsorption process reaches the equilibrium after only 1 h. Thus, the lack of direct competition appears to be related to the much slower adsorption kinetics of DOC compared to E2. In this sense, the size of DOC fractions may be the critical factor that slower the kinetics because DOC molecules are hindered from accessing the majority of the pores of PBSAC, confirming previous findings [149, 150].

In the last section, the accessibility of different common and easy-to-detect dyes with increased MW was investigated by comparing the adsorption isotherms on PBSAC.

5.3.7 Adsorption isotherms of dyes with different MW

Some dyes were selected to cover a meaningful MW range (317-1373 Da, Table 5.5). The adsorption isotherms of the dyes on PBSAC are reported in Fig. 5.12A.

5.3. Results and discussion

Table 5.5: List of the dyes used as tracers with increasing MW. Information about the size and the charge.

| Dye | Molecular weight <i>Da</i> or $g\ mol^{-1}$ | Charge characteristics at pH 8 |
|-----------------------------------|--|--|
| Methylene blue (MB) | 317 | <i>positively charged</i> |
| Methylene orange (MO) | 321 | <i>negatively charged</i> |
| Malachite green (MG) (oxalate) | 364 (128) | <i>positively charged (negatively charged)</i> |
| Rhodamine B (RhB) | 479 | <i>overall neutral but with 1 positive and 1 negative charge</i> |
| Titan yellow (TY) | 695 | <i>negatively charged</i> |
| Red direct 80 (RD80) | 1373 | <i>negatively charged</i> |

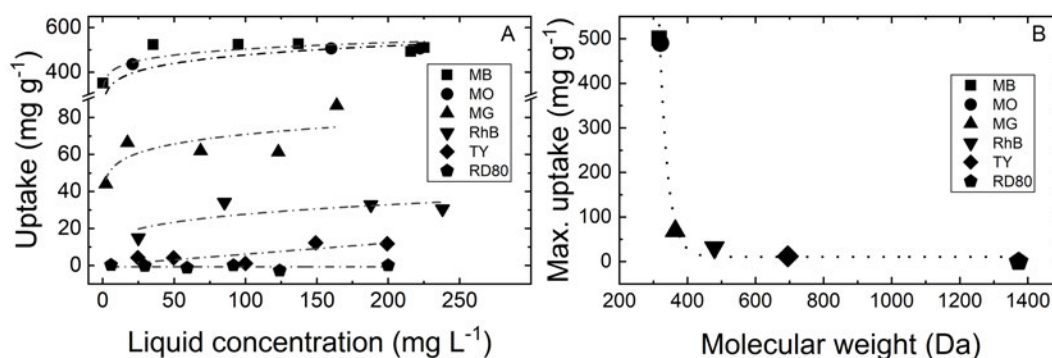


Figure 5.12: (A) adsorption isotherms of dyes with increasing MW; (B) maximum experimental uptake as a function of MW. PBSAC (200 μ m) concentration 0.5 $g\ L^{-1}$. Temperature 20 $^{\circ}C$. Equilibrium time 96 h.

The maximum uptake by PBSAC is clearly affected by the MW of the compound, as shown in Fig. 5.12B. For the smaller dyes (MB and MO), the maximum uptake is $\approx 500\ mg\ g^{-1}$. Increasing the MW, it drops to 10-90 $mg\ g^{-1}$. For the largest dyes used (1373 Da), no adsorption at all is measurable. Adsorption to the external PBSAC surface might be occurring but leading to a really small uptake that is not measurable with UV-vis.

These results suggest that the PBSAC porosity can be fully accessed only by molecules of ~ 300 Da. However, Table 5.5 indicates that the dyes used have different charge characteristics that may also affect the adsorption. Thus the size of the molecule is not the only parameter varied. The role of the chemistry of the dye in the adsorption isotherm needs to be further clarified to draw solid conclusions about the influence of the size. It is also worth mentioning that malachite green (MG) was actually used in the form of malachite green oxalate. Oxalate molecules may also adsorb to PBSAC, covering part of the surface area available for MG. In brief, the maximum uptake for MG reported in Fig. 5.12B may be underestimated.

5.3.8 Considerations about membrane cleaning

Membrane fouling is a phenomenon known to affect severely the performance of membrane filtration. As a consequence, cleaning of the membrane is a required operation to remove foulants deposited on the membrane active layer. The saturation time of PBSAC was discussed to be in order of years in Section 2.3.5, while membrane cleaning can range between 20 min to several months (Table 5.6) depending on the cleaning strategy used. For this reason, membrane cleaning is expected to take place many times before the PBSAC layer get saturated (and thus needs to be replaced).

Thus, it is relevant to discuss the compatibility of a permeate-side PBSAC layer with membrane cleaning. Table 5.6 reports two common strategies to clean fouled membranes, namely hydraulic backwash and chemical cleaning. Hydraulic backwash for UF membranes is performed at pressure ranging between 0.2 bar and 2 bar. On the other hand, chemical cleaning is typically performed either with strong acidic or basic solution. The intrinsic adsorptive properties of PBSAC should not be affected by backwash or contact with acid or base (indeed, adsorption of hormones onto PBSAC was previously shown to be unaffected by the pH in the range 2 to 12 [54]). In summary, the PBSAC layer on the permeate side is expected to be compatible with conventional membrane cleaning strategies.

Table 5.6: Cleaning frequency and typical conditions of conventional cleaning processes for fouled UF membranes. Adapted from [144].

| Cleaning process | Frequency [161] | Conditions [162, 163] |
|--------------------|--|------------------------------|
| Hydraulic backwash | 20-90 min or daily if coupled with chemical cleaning | Backwash pressure: 0.2-2 bar |
| Chemical cleaning | 1-3 months (in case of cleaning in place) | pH: 2-12 |

5.4 Conclusions

- LC-OCD results show that the two types of DOC used, namely HA and NOM, have different characteristics. In particular, SUVA is 13.7 and 6.0 L mg⁻¹ m⁻¹ for HA and NOM, respectively.
- In the presence of HA, the rejection of E2 by UF increases, as reported in the literature. However, the increase of the rejection in the presence of NOM is not significant. The different behavior highlights that HA interacts stronger with E2 compared to NOM, which in turn is related to its higher SUVA.
- UF membranes can contribute to the removal of E2 in the UF-PBSAC due to adsorption. Adsorption of E2 by UF is independent of the MWCO, but it is

related to the UF series. Millipore PL membranes adsorb a significant amount of hormones, while adsorption is negligible for PLH membranes.

- Overall, the presence of DOC (10 mgC L⁻¹) does not compromise the adsorption process of E2 (100 ng L⁻¹) in the PBSAC layer. No early breakthrough was observed independently of the membrane MWCO and the type of DOC used.
- Minor interference by HA was observed for UF MWCO > 10 kDa. The mass of E2 adsorbed in the layer was calculated by means of a mass balance. The mass adsorbed is reduced from 70 % (MWCO of 10 kDa) to 56 and 61 % (MWCO of 100 and 300 kDa, respectively).
- The larger HA fractions can indirectly compete due to the interaction between E2 and HA molecules. The E2 molecules bound to HA flow through the PBSAC mat without being adsorbed.
- The lack of an early breakthrough scenario was attributed to the lack of direct competition for the adsorption sites. Batch kinetics experiments highlighted that, although DOC can adsorb partially to PBSAC, its adsorption kinetics is significantly slower compared to the one of E2.
- The slow adsorption kinetics of all DOC fractions (including LMW neutrals) appears to be caused by the size-based-exclusion of DOC molecules to the major part of the PBSAC porosity. The adsorption capacity of dyes (used as tracers of different MW) decreased from 500 mg g⁻¹ for MW of 320 Da to less than 30 mg g⁻¹ for MW higher than 500 Da.

Chapter 6

Conclusion and outlook

Chapter 2 demonstrates that permeate side PBSAC adsorption of estrogens is a promising approach to reduce the concentration of these compounds from water. Significant removals from 60 to 80 % were achieved for four steroid estrogens when a 2.2 mm thick commercial PBSAC filter was placed on the permeate side of a UF membrane. In this PBSAC filter, particles (450 μm in diameter) are held together employing a glue. The adsorption process is effective even if the empty bed contact time applied (≈ 1 min) is remarkably reduced compared to that of conventional activated carbon processes. The removal for the most estrogenic hormone, estradiol, was further increased to 94 % by placing five PBSAC filters corresponding to a total thickness of the adsorbent bed of 11 mm.

Using a millimetric adsorbent layer brings not only short contact time but also an expected reduced maximum pollutant uptake (hence the lifetime of the adsorbent). The experimental evidence from this work shows that reduced maximum uptake of the thin layer may not be a limiting factor when only trace pollutants adsorb to the PBSAC layer. Further, the adsorption process revealed to be more efficient when PBSAC particles are packed in a millimetric layer (e.g., without the use of the glue). In this case, the maximum removal of 94 % could be achieved with an adsorbent layer of only 2 mm (compared to 11 mm for the commercial PBSAC filter).

The systematic investigation of the material characteristics of PBSAC (Chapter 3) has highlighted room for further advancement of the adsorption process in a millimetric adsorbent layer. The most critical parameter able to improve the adsorption process is the size of the particles packed in the layer. Smaller PBSAC translates into a larger external surface area available for immediate adsorption. As a consequence, the removal of estradiol can be increased to 99 % by decreasing the diameter of PBSAC down to 80 μm . The implication on the process is that estradiol can be reduced to the required drinking water level using a layer of 2 and 4 mm for PBSAC of 80 and 200 μm , respectively (for a feed concentration of 100 ng L^{-1}).

On the other side, the internal porous morphology (specific surface and micropores volume) was shown to have no influence on the initial rate adsorption of estradiol. However, the adsorption isotherms for methylene blue (at high concentration) highlighted that higher specific surface area and micropores volume are expected to influence the maximum uptake (hence the lifetime) of the PBSAC layer.

Some interesting outcomes were provided by the investigation of the surface chemistry of PBSAC. By increasing the oxygen content on the adsorbent surface (from 4.1 to 9.1 %atomic), the removal of OH-containing estrogens (estradiol) was

increased. This behavior was attributed to the formation of hydrogen bonds between the pollutant and the surface of PBSAC, resulting in enhanced adsorption kinetics. Again, the implication on the process is the possibility to reduce estrogens concentration to the desired level using a thinner layer (for PBSAC with a diameter of 200 μm , from 4 mm to 2 mm at a "standard" and increased oxygen content, respectively).

The primary role of the diameter of PBSAC compared to its porous morphology suggested that the adsorption process is dominated by film diffusion compared to diffusion inside the adsorbent. To confirm this hypothesis, a transport-adsorption model was formulated and the simulated breakthrough curves compared to the experimental one for three PBSAC diameters (Chapter 4). The peculiar thin adsorbent bed used influences the axial dispersion of pollutants. Empirical correlations available in the literature to estimate the dispersion coefficient can not be applied in the case of a millimetric layer. The dispersion coefficient estimated via the best-fitting to the experimental data was shown to depend mainly on the ratio between bed thickness and particle diameter. Using the axial dispersion coefficients obtained by the best-fitting procedure, the developed model can be used to simulate a priori the breakthrough curve of micropollutants. In particular, the minimum layer thickness in order to meet the target permeate concentration (for estradiol: 1 ng L^{-1} , drinking water) was predicted for a realistically wide range of feed concentrations (5 - 200 ng L^{-1}).

Finally, in Chapter 5, the impact of background organic carbon on the adsorption of estradiol in the UF-PBSAC mat was assessed. The adsorption process revealed to be strong and only minorly affected by the presence of organic matter, although present in water at much higher concentration (10 mgC L^{-1}) compared to estradiol (100 ng L^{-1}). Minor competitive effects, reducing estradiol adsorption on PBSAC of about 10 %, were observed for commercial humic acid (as the source of organic matter) only when the molecular weight cut-off of the UF was equal or larger of 10 kDa. These results indicate that the larger fraction of humic acid can reduce the adsorption of estradiol if they access the adsorbing layer. However, the same effect was not observed for a natural surface water, which is characterized by a lower specific UV absorbance (hence aromatic content). For this reason, the competitive effect of humic acid (not observed with natural water) was attributed to the binding of estradiol to the organic matter molecules, a phenomenon known to be enhanced for high aromaticity organic carbon.

Static adsorption experiments have further highlighted that both types of organic matter can adsorb to PBSAC, but they present a notably lower adsorption kinetics compared to E2. The size-based exclusion of organic matter molecules to the PBSAC porosity was identified as the reason for this slow adsorption kinetic. In fact, the adsorption capacity of dyes (used as tracers of different MW) decreased from 500 mg g^{-1} for MW of 320 Da (similar to hormones) to less than 30 mg g^{-1} for MW higher than 500 Da.

The work presented in this thesis opens to additional research questions. Future work should focus on the experimental determination of the breakthrough time of hormones in the UF-PBSAC. The estimation reported in Chapter 2 and Chapter 3 are helpful to have an order of magnitude of this breakthrough time, but it is based on rather weak assumptions that should be further verified. Alternatively, the breakthrough time could be predicted using the model formulated in Chapter 3 coupled with an adsorption isotherm measured in the non-linear range. The latter is challenging to obtain at a laboratory scale due to the low solubility of hormones in water ($\approx 1 \text{ mg L}^{-1}$ for estradiol). An attempt should be made by employing an extremely low PBSAC concentration, so either by increasing the volume of hormones or reducing the amount of PBSAC placed in the flask.

Besides, several intriguing phenomena were observed that could be elaborate in different research projects. First, the deteriorated filtration performance of nanofiltration membranes when an adsorbing layer is placed on the permeate side could be clarified by targeted experiments. The permeate side adsorbent can affect the rejection mechanism described by the solution-diffusion theory. Thus, the filtration of hormones in the NF-PBSAC could be investigated by varying the parameters that most affect the permeate side concentration (e.g., PBSAC size and layer thickness). Second, Chapter 3 reports interesting results on the influence of oxygen content on the adsorption kinetic of hormones. In the literature, the studies on the surface chemistry of activated have mainly focused on the equilibrium adsorption characteristics (rather the kinetics). The possibility to tune the adsorption kinetic towards different pollutants by varying the surface chemistry on the carbon is indeed intriguing. However, kinetics tests should be performed by using micropollutants with chemical properties very different from each other to provide a systematic understanding of this phenomenon.

Further effort is indeed needed in the modeling of hormones adsorption in the thin packed-layer. While the results presented in Chapter 4 helps to have insight into the mechanism, a satisfying validation of this model was not achieved. At the current state, the model can not be used to predict the breakthrough curve of any micropollutants from its adsorption isotherm. In particular, the role of the axial dispersion needs further investigation. Modeling the breakthrough curve of a solute that does not adsorb and enter the pores would be the first step. In these conditions, the film transport and the equilibrium adsorption step could be neglected. The axial dispersion coefficients could be determined in an independent way compared to the best-fit of hormones breakthrough curves.

Finally, the assessment of the impact of more complex real water (for example wastewater) would be interesting. The chemical characteristics of background organic carbon vary much depending on the type of water (e.g., surface or wastewater) and on other factors such as geography. In the last section of Chapter 5, the proof of principle of a simple methodology to estimate a sort of pore-exclusion-molecular-weight of organic carbon (thus the maximum molecular weight that allows organic

molecules to enter the porosity of PBAC) was presented. Due to its simplicity, this methodology may be really helpful in predicting the impact of organic carbon on the adsorption of micropollutants onto activated carbon.

Appendix A

Supporting information on analytical methodology

A.1 Hormones solution preparation

Native hormone solutions from Perkin Elmer are supplied in 1 mL ethanol solution. They have a total activity of 1 mCi (3.7×10^7 Bq) and a specific activity that varies depending on the batch (from 70 to 94 Ci mmol^{-1}). The actual concentration of hormones in the supplied bottles can be calculated from a total and specific activity. For example, for E2(Ch 18/08/17) batch that has a specific activity of 94 Ci mmol^{-1} (3.478×10^{15} Bq mmol^{-1}) it follows:

$$\begin{aligned} \text{mass E2 in the bottle} &= \frac{\text{Total activity}}{\text{Specific activity}} \text{MW} = \\ &= \frac{3.7 \cdot 10^7 \text{ Bq}}{3.478 \cdot 10^{15} \text{ Bq mol}^{-1}} 272 \text{ g mol}^{-1} = 2.90 \cdot 10^{-6} \text{ g} \quad (\text{A.1}) \end{aligned}$$

$$\begin{aligned} \text{concentration E2 in the bottle} &= \frac{\text{mass of E2}}{\text{volume}} = \\ &= \frac{2.90 \cdot 10^{-6} \text{ g}}{10^{-3} \text{ L}} = 2.90 \text{ mg L}^{-1} \quad (\text{A.2}) \end{aligned}$$

For a solution with hormone concentration higher than 100 ng L^{-1} , non labeled hormones are also used. The volume needed of non-labeled (nL) stock solution (10 mg L^{-1} in 100 % methanol), V_{nL} is calculated using the following mass balance:

$$\text{conc}_{total} \text{Vol}_{total} = \text{conc}_{3H} \text{Vol}_{3H} + \text{conc}_{nL} \text{Vol}_{nL} \quad (\text{A.3})$$

Considering that $\text{conc}_{3H} = 100 \text{ ng L}^{-1}$ and introducing $\text{Vol}_{3H} = \text{Vol}_{tot} - \text{Vol}_{nL}$, it results:

$$\text{Vol}_{nL} = \frac{\text{conc}_{total} - \text{conc}_{3H}}{\text{conc}_{nL} - \text{conc}_{3H}} \quad (\text{A.4})$$

So, the solution of estradiol 100 $\mu\text{g L}^{-1}$ used in Fig. A.1 is prepared by adding 9.99 mL of non-labeled E2 stock (10 mg L^{-1}) per L of solution. This solution contains 1 %vol of methanol. In order to verify what is the effect (or interference) of methanol

on the adsorption of E2, a static adsorption kinetic experiment was carried using 10 %vol of methanol and compared to the results in the absence of methanol.

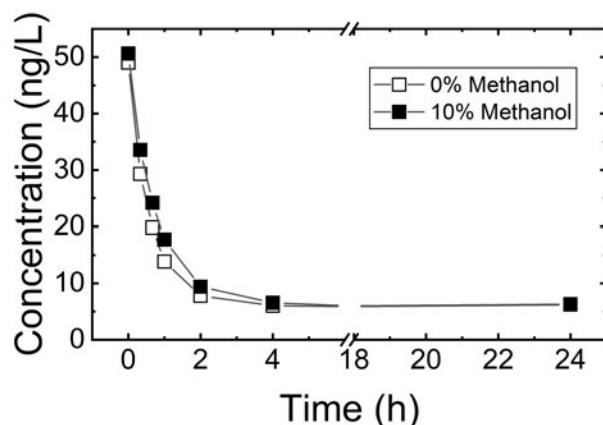


Figure A.1: E2 concentration as a function of time for the normal buffer (1 mM NaHCO₃, 10 mM NaCl) and the same buffer containing 10 % in volume of methanol (initial concentration: 50 ng L⁻¹, 20 °C, 260 rpm, pH 8).

The presence of methanol did not affect the equilibrium (high contact times) concentration of estradiol (E2). On the contrary, the kinetic is slightly slower when methanol is present. This means that for dynamic adsorption experiments, the methanol could have a negative effect because the contact time are generally lower or equal to 1 min.

A.2 Calibration curves of hormones

The tritium-labeled hormones used in Chapter 1 have a specific activity of 70, 94, 98 and 80 Ci mmol⁻¹ for E2, E1, P and T respectively. Calibration curves were obtained by preparing standards with different concentrations and measuring their activity. Initially, 7 points (0, 0.1, 1, 5, 12.5, 25, 50, 100 ng L⁻¹) calibration was performed for E2. For the other hormones, the calibration was limited to 3 points and the blank (0, 1, 10, 100 ng L⁻¹). The calibration curves used in Chapter 1 are reported in Fig. A.2.

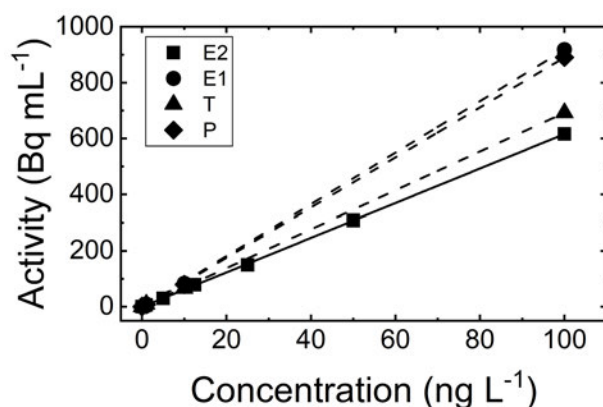


Figure A.2: Calibration curves of E2, E1, T and P solutions used in Chapter 2. Standards were prepared in 1 mM NaHCO₃, 10 mM NaCl.

The calibration curves for E1, T and P used in Chapter 2 are reported in Fig. A.3. The calibration of E2 used in Chapter 4 is reported in Fig. A.4.

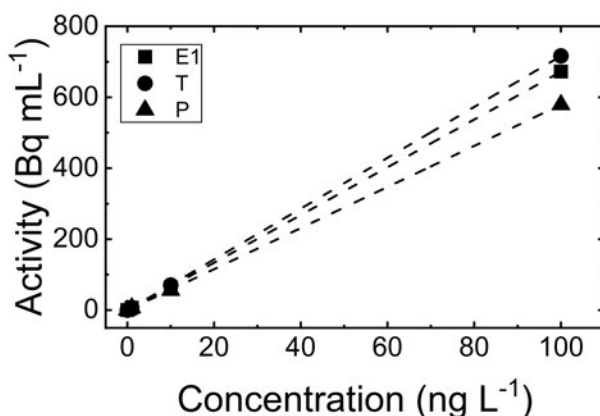


Figure A.3: Calibration curves of E1, T and P solutions used in Chapter 3. Standards were prepared in 1 mM NaHCO₃, 10 mM NaCl.

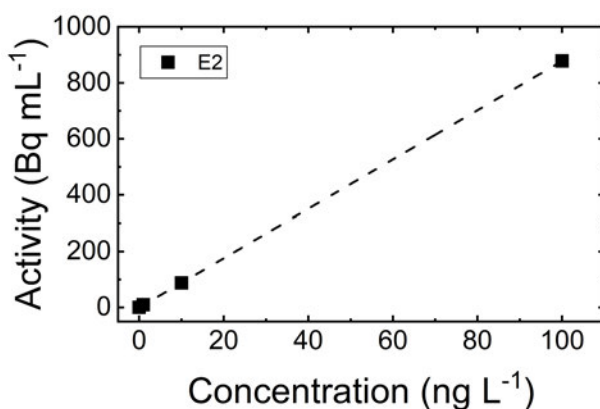


Figure A.4: Calibration curves of E2 used in Chapter 5. Standards were prepared in 1 mM NaHCO₃, 10 mM NaCl.

A.3 Ethanol interference in LC-OCD analysis

LC-OCD gives a significant OCD signal at approximately 40 min (Fig. A.5). After the addition of E2 to the feed waters, the values for organic matter, SUVA and LMW neutrals are heavily distorted by the solvent ethanol (Table A.1). Therefore, these values cannot be used for analyzing the samples. Besides, LMW acids are neither reliable nor significant since their concentration is so low that changes are mostly within the error. On the contrary, the HS peak is (retention time 20 min) is not affected by the ethanol peak (retention time 40 min).

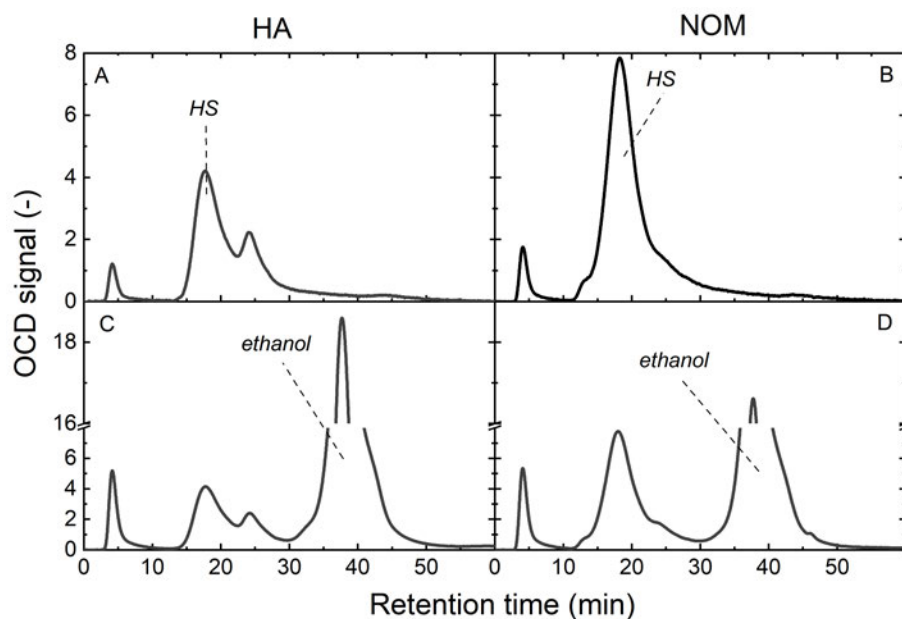


Figure A.5: LC-OCD chromatograms of HA and NOM feed solution diluted by a factor of 4 with Milli-Q before (A and B) and after the addition of 100 ng L^{-1} E2 solved in a 0.004 %vol ethanol aqueous solution (C and D).

Table A.1: Comparison between the concentrations of the different fractions of HA before and after the addition of E2 (and consequently ethanol).

| | | HA | HA+E2 |
|------------------------|-----------------------------------|------|-------------|
| TOC (= organic matter) | mgC L^{-1} | 7.3 | 24.4 |
| SUVA | $\text{L mg}^{-1} \text{ m}^{-1}$ | 14.4 | 4.8 |
| HS | mgC^{-1} | 3.9 | 3.9 |
| SUVA-HS | $\text{L mg}^{-1} \text{ m}^{-1}$ | 13.7 | 13.9 |
| MW | g mol^{-1} | 876 | 816 |
| Building Blocks | mgC L^{-1} | 1.4 | 1.3 |
| LMW Neutrals | mgC L^{-1} | 1.3 | 17.9 |
| LMW Acids | mgC L^{-1} | 0.5 | 0.3 |

Appendix B

Supporting information on experimental methodology

B.1 Filtration protocols

Table B.1: Filtration protocols of the dynamic adsorption experiments for the UF-PBSAC mat.

| No. | Step | Conditions | Justification |
|-----|-------------------------------|---|---|
| 1 | Conditioning | Soak the membrane and the PBSAC mat in MilliQ water for 1 h | Remove glycerine coating from the membrane (if present). For hydrophobic membranes, ethanol solution is used in order to favour wetting in the next steps |
| 2 | Filtration medium preparation | Place the stainless steel support layer inside the bottom part. Place the PBSAC mat on the top of the support layer. Place the membrane on the top of the PBSAC mat. Place the internal o-ring on the top of the membrane. Mount the top part of the stirred cell and close with the clamp. | |
| 3 | Compaction wetting | Fill the cell with MilliQ water ^a , open the valve for synthetic air and adjust the pressure to 2 times the one used in the experiment (3 bar for 10 kDa RC membrane and desire flux of 100 L m ⁻² h ⁻¹). Run MilliQ through the membrane-PBSAC for 1 h. Close the valve for synthetic air and open the valve on the top part of the stirred cell in order to de-pressurize the system. | |

^a volume needed depends on the flow rate, it needs to be enough to run water for 1 h without that the cell gets completely empty

| | | | |
|---|---------------------------|--|--|
| 4 | PWF before | <p>Fill the cell with MilliQ water, open the valve for synthetic air (pressure was already adjusted in the previous step). Run MilliQ water for 30 min. Plot the mass collected in the permeate beaker as a function of time. Obtain the flowrate, 2 possible way: i) take the slope of the mass vs time curve ii) divide the total mass collected in the beaker by the time of filtration. Obtain the flux dividing the flow rate (volumetric) by the membrane area (unit: $\text{L m}^{-2} \text{h}^{-1}$). Obtain the permeability by dividing the flux by the pressure applied ($\text{L m}^{-2} \text{h}^{-1} \text{bar}^{-1}$).</p> | <p>Measure permeability of the membrane and make sure that is within the acceptable range. This is done by comparing the experimental result with the value reported by manufacturer).</p> |
| 5 | Filtration test | <p>Pour 700 mL of the feed^a solution inside the cell (ensure that the feed solution is at room temperature). Start stirring at 400 rpm if needed^b. Open the synthetic air valve (pressure was already adjusted in the previous step), the feed solution will start to flow through the membrane. Once the desired amount of permeate volume is collected in a vial, move manually the tube to the subsequent vial. Repeat the last step until the desired amount of permeate (or number of permeate samples) is reached. Open the cell and collect 10 mL of retentate from inside the cell (required for mass balance).</p> <p>^a hormone concentration of 100 ng/L and background solution composed by 10 mM NaCl and 1 mM NaHCO₃</p> <p>^b Stirring is used only if there are compounds in the feed solution that could be rejected (e.g., humic acid).</p> | <p>Perform the filtration of water contaminated. Collect different samples as a function of volume filtrated for further analysis. Obtain the graph permeate conc. vs permeate volume.</p> |
| 6 | Samples and data analysis | <p>Measure the concentration of hormones in the collected samples (including feed and retentate). Plot the permeate concentration as a function of permeate volume or time. In case a single performance parameters (such as removal or permeate concentration) needs to be used, define a fixed permeate volume (e.g. 600 mL) at which the parameter is derived.</p> | <p>Measure the concentration of hormones. Plot the breakthrough curve.</p> |

B.1. Filtration protocols

Table B.2: Filtration protocols of the dynamic adsorption experiments for the UF-PBSAC packed layer.

| No. | Step | Conditions | Justification |
|-----|-------------------------|--|--|
| 1 | Conditioning | Soak the membrane in MilliQ water for 1 h | Remove glycerine coating from the membrane (if present). For hydrophobic membranes, ethanol solution is used in order to favour wetting in the next steps. |
| 2 | PBSAC layer preparation | Weight the desired amount of PBSAC on the balance. Pour the PBSAC in the bottom part of the stirred cell. Shake gently the bottom part in order to obtain a uniform PBSAC layer. Place the membrane on the top of the PBSAC layer. Place the internal o-ring on the top of the membrane. Mount the top part of the stirred cell and close with the clamp. | |
| 3 | Wetting and PWF | Fill the cell with 900 mL of MilliQ water, open the valve for synthetic air and adjust the pressure to the one used in the experiment. Run MilliQ through the membrane-PBSAC until 600 mL of permeate is collected ^a . Close the valve for synthetic air and open the valve on the top part of the stirred cell in order to de-pressurize the system. Convert the mass collected shown in LabView to volume collected using the density (at the average temperature reported in LabView). Obtain the flowrate, 2 possible way: i) take the slope of the volume vs time curve ii) divide the total volume collected in the beaker by the time of filtration. Obtain the flux dividing the flow rate (volumetric) by the membrane area (unit: $L m^{-2} h^{-1}$). Obtain the permeability by dividing the flux by the pressure applied ($L m^{-2} h^{-1} bar^{-1}$). | Wet the PBSAC layer for determined amount of time (in order to obtain reproducible adsorption process). Measure the PWF of the UF-PBSAC (completely controlled by the UF). |

^a In this way, 300 mL of MilliQ will be in the cell after this step.

| | | | |
|---|---------------------------|--|--|
| 4 | Filtration test | <p>Pour 400 mL of the feed^a solution inside the cell (ensure that the feed solution is at room temperature). Stirred at 300 rpm for 30 seconds. Open the synthetic air valve (pressure was already adjusted in the previous step), the feed solution will start to flow through the membrane. Once the desired amount of permeate volume^b is collected in a vial, move manually the tube to the following vial. Repeat the last step until the desired amount of permeate (or number of permeate samples) is reached. Open the cell and collect 10 mL of retentate from inside the cell (required for mass balance).</p> | <p>Perform the filtration of water contaminated. Collect different samples as a function of volume filtered for further analysis. Obtain the graph permeate conc. vs permeate volume</p> |
| | | <p>^a for a desired final feed solution of 700 mL and hormone concentration of 100 ng L⁻¹, this solution needs to have hormone concentration of 175 ng L⁻¹</p> | |
| | | <p>^b sampling volume and total permeate volume collected varies depending on the experiment</p> | |
| 5 | Samples and data analysis | <p>Measure the concentration of hormones in the collected samples (including feed and retentate). Plot the permeate concentration as a function of permeate volume or time. In case a single performance parameters (such as removal or permeate concentration) needs to be used, define a fixed permeate volume (e.g. 600 mL) at which the parameter is derived.</p> | <p>Measure the concentration of hormones. Plot the breakthrough curve.</p> |

B.2 Repeatability analysis of E2 breakthrough curve

The repeatability of dynamic adsorption experiments was assessed by means of triplicate experiments in the same conditions. An experimental error was then associated with the permeate concentration or the mass adsorbed by considering the relative deviation of the maximum and minimum value from the average.

$$\%error = \frac{CONC_{max} - CONC_{min}}{CONC_{average}} \cdot 100 \quad (B.1)$$

The repeatability of the filtration of hormones in background solution (1 mM NaHCO₃ and 10 mM NaCl) through the UF coupled with the PBSAC filter mat (experiments in Chapter 1) was assessed using the following conditions: the flux of 125 ± 3 L m⁻² h⁻¹, E2 feed concentration of 101 ± 1 ng L⁻¹, 24.4 ± 1.8 °C. Fig. B.1 shows that the dynamic adsorption of E2 for the UF-PBSAC mat is repeatable. However, the error is relative high. The average error considering of all the permeate sample is 11 %.

The repeatability of the dynamic adsorption of E2 for the UF-PBSAC packed-layer was assessed using PBSAC sample with increased oxygen content. The other

B.2. Repeatability analysis of E2 breakthrough curve

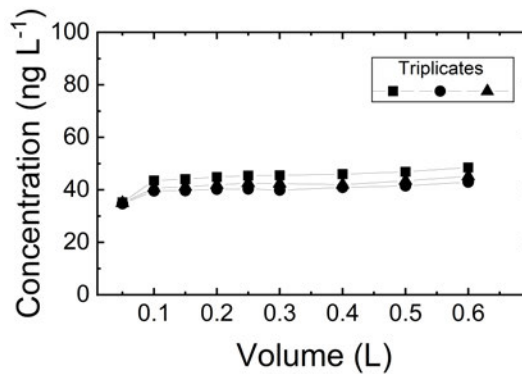


Figure B.1: Permeate concentration of E2 as a function of permeate volume for the UF-PBSAC mat in three experiments in the same conditions (flux of $125 \pm 3 \text{ L m}^{-2} \text{ h}^{-1}$, E2 feed concentration of $101 \pm 1 \text{ ng L}^{-1}$, $24.4 \pm 1.8 \text{ }^\circ\text{C}$).

experimental conditions are: flux of $397 \pm 11 \text{ L m}^{-2} \text{ h}^{-1}$, E2 feed concentration of $101 \pm 1 \text{ ng L}^{-1}$, $25.8 \pm 1.7 \text{ }^\circ\text{C}$. This is sample which give the higher removal and the lowest permeate concentration. So the experimental error for a layer containing the PBSAC with increased oxygen content is expected to be the highest because of the highest contribution of analytical error (at the lowest concentration). The relative concentration of the triplicates are shown in Fig. B.2. The relative errors on the concentration in each permeate sample ranges from 20 to 30 %. It corresponds to an absolute error of $1.5 - 2.5 \text{ ng L}^{-1}$. Considering that the difference in E2 permeate concentration between sample with increased and standard oxygen content (Fig. 3.10) is 6 ng L^{-1} , it can be concluded that this difference is related to enhanced adsorption at higher oxygen content and not simply by experimental error.

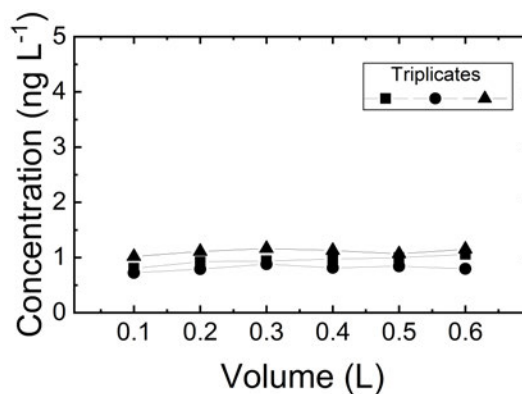


Figure B.2: Permeate concentration of E2 as a function of permeate volume for the UF-PBSAC packed-layer (PBSAC O+, see Table 3.1) in three experiments in the same conditions (flux of $397 \pm 11 \text{ L m}^{-2} \text{ h}^{-1}$, E2 feed concentration of $101 \pm 1 \text{ ng L}^{-1}$, $25.8 \pm 1.7 \text{ }^\circ\text{C}$).

Finally, the repeatability of the dynamic adsorption of E2 in presence of DOC was considered (Fig. B.3). In this case, the error on the mass adsorbed to the PBSAC mat compared to the available for adsorption is the most critical parameter because it was used to discriminate whether indirect competition is occurring. The relative error on the mass adsorbed resulted in 7 and 9 % for HA and NOM, respectively

(Table B.3). So, the difference of 10-15 % reported in Fig. 5.9 is significant even if really close to the experimental error

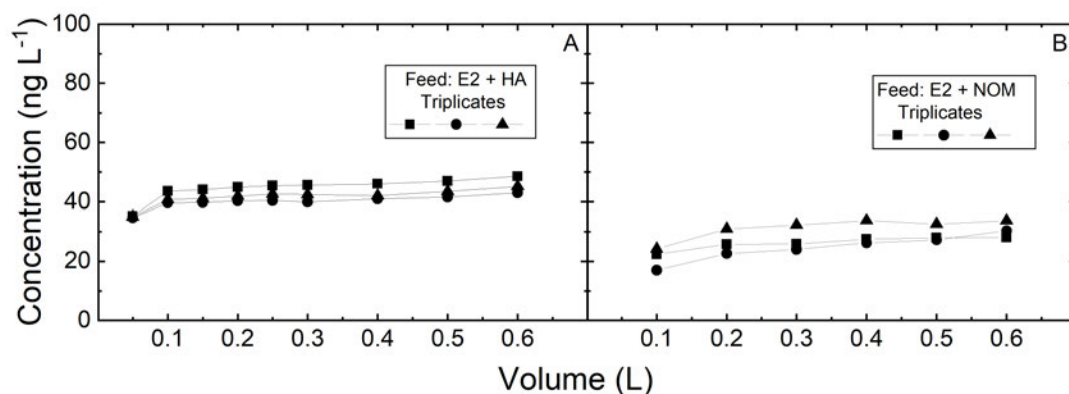


Figure B.3: Permeate concentration of E2 in presence of HA (A) and NOM (B) as a function of permeate volume for the UF-PBSAC mat in three experiments in the same conditions (flux of $125 \pm 4 \text{ L m}^{-2} \text{ h}^{-1}$, E2 feed concentration of $99 \pm 3 \text{ ng L}^{-1}$, $23.8 \pm 1.3 \text{ }^\circ\text{C}$).

Table B.3: Mass of E2 adsorbed to PBSAC at the end of the dynamic adsorption experiments reported in Fig. B.3.

| Mass of E2 adsorbed relative to the available ^a | | | |
|--|-------|-------|--------------------|
| Rep 1 | Rep 2 | Rep 3 | Error ^b |
| % | % | % | % |
| <i>Humic acid</i> | | | |
| 73 | 73 | 67 | 7 |
| <i>Natural organic matter</i> | | | |
| 81 | 75 | 79 | 9 |

^acalculated based on Eq. (5.5) (Chapter 5)

^bcalculated based on Eq. (B.1)

Appendix C

Supporting results

C.1 Influence of the thickness on E2 removal for the UF-PBSAC mat

In this section, the E2 concentration measured at an increasing number of PBSAC mat is compared to the expected one in the ideal case (as if each layer is characterized by the same removal, and they act as separated layers in series) (Fig. C.1). The permeate concentration after n layer can be calculated based on the removal R and the inlet concentration in the first layer (c_{feed}) from Eq. (C.1):

$$c_{permeate,n} = c_{feed} (1 - R)^n \quad (C.1)$$

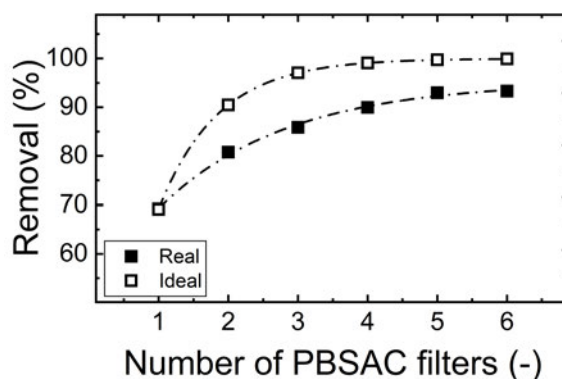


Figure C.1: Comparison between experimental and ideal (see Eq. (C.1)) for definition) removal of E2 at an increasing number of PBSAC mat.

From (Fig. C.1) it is evident that the experimental removal is lower than the ideal one. The adsorption process is then not independent in each layer, but increasing the thickness may change the mass transport regime compared to the single layer.

C.2 Estimation of the mass of PBSAC in the mat

The mass of PBSAC per gram of PBSAC mat was obtained in the following way: (i) a PBSAC mat sample was heated in a glass beaker containing water at 100 °C for 48 h in order to remove the water-soluble glue; (ii) the glass beaker was put in the oven at 80 °C overnight in order to evaporate the water; (iii) the PBSAC remained in the beaker after water evaporation was weighted on an analytic balance; (iv) the mass

of PBSAC was divided by the initial mass of the mat (resulting in 0.8 g of PBSAC per gram of mat).

C.3 Estimation of PBSAC lifetime (breakthrough volume)

The breakthrough volume can be defined as the total volume that can be processed before the permeate concentration rises to a level higher than a target value (e.g., the limit E2 concentration for drinking water). Translating to a hypothetical real process, the breakthrough volume is the lifetime of the PBSAC layer; once it is reached, the process needs to be discontinued, and the adsorbent layer either replaced or regenerated.

The real breakthrough volume could not be determined experimentally. So the ideal breakthrough volume (Fig. C.2) was estimated in Section 2.3.5 (Chapter 2).

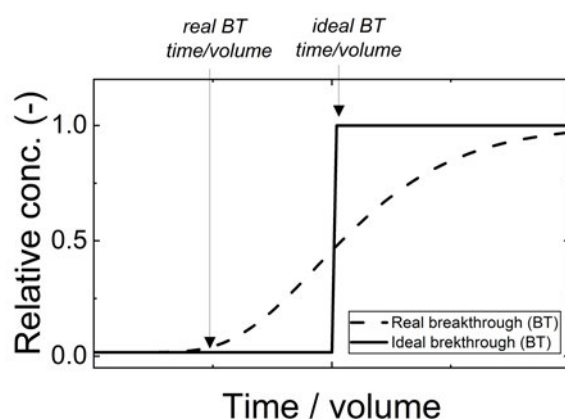


Figure C.2: Conceptual comparison between real and ideal breakthrough curves and breakthrough volume / time.

C.4 Considerations about pressure drop

The diameter of PBSAC in the packed thin layer is the most critical parameter allowing to improve the effectiveness in terms of MP removal. Using smaller adsorbents in a packed-bed also has the negative consequence of increasing the pressure drop across the bed. In this section, the pressure drop of low-pressure membranes is compared to the pressure drop across a millimetric PBSAC layer. The pressure drop across a membrane at a fixed flux can be estimated from the water permeability coefficient (C.2).

$$J_w = A \Delta P \quad (\text{C.2})$$

where J_w is the water flux (equivalent to a superficial velocity), A is the water permeability coefficient and ΔP is the pressure difference across the membrane.

C.4. Considerations about pressure drop

Table C.1 reports the values of permeability for the ultrafiltration (UF) membranes used in Chapter 5. In addition, permeability values for more open membranes (microfiltration, MF) are collected from the literature. Based on these permeabilities, the pressure drop across the membrane at a flux of $200 \text{ L m}^{-2} \text{ h}^{-1}$ can be calculated (Table C.1).

Table C.1: Permeability reported in this work (for UF) and in the literature (for MF) for some commercial low pressure membranes.

| Class | Membrane | Reported permeability | Pressure drop at $200 \text{ L m}^{-2} \text{ h}^{-1}$ |
|-------|------------------------------------|---|--|
| | | $\text{L m}^{-2} \text{ h}^{-1} \text{ bar}^{-1}$ | bar |
| UF | Millipore® Ultracel PLAC 1 kDa | 4 | 50.0 |
| | Millipore® Ultracel PLCBC 3 kDa | 5.4 | 37.0 |
| | Millipore® Ultracel PL CC 5 kDa | 13.2 | 15.2 |
| | Millipore® Ultracel PL GC 10 kDa | 86 | 2.3 |
| | Millipore® Ultracel PLC HK 100 kDa | 155 | 1.3 |
| MF | Pall® PVDF $0.1 \mu\text{m}$ | 3300 [164] | 0.06 |
| | Pall® PVDF $0.2 \mu\text{m}$ | 5900 [164] | 0.03 |
| | Millipore® PVDF $0.2 \mu\text{m}$ | 3900 [165] | 0.05 |
| | Pall® PVDF $0.45 \mu\text{m}$ | 20000 [164] | 0.01 |

The pressure drop across a packed-bed can be estimated using the Carman-Kozeny equation [166], which, for a bed packed with spherical particles, has the form of Eq. (C.3):

$$\frac{\Delta P}{L} = \frac{150 \mu}{d_p^2} \frac{(1 - \varepsilon_b)^2}{\varepsilon_b^3} u \quad (\text{C.3})$$

where ΔP is the pressure drop across the packed-bed, L is the length of the bed, μ is the dynamic viscosity, d_p is the diameter of the spherical particle packed in the bed, ε_b is the bed porosity and u is the superficial velocity.

The pressure drop at $200 \text{ L m}^{-2} \text{ h}^{-1}$ across a thin layer ($L = 2$ and 10 mm) was estimated in a particle diameter range from $600 \mu\text{m}$ to an hypothetical extremely small diameter of $10 \mu\text{m}$ (note that the smallest PBSAC used in the literature has a diameter of $80 \mu\text{m}$). Fig. C.3 shows that the pressure drop of the PBSAC layer is always at least one order of magnitude lower than the one of the membrane (even for an hypothetical PBSAC diameter of only $10 \mu\text{m}$). In a realistic PBSAC diameter range ($D_p \geq 80 \mu\text{m}$), the PBSAC layer pressure drop (highest $2 \cdot 10^{-6} \text{ bar}$) is four

order of magnitude higher than the membrane pressure drop (lowest 10^{-2} bar for MF with pore size of $0.45\ \mu\text{m}$).

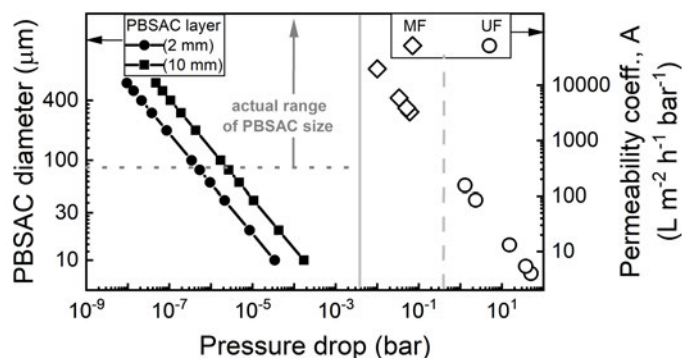


Figure C.3: Comparison of the estimated pressure drop in a PBSAC layer for decreasing particle diameter and the pressure drop in low pressure membranes estimated based on water permeability.

Focusing only the adsorbing layer, it should be noted that the pressure drop does not depend only the adsorbent size but it increases with the bed length. Thus, a thin layer has a smaller pressure drop compared to a column. For this reason, the pressure drop across a millimetric layer was compared to the one of a packed-column ($L = 0.5, 1$ and $2\ \text{m}$) in Fig. C.4.

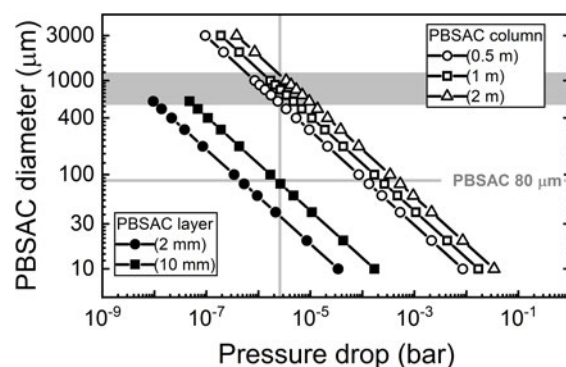


Figure C.4: Comparison of the estimated pressure drop in a PBSAC layer (2 and 10 mm) and a PBSAC column (0.5, 1 and 2 m)

Fig. C.4 shows that a layer of 10 mm thickness packed with the smallest PBSAC used ($80\ \mu\text{m}$) is characterized by a pressure drop similar to a column packed with adsorbent with a size in the range $0.6\text{--}1\ \text{mm}$.

C.5 Electrokinetic surface potential of UF membranes

The electrokinetic potential (or zeta potential) of all UF membranes used in Chapter 5 was measured using an electrokinetic analyzer (SurPASS, Anton Paar, Austria) in the streaming current mode using the adjustable gap cell for planar samples.

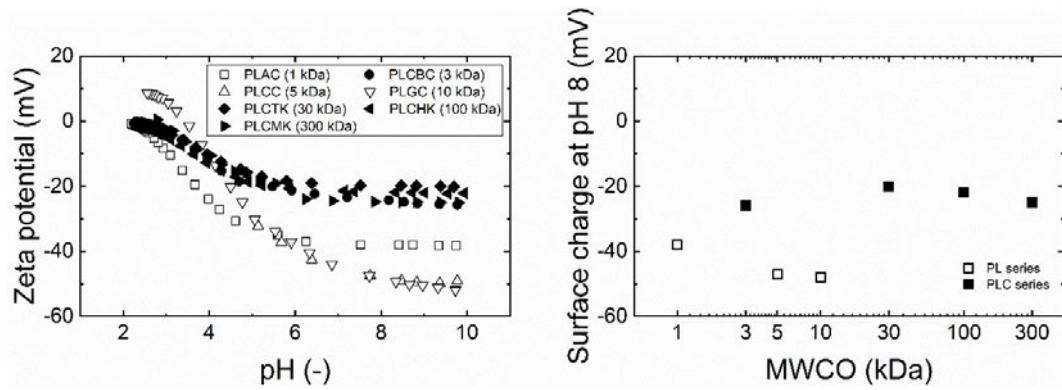


Figure C.5: Electrokinetic potential of the UF membranes as a function of pH (left) and zeta potential for the different MWCO at pH 8 (right).

Fig. C.5 shows that the zeta potential is different for UF belonging to PLC and PLH series. The electrokinetic potential for PLH membranes (-38 to -48 mV) is more negative compared to PLC (-20 to -28).

C.6 Real breakthrough curves for high-pressure UF

For the higher pressure UF membranes, MPs partitioned to organic matter are rejected by the UF. These subsequently accumulate in the cell, which leads to an increase in stirred cell concentration. The permeate concentration relative to the initial feed concentration is plotted in Fig. C.6 for the membranes with smaller MWCO.

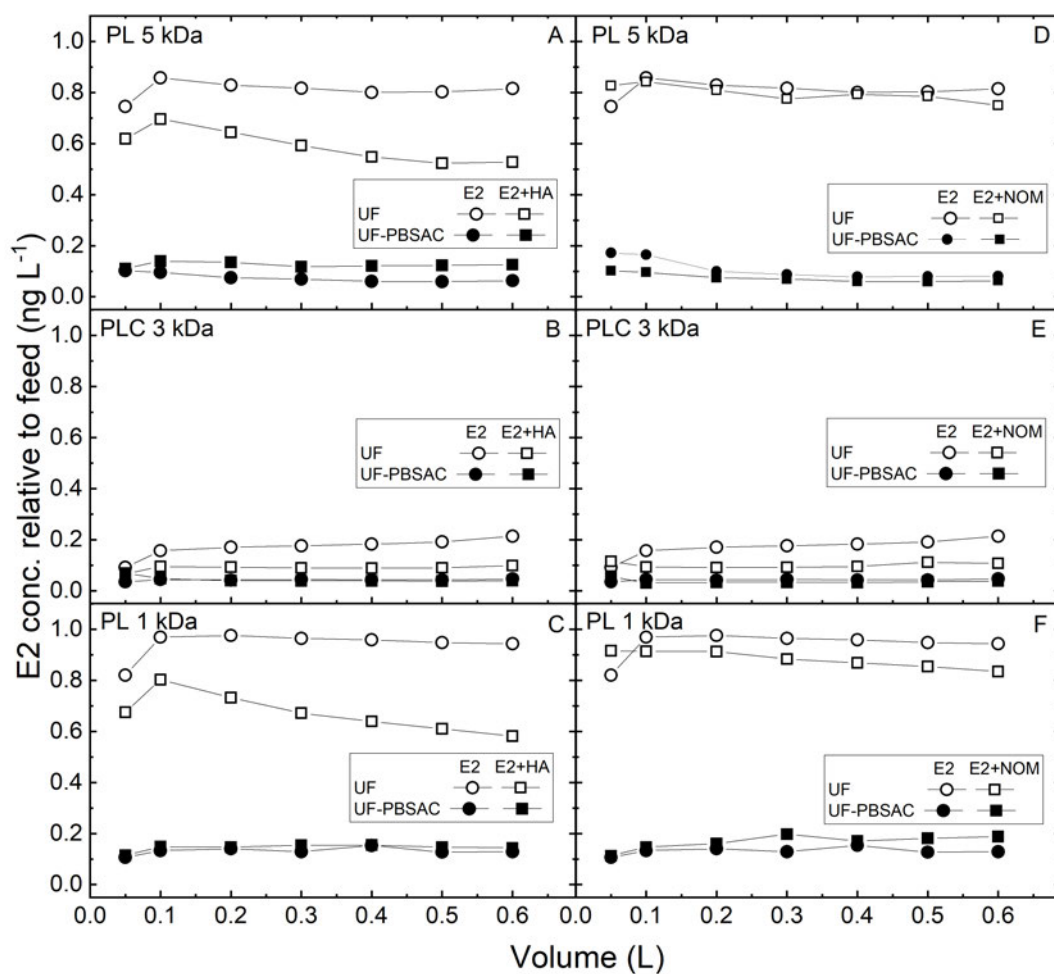


Figure C.6: Permeate E2 concentration relative to the feed as a function of permeate volume.

Appendix D

Supporting information on modeling

D.1 Membrane and system dispersion

When modeling the breakthrough curve of a fixed-bed adsorption process, the so-called "system dispersion" needs to be taken into account. Typically, system dispersion is caused by the dead-volume present in the filtration system (e.g., pump, tubing, fittings). In the case of PBSAC, the membrane is also present before the PBSAC packed-layer Fig. D.1. The UF membrane used in the first two chapters presents negligible adsorption and it can be assumed to behave as thin dispersive porous media.

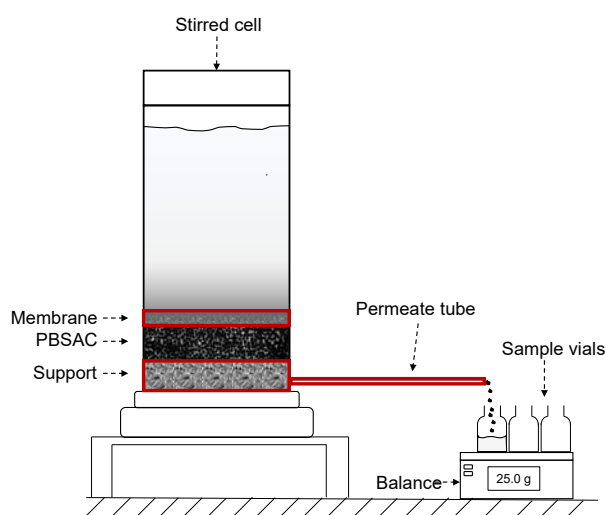


Figure D.1: Schematics of the components other than the PBSAC layer that may affect the shape the experimentally measured breakthrough curves.

Modeling the system dispersion in this case revealed to be challenging for two main reasons. First, in the stirred-cell set-up, the pressure start to rise slowly as soon as the synthetic air valve is open and some time is needed before reaching the desired pressure (set on the valve). As a consequence, the flow rate is not constant at the beginning but it increases in the first 250 s (Fig. D.2). The model formulate in Chapter 4 is based on the assumption of constant superficial velocity. This non-constant velocity does not compromise modeling the PBSAC layer where filtration is carried out for almost 4000 s. On the other hand, the breakthrough curve of E2 in the membrane (plus the support layer and the tubing) occurs in the first 120 s. Second, the behavior of porous support layer is difficult to investigate. In fact, it

Table D.1: Dead volume of the permeate tube and support layer, and consequent delay times.

| Flow rate (mL s ⁻¹) | Dead volume (mL) | | Delay time (s) | |
|------------------------------------|------------------|---------|----------------|----------------|
| | Tube | Support | Tube | Tube + Support |
| 0.088 | 1.5 | 6.6 | 17 | 92 |

is too porous to perform a targeted experiment where its characteristics dispersion curve (without the membrane) could be measured.

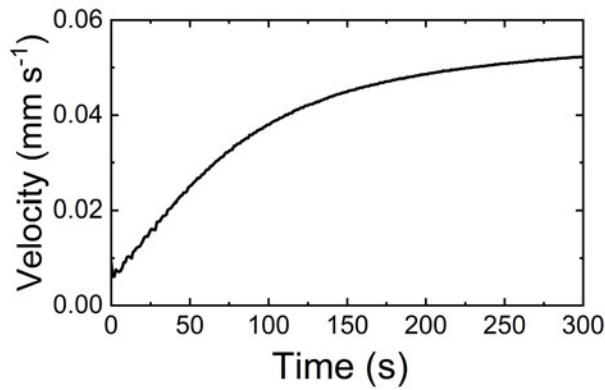


Figure D.2: Superficial velocity as a function of filtration time for the first 300 s after the synthetic air valve is opened and the pressure inside the cell start to increase.

For this reason, the main focus was to understand if the system dispersion has an effect or could be neglected in case of UF membrane with negligible adsorption. The system dispersion breakthrough was modeled in the two following case:

Case 1: The UF membrane (thickness 0.3 mm) is the only dispersive medium, both the tube and the support layer (2 mm thickness) are assumed to only contribute to a "convective delay" of the hormones concentration in the permeated.

Case 2: The UF and the support layer are assumed to be both dispersive media.

The delay due either to the permeate tube or the permeate tube and the supporting layer was simply modeled as a delay injection. The delay time was calculated from the volume of the dead volume and the average flow rate in the first 120 s.

In Fig. D.3C&D, it can be seen the comparison of E2 breakthrough if system dispersion is considered or neglected. The two curves are slightly deviating only for the 500 s. In the experimental breakthrough curves used in Chapter 4, the first point (e.g. the first sample measured) is around at 550 s of filtration time. In conclusion, the effect of the membrane can be neglected if it presents negligible adsorption. On the other hand, for a UF with significant adsorption (such the ones used in Chapter 5, see Fig. 5.8), parameters such as porosity, dispersion coefficient and adsorption isotherm need to be estimated and the transport through the membrane modeled as shown in Chapter 4.

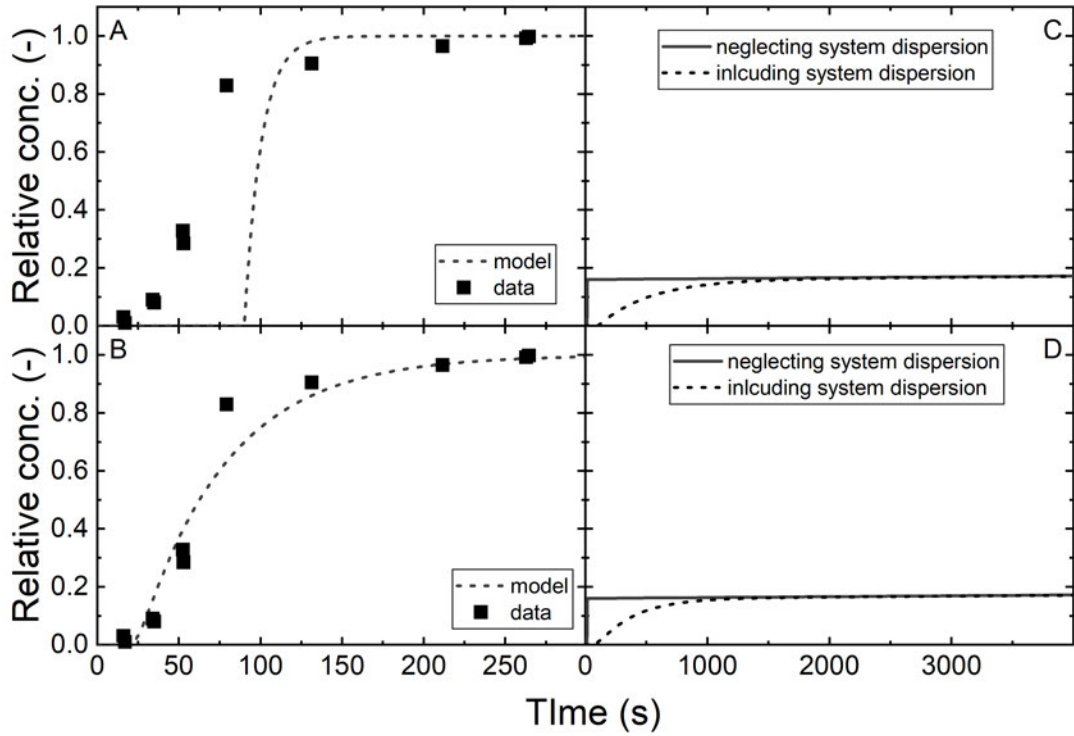


Figure D.3: Comparison of the model and the experimental data of system dispersion in case 1 (A) and case 2 (B). Effect of system dispersion on the breakthrough curve of E2 in the UF-PBSAC (C and D). Parameters for Case 1: L of 0.3 mm, D_{UF} of $1 \text{ mm}^2 \text{ s}^{-1}$, ε of 0.8. Parameters for case 2: L of 2.3 mm, D_{UF} of $0.1 \text{ mm}^2 \text{ s}^{-1}$, ε of 0.7.

D.2 Solution of the model

The partial differential equations (PDE) are solved by means of space discretization using linear finite element (LFE) following the procedure reported [138]. The result is a set of ordinary differential equations (ODE) that can be solved using Matlab ODE solver (function *ode15s* that automatically perform the time discretization).

As the first step, all the parameters are assigned, including the size of the grid of the discretization. The parameters are grouped in a structured array *par*:

D.2. Solution of the model

isotherm (Eq. (4.17)) can be rewritten in the form of Eq. (D.3) and, under the LFE discretization becomes Eq. (D.4):

$$\frac{dc_p}{dt}(1 + \rho_{app} K_{eq}) = \frac{6}{d_p} k_f (c - c_p) \quad (D.3)$$

$$M \frac{dc_p}{dt}(1 + \rho_{app} K_{eq}) = \frac{6}{d_p} k_f M (c - c_p) \quad (D.4)$$

The model is implemented in Matlab in the following way:

```
function dcdt = model(time,conc)
%membrane concentration
dcdt(:,3) = -(par.v/par.epsm*Cm + par.dm*Am)* conc(:,3);
dcdt(1,3) = dcdt(1,3) - par.v/par.epsm*(conc(1,1)-inlet(time)); %boundary conditions
dcdt(:,3) = Mm*dcdt(:,3);
%bulk PBSAC layer concentration
dcdt(:,1) = -(par.v/par.epsb*C + par.dax*A)* conc(:,1)-...
- ((1-par.epsb)/par.epsb)*par.kf*(3/par.rp)*M*(conc(:,1)-conc(:,2));
dcdt(1,1) = dcdt(1,1) - par.v/par.epsb*(conc(1,1)-conc(end,3)); %boundary conditions
dcdt(:,1) = M*dcdt(:,1);
%pore concentration
dcdt(:,2) = (par.kf*(3/par.rp)*(conc(:,1)-conc(:,2))) ;
dcdt(:,2) = (1+par.density*par.Keq)\dcdt(:,2);
```

The feed concentration function is then defined. To take into account the delay in the breakthrough caused by the dead-volume in the system (mainly the permeate tube), a delay injection is used (see Appendix D.1):

```
function infun = inlet(t)
if t < par.tdealy
infun = zeros (size(t));
else
infun = ones(size(t))*par.feed;
end
end
```

The model is solved using Matlab function *ode15s*, after defining the initial concentration (c_0 , which is 0 both in the bulk and pore phase) and selecting only the outlet concentration (last node):

```
c0=zeros(3 * dim ,1);
selection=par.axialgrid;
options =odeset('MaxStep',1,'InitialStep',1,'OutputFcn',@odeplot,'OutputSel',selection);
[time,conc]=ode15s(@model,[0 par.duration],c0,options);
```

D.3 Conceptual flow diagram

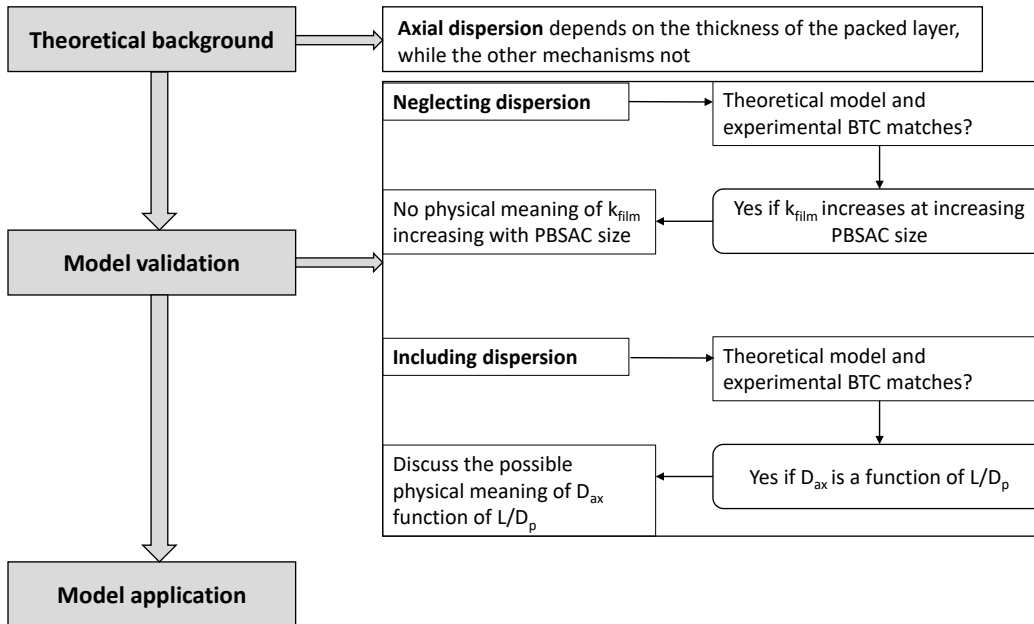


Figure D.4: The conceptual workflow of the paper, from Theoretical background, through model validation to model application.

Bibliography

- [1] R. P. Schwarzenbach, B. I. Escher, K. Fenner, T. B. Hofstetter, C. A. Johnson, U. von Gunten, and B. Wehrli. "The challenge of micropollutants in aquatic systems". In: *Science* 313.5790 (2006), pp. 1072–1077. DOI: 10.1126/science.1127291.
- [2] T. A. Ternes, M. Stumpf, J. Mueller, K. Haberer, R. D. Wilken, and M. Servos. "Behavior and occurrence of estrogens in municipal sewage treatment plants — I. Investigations in Germany, Canada and Brazil". In: *Science of the Total Environment* 225.1 (1999), pp. 81–90. DOI: 10.1016/S0048-9697(98)00334-9.
- [3] M. Adeel, X. Song, Y. Wang, D. Francis, and Y. Yang. "Environmental impact of estrogens on human, animal and plant life: A critical review". In: *Environment International* 99 (2017), pp. 107–119. DOI: 10.1016/j.envint.2016.12.010.
- [4] M. Y. Gross-Sorokin, S. D. Roast, and G. C. Brighty. "Assessment of feminization of male fish in English rivers by the Environment Agency of England and Wales". In: *Environmental Health Perspectives* 114 Suppl 1 (2006), pp. 147–51. DOI: 10.1289/ehp.8068.
- [5] K. A. Kidd, P. J. Blanchfield, K. H. Mills, V. P. Palace, R. E. Evans, J. M. Lazorchak, and R. W. Flick. "Collapse of a fish population after exposure to a synthetic estrogen". In: *Proceedings of the National Academy of Sciences* 104.21 (2007), pp. 8897–8901. DOI: 10.1073/pnas.0609568104.
- [6] P. D. Anderson, A. C. Johnson, D. Pfeiffer, D. J. Caldwell, R. Hannah, F. Mastrocchio, J. P. Sumpter, and R. J. Williams. "Endocrine disruption due to estrogens derived from humans predicted to be low in the majority of U.S. surface waters". In: *Environmental Toxicology and Chemistry* 31.6 (2012), pp. 1407–1415. DOI: 10.1002/etc.1824.
- [7] J. S. Toor and S. C. Sikka. "Role of endocrine disruptors in testicular toxicity". In: *Reproductive and Developmental Toxicology*. Academic Press, 2017. ISBN: 9780128042397. DOI: 10.1016/b978-0-12-804239-7.00059-7.
- [8] L. Trasande, R. T. Zoeller, U. Hass, A. Kortenkamp, P. Grandjean, J. P. Myers, J. DiGangi, M. Bellanger, R. Hauser, J. Legler, N. E. Skakkebaek, and J. J. Heindel. "Estimating burden and disease costs of exposure to endocrine-disrupting chemicals in the European union". In: *Journal of Clinical Endocrinology & Metabolism* 100.4 (2015), pp. 1245–55. DOI: 10.1210/jc.2014-4324.

- [9] L. S. Treviño, Q. Wang, and C. L. Walker. "Hypothesis: Activation of rapid signaling by environmental estrogens and epigenetic reprogramming in breast cancer". In: *Reproductive Toxicology* 54 (2015), pp. 136–140. DOI: 10.1016/j.reprotox.2014.12.014.
- [10] W. Jiang, Y. Yan, M. Ma, D. Wang, Q. Luo, Z. Wang, and S. K. Satyanarayanan. "Assessment of source water contamination by estrogenic disrupting compounds in China". In: *Journal of Environmental Sciences* 24.2 (2012), pp. 320–328. DOI: 10.1016/s1001-0742(11)60746-8.
- [11] P. Y. Kunz, C. Kienle, M. Carere, N. Homazava, and R. Kase. "In vitro bioassays to screen for endocrine active pharmaceuticals in surface and waste waters". In: *Journal of Pharmaceutical and Biomedical Analysis* 106 (2015), pp. 107–115. DOI: 10.1016/j.jpba.2014.11.018.
- [12] W. C. Li. "Occurrence, sources, and fate of pharmaceuticals in aquatic environment and soil". In: *Environmental Pollution* 187 (2014), pp. 193–201. DOI: 10.1016/j.envpol.2014.01.015.
- [13] P. Verlicchi, A. Galletti, M. Petrovic, and D. Barceló. "Hospital effluents as a source of emerging pollutants: An overview of micropollutants and sustainable treatment options". In: *Journal of Hydrology* 389.3-4 (2010), pp. 416–428. DOI: 10.1016/j.jhydro1.2010.06.005.
- [14] M. Avbersek, J. Somen, and E. Heath. "Dynamics of steroid estrogen daily concentrations in hospital effluent and connected waste water treatment plant". In: *Journal of Environmental Monitoring* 13.8 (2011), pp. 2221–6. DOI: 10.1039/c1em10147a.
- [15] O. Cardoso, J.-M. Porcher, and W. Sanchez. "Factory-discharged pharmaceuticals could be a relevant source of aquatic environment contamination: Review of evidence and need for knowledge". In: *Chemosphere* 115 (2014), pp. 20–30. DOI: 10.1016/j.chemosphere.2014.02.004.
- [16] C. W. Cui, S. L. Ji, and H. Y. Ren. "Determination of steroid estrogens in wastewater treatment plant of a contraceptives producing factory". In: *Environmental Monitoring and Assessment* 121.1-3 (2006), pp. 409–19. DOI: 10.1007/s10661-005-9139-8.
- [17] M. Ma, K. Rao, and Z. Wang. "Occurrence of estrogenic effects in sewage and industrial wastewaters in Beijing, China". In: *Environmental Pollution* 147.2 (2007), pp. 331–6. DOI: 10.1016/j.envpol.2006.05.032.
- [18] T. aus der Beek, F. A. Weber, A. Bergmann, S. Hickmann, I. Ebert, A. Hein, and A. Kuster. "Pharmaceuticals in the environment - Global occurrences and perspectives". In: *Environmental Toxicology and Chemistry* 35.4 (2016), pp. 823–35. DOI: 10.1002/etc.3339.

- [19] D. Eike, R. Marcus, and J. Dirk. *The database "Pharmaceuticals in the Environment" - Update and new analysis*. 2019. URL: <https://www.umweltbundesamt.de/en/publikationen/the-database-pharmaceuticals-in-the-environment>.
- [20] S. Y. Wee and A. Z. Aris. "Endocrine disrupting compounds in drinking water supply system and human health risk implication". In: *Environment International* 106 (2017), pp. 207–233. DOI: 10.1016/j.envint.2017.05.004.
- [21] R. Triebskorn and H. Hetzenauer. "Micropollutants in three tributaries of Lake Constance, Argen, Schussen and Seefelder Aach: a literature review". In: *Environmental Sciences Europe* 24.1 (2012), p. 8. DOI: 10.1186/2190-4715-24-8.
- [22] European Commission. *Communication from the Commission to the Council and the European Parliament on the implementation of the Community Strategy for Endocrine Disruptors*. 1999. URL: https://ec.europa.eu/environment/archives/docum/01262_en.htm.
- [23] European Commission. *Communication from the Commission to the Council and the European Parliament on the implementation of the Community Strategy for Endocrine Disruptors - a range of substances suspected of interfering with the hormone systems of humans and wildlife (COM (99) 706)*. 2001. URL: <https://ec.europa.eu/environment/archives/docum/99706sm.htm>.
- [24] European Commission. *Proposal for a directive of the European parliament and of the council amending Directives 2000/60/EC and 2008/105/EC as regards priority substances in the field of water policy (COM(2011) 876)*. 2011. URL: <https://op.europa.eu/en/publication-detail/-/publication/859825c3-d7c7-424b-96dd-84eb700ef0bf/language-en>.
- [25] F. Lahnsteiner, B. Berger, M. Kletzl, and T. Weismann. "Effect of 17beta-estradiol on gamete quality and maturation in two salmonid species". In: *Aquatic Toxicology* 79.2 (2006), pp. 124–31. DOI: 10.1016/j.aquatox.2006.05.011.
- [26] SCHER (Scientific Committee on Health and Environmental Risks). *Opinion on "chemicals and the water framework directiveDraft environmental quality standards" (17β-estradiol (E2))*. 2011. URL: <https://op.europa.eu/en/publication-detail/-/publication/cf1e0983-cec5-4e64-93f0-45940d94af1b/language-en>.
- [27] European Commission. *Directive of the european parliament and of the council on the quality of water intended for human consumption (recast)*. 2018. URL: <https://op.europa.eu/en/publication-detail/-/publication/8c5065b2-074f-11e8-b8f5-01aa75ed71a1>.
- [28] C. P. Gerba and I. L. Pepper. "Municipal wastewater treatment". In: *Environmental and Pollution Science*. Elsevier, 2019, pp. 393–418. ISBN: 978-0-12-814719-1. DOI: 10.1016/B978-0-12-814719-1.00022-7.

- [29] H. Hamid and C. Eskicioglu. "Fate of estrogenic hormones in wastewater and sludge treatment: A review of properties and analytical detection techniques in sludge matrix". In: *Water Research* 46.18 (2012), pp. 5813–33. DOI: 10.1016/j.watres.2012.08.002.
- [30] S. K. Khanal, B. Xie, M. L. Thompson, S. Sung, S.-K. Ong, and J. van Leeuwen. "Fate, transport, and biodegradation of natural estrogens in the environment and engineered systems". In: *Environmental Science & Technology* 40.21 (2006), pp. 6537–6546. DOI: 10.1021/es0607739.
- [31] H. Lee and D. Liu. "Degradation of 17- β estradiol and its metabolites by sewage bacteria". In: *Water, Air, & Soil Pollution* 4 (2004), pp. 351–366. DOI: 10.1023/A:1014117329403.
- [32] M. Carballa, F. Omil, J. M. Lema, M. Llompart, C. Garcia-Jares, I. Rodriguez, M. Gomez, and T. Ternes. "Behavior of pharmaceuticals, cosmetics and hormones in a sewage treatment plant". In: *Water Research* 38.12 (2004), pp. 2918–26. DOI: 10.1016/j.watres.2004.03.029.
- [33] T. Hashimoto and T. Murakami. "Removal and degradation characteristics of natural and synthetic estrogens by activated sludge in batch experiments". In: *Water Research* 43.3 (2009), pp. 573–82. DOI: 10.1016/j.watres.2008.10.051.
- [34] World Health Organization. *Pharmaceuticals in drinking-water*. 2011. URL: https://www.who.int/water_sanitation_health/publications/2012/pharmaceuticals/en/.
- [35] A. G. Fane, R. Wang, and Y. Jia. "Membrane technology: Past, present and future". In: *Membrane and Desalination Technologies*. Springer, 2011, pp. 1–45. ISBN: 978-1-58829-940-6. DOI: 10.1007/978-1-59745-278-6_1.
- [36] F. Li, K. Wichmann, and R. Otterpohl. "Review of the technological approaches for grey water treatment and reuses". In: *Science of the Total Environment* 407.11 (2009), pp. 3439–49. DOI: 10.1016/j.scitotenv.2009.02.004.
- [37] I. Owusu-Agyeman, A. Jeihanipour, T. Luxbacher, and A. I. Schäfer. "Implications of humic acid, inorganic carbon and speciation on fluoride retention mechanisms in nanofiltration and reverse osmosis". In: *Journal of Membrane Science* 528 (2017), pp. 82–94. DOI: 10.1016/j.memsci.2016.12.043.
- [38] N. K. Khanzada, M. U. Farid, J. A. Kharraz, J. Choi, C. Y. Tang, L. D. Nghiem, A. Jang, and A. K. An. "Removal of organic micropollutants using advanced membrane-based water and wastewater treatment: A review". In: *Journal of Membrane Science* 598 (2020). DOI: 10.1016/j.memsci.2019.117672.
- [39] A. I. Schafer, I. Akanyeti, and A. J. Semiao. "Micropollutant sorption to membrane polymers: a review of mechanisms for estrogens". In: *Advances in Colloid and Interface Science* 164.1-2 (2011), pp. 100–17. DOI: 10.1016/j.cis.2010.09.006.

- [40] Y. Yoon, P. Westerhoff, S. A. Snyder, and E. C. Wert. "Nanofiltration and ultrafiltration of endocrine disrupting compounds, pharmaceuticals and personal care products". In: *Journal of Membrane Science* 270.1-2 (2006), pp. 88–100. DOI: 10.1016/j.memsci.2005.06.045.
- [41] C. Bellona, J. E. Drewes, P. Xu, and G. Amy. "Factors affecting the rejection of organic solutes during NF/RO treatment—a literature review". In: *Water Research* 38.12 (2004), pp. 2795–809. DOI: 10.1016/j.watres.2004.03.034.
- [42] L. D. Nghiem, A. Manis, K. Soldenhoff, and A. I. Schäfer. "Estrogenic hormone removal from wastewater using NF/RO membranes". In: *Journal of Membrane Science* 242.1-2 (2004), pp. 37–45. DOI: 10.1016/j.memsci.2003.12.034.
- [43] A. J. C. Semião and A. I. Schäfer. "Removal of adsorbing estrogenic micropollutants by nanofiltration membranes. Part A—Experimental evidence". In: *Journal of Membrane Science* 431 (2013), pp. 244–256. DOI: <http://dx.doi.org/10.1016/j.memsci.2012.11.080>.
- [44] L. D. Nghiem, A. I. Schäfer, and M. Elimelech. "Removal of natural hormones by nanofiltration membranes: Measurement, modeling, and mechanisms". In: *Environmental Science & Technology* 38.6 (2004), pp. 1888–1896. DOI: 10.1021/es034952r.
- [45] H. Guo, Y. Deng, Z. Tao, Z. Yao, J. Wang, C. Lin, T. Zhang, B. Zhu, and C. Y. Tang. "Does hydrophilic polydopamine coating enhance membrane rejection of hydrophobic endocrine-disrupting compounds?" In: *Environmental Science & Technology Letters* 3.9 (2016), pp. 332–338. DOI: 10.1021/acs.estlett.6b00263.
- [46] Y.-l. Liu, X.-m. Wang, H.-w. Yang, Y. F. Xie, and X. Huang. "Preparation of nanofiltration membranes for high rejection of organic micropollutants and low rejection of divalent cations". In: *Journal of Membrane Science* 572 (2019), pp. 152–160. DOI: <https://doi.org/10.1016/j.memsci.2018.11.013>.
- [47] Y.-L. Liu, Y.-Y. Zhao, X.-M. Wang, X.-H. Wen, X. Huang, and Y. F. Xie. "Effect of varying piperazine concentration and post-modification on prepared nanofiltration membranes in selectively rejecting organic micropollutants and salts". In: *Journal of Membrane Science* 582 (2019), pp. 274–283. DOI: <https://doi.org/10.1016/j.memsci.2019.04.018>.
- [48] H. Guo, Z. Yao, Z. Yang, X. Ma, J. Wang, and C. Y. Tang. "A one-step rapid assembly of thin film coating using green coordination complexes for enhanced removal of trace organic contaminants by membranes". In: *Environmental Science & Technology* 51.21 (2017), pp. 12638–12643. DOI: 10.1021/acs.est.7b03478.

- [49] H. Sontheimer, J. C. Crittenden, and R. S. Summers. *Activated carbon for water treatment*. DVGW-Forschungsstelle, Engler-Bunte-Institut, Universität Karlsruhe (TH), 1988. URL: <http://books.google.com/books?id=9g5SAAAAAAAJ>.
- [50] F. Bonvin, L. Jost, L. Randin, E. Bonvin, and T. Kohn. "Super-fine powdered activated carbon (SPAC) for efficient removal of micropollutants from wastewater treatment plant effluent". In: *Water Research* 90 (2016), pp. 90–9. DOI: 10.1016/j.watres.2015.12.001.
- [51] E. Worch. *Adsorption technology in water Treatment*. De Gruyter, 2012. ISBN: 978-3-11-024023-8. DOI: 10.1515/9783110240238.
- [52] M. Fürhacker, A. Dürauer, and A. Jungbauer. "Adsorption isotherms of 17 β -estradiol on granular activated carbon (GAC)". In: *Chemosphere* 44.7 (2001), pp. 1573–1579. DOI: 10.1016/S0045-6535(00)00543-9.
- [53] Y. Yoon, P. Westerhoff, and S. A. Snyder. "Adsorption of 3H-labeled 17 β -estradiol on powdered activated carbon". In: *Water, Air, & Soil Pollution* 166.1 (2005), pp. 343–351. DOI: 10.1007/s11270-005-7274-z.
- [54] M. Tagliavini, F. Engel, P. G. Weidler, T. Scherer, and A. I. Schäfer. "Adsorption of steroid micropollutants on polymer-based spherical activated carbon (PBSAC)". In: *Journal of Hazardous Materials* 337 (2017), pp. 126–137. DOI: 10.1016/j.jhazmat.2017.03.036.
- [55] Y. Luo, W. Guo, H. H. Ngo, L. D. Nghiem, F. I. Hai, J. Zhang, S. Liang, and X. C. Wang. "A review on the occurrence of micropollutants in the aquatic environment and their fate and removal during wastewater treatment". In: *Science of the Total Environment* 473-474 (2014), pp. 619–41. DOI: 10.1016/j.scitotenv.2013.12.065.
- [56] E. J. Rosenfeldt, K. G. Linden, S. Canonica, and U. von Gunten. "Comparison of the efficiency of *OH radical formation during ozonation and the advanced oxidation processes O₃/H₂O₂ and UV/H₂O₂". In: *Water Research* 40.20 (2006), pp. 3695–704. DOI: 10.1016/j.watres.2006.09.008.
- [57] D. Kanakaraju, B. D. Glass, and M. Oelgemoller. "Advanced oxidation process-mediated removal of pharmaceuticals from water: A review". In: *Journal of Environmental Management* 219 (2018), pp. 189–207. DOI: 10.1016/j.jenvman.2018.04.103.
- [58] Q. Sun, G. Zhu, C. Wang, Z. Yang, and Q. Xue. "Removal characteristics of steroid estrogen in the mixed system through an ozone-based advanced oxidation process". In: *Water, Air, & Soil Pollution* 230.9 (2019). DOI: 10.1007/s11270-019-4275-x.
- [59] R. Pesoutova, L. Stritesky, and P. Hlavinek. "A pilot scale comparison of advanced oxidation processes for estrogenic hormone removal from municipal wastewater effluent". In: *Water Science & Technology* 70.1 (2014), pp. 70–5. DOI: 10.2166/wst.2014.196.

- [60] J. Wang, X. Zhou, M. Gatheru Waigi, F. Owino Gudda, P. Cheng, and W. Ling. "Simultaneous removal of estrogens and antibiotics from livestock manure using fenton oxidation technique". In: *Catalysts* 9.8 (2019). DOI: 10.3390/catal9080644.
- [61] F. A. Almomani, M. Shawaqfah, R. R. Bhosale, and A. Kumar. "Removal of emerging pharmaceuticals from wastewater by ozone-based advanced oxidation processes". In: *Environmental Progress & Sustainable Energy* 35.4 (2016), pp. 982–995. DOI: 10.1002/ep.12306.
- [62] J. Margot, C. Kienle, A. Magnet, M. Weil, L. Rossi, L. F. de Alencastro, C. Abegglen, D. Thonney, N. Chevre, M. Scharer, and D. A. Barry. "Treatment of micropollutants in municipal wastewater: ozone or powdered activated carbon?" In: *Science of the Total Environment* 461-462 (2013), pp. 480–98. DOI: 10.1016/j.scitotenv.2013.05.034.
- [63] M. R. Esfahani, J. L. Tyler, H. A. Stretz, and M. J. M. Wells. "Effects of a dual nanofiller, nano-TiO₂ and MWCNT, for polysulfone-based nanocomposite membranes for water purification". In: *Desalination* 372 (2015), pp. 47–56. DOI: 10.1016/j.desal.2015.06.014.
- [64] Y. F. Wang, Y. Liu, Y. Yu, and H. O. Huang. "Influence of CNT-rGO composite structures on their permeability and selectivity for membrane water treatment". In: *Journal of Membrane Science* 551 (2018), pp. 326–332. DOI: 10.1016/j.memsci.2018.01.031.
- [65] P. Amaral, E. Partlan, M. Li, F. Lapolli, O. T. Mefford, T. Karanfil, and D. A. Ladner. "Superfine powdered activated carbon (S-PAC) coatings on microfiltration membranes: Effects of milling time on contaminant removal and flux". In: *Water Research* 100 (2016), pp. 429–438. DOI: 10.1016/j.watres.2016.05.034.
- [66] J. R. Ellerie, O. G. Apul, T. Karanfil, and D. A. Ladner. "Comparing graphene, carbon nanotubes, and superfine powdered activated carbon as adsorptive coating materials for microfiltration membranes". In: *Journal of Hazardous Materials* 261 (2013), pp. 91–98. DOI: 10.1016/j.jhazmat.2013.07.009.
- [67] K. Niedergall, M. Bach, T. Schiestel, and G. E. M. Tovar. "Nanostructured composite adsorber membranes for the reduction of trace substances in water: The example of Bisphenol A". In: *Industrial & Engineering Chemistry Research* 52.39 (2013), pp. 14011–14018. DOI: 10.1021/ie303264r.
- [68] M. Tagliavini and A. I. Schäfer. "Removal of steroid hormone micropollutants from water using a membrane composite of UF with permeate side adsorption". In: *Membrane Technology* 2021.5 (2021), pp. 5–7. ISSN: 0958-2118. DOI: 10.1016/S0958-2118(21)00074-4.

- [69] C. Stoquart, P. Servais, P. R. Bérubé, and B. Barbeau. "Hybrid membrane processes using activated carbon treatment for drinking water: a review". In: *Journal of Membrane Science* 411-412 (2012), pp. 1–12. DOI: 10.1016/j.memsci.2012.04.012.
- [70] J. Kim, Z. Cai, and M. M. Benjamin. "Effects of adsorbents on membrane fouling by natural organic matter". In: *Journal of Membrane Science* 310.1-2 (2008), pp. 356–364. DOI: 10.1016/j.memsci.2007.11.007.
- [71] C.-W. Li and Y.-S. Chen. "Fouling of UF membrane by humic substance: Effects of molecular weight and powder-activated carbon (PAC) pre-treatment". In: *Desalination* 170.1 (2004), pp. 59–67. DOI: 10.1016/j.desal.2004.03.015.
- [72] W. Tsujimoto, H. Kimura, T. Izu, and T. Irie. "Membrane filtration and pre-treatment by GAC". In: *Desalination* 119.1 (1998), pp. 323–326. DOI: 10.1016/S0011-9164(98)00176-3.
- [73] M. Campinas and M. J. Rosa. "Assessing PAC contribution to the NOM fouling control in PAC/UF systems". In: *Water Research* 44.5 (2010), pp. 1636–44. DOI: 10.1016/j.watres.2009.11.012.
- [74] S. Mozia and M. Tomaszewska. "Treatment of surface water using hybrid processes—adsorption on PAC and ultrafiltration". In: *Desalination* 162 (2004), pp. 23–31. DOI: 10.1016/S0011-9164(04)00023-2.
- [75] A. S. Ruhl, J. Altmann, F. Zietzschmann, F. Meinel, A. Sperlich, and M. Jekel. "Integrating micro-pollutant removal by powdered activated carbon into deep bed filtration". In: *Water, Air, & Soil Pollution* 225.3 (2014), p. 1877. DOI: 10.1007/s11270-014-1877-1.
- [76] A. B. Dichiara, S. J. Weinstein, and R. E. Rogers. "On the choice of batch or fixed bed adsorption processes for wastewater treatment". In: *Industrial & Engineering Chemistry Research* 54.34 (2015), pp. 8579–8586. DOI: 10.1021/acs.iecr.5b02350.
- [77] K. Haberer and S. Normann-Schmidt. "The haberer process: combining contact flocculation, filtration, and PAC adsorption". In: *Journal - AWWA* 83.9 (1991), pp. 82–89. DOI: 10.1002/j.1551-8833.1991.tb07217.x.
- [78] M. N. Nguyen, P. B. Trinh, C. J. Burkhardt, and A. I. Schäfer. "Incorporation of single-walled carbon nanotubes in ultrafiltration support structure for the removal of steroid hormone micropollutants". In: *Separation and Purification Technology* (2021), p. 118405. DOI: 10.1016/j.seppur.2021.118405.
- [79] S.-E. Wu, K.-J. Hwang, T.-W. Cheng, Y.-C. Lin, and K.-L. Tung. "Dynamic membranes of powder-activated carbon for removing microbes and organic matter from seawater". In: *Journal of Membrane Science* 541 (2017), pp. 189–197. DOI: 10.1016/j.memsci.2017.07.006.

- [80] M. Tagliavini, P. G. Weidler, C. Njel, J. Pohl, D. Richter, B. Böhringer, and A. I. Schäfer. "Polymer-based spherical activated carbon – ultrafiltration (UF-PBSAC) for the adsorption of steroid hormones from water: Material characteristics and process configuration". In: *Water Research* 185 (2020), p. 116249. ISSN: 0043-1354. DOI: 10.1016/j.watres.2020.116249.
- [81] J. Altmann, D. Rehfeld, K. Träder, A. Sperlich, and M. Jekel. "Combination of granular activated carbon adsorption and deep-bed filtration as a single advanced wastewater treatment step for organic micropollutant and phosphorus removal". In: *Water Research* 92 (Apr. 2016), pp. 131–139. DOI: 10.1016/j.watres.2016.01.051.
- [82] A. M. Kennedy, A. M. Reinert, D. R. U. Knappe, I. Ferrer, and R. S. Summers. "Full- and pilot-scale GAC adsorption of organic micropollutants". In: *Water Research* 68 (2015), pp. 238–248. DOI: 10.1016/j.watres.2014.10.010.
- [83] F. Meinel, A. S. Ruhl, A. Sperlich, F. Zietzschmann, and M. Jekel. "Pilot-scale investigation of micropollutant removal with granular and powdered activated carbon". In: *Water, Air, & Soil Pollution* 226.1 (2014), p. 2260. DOI: 10.1007/s11270-014-2260-y.
- [84] A. Rostvall, W. Zhang, W. Dürig, G. Renman, K. Wiberg, L. Ahrens, and P. Gago-Ferrero. "Removal of pharmaceuticals, perfluoroalkyl substances and other micropollutants from wastewater using lignite, Xylit, sand, granular activated carbon (GAC) and GAC+Polonite® in column tests – role of physico-chemical properties". In: *Water Research* 137 (2018), pp. 97–106. DOI: 10.1016/j.watres.2018.03.008.
- [85] M. T. Amin, A. A. Alazba, and U. Manzoor. "A review of removal of pollutants from water/wastewater using different types of nanomaterials". In: *Advances in Materials Science and Engineering* 2014 (2014), pp. 1–24. DOI: 10.1155/2014/825910.
- [86] D. S. Dlamini, B. B. Mamba, and J. Li. "The role of nanoparticles in the performance of nano-enabled composite membranes - A critical scientific perspective". In: *Science of the Total Environment* 656 (2019), pp. 723–731. DOI: 10.1016/j.scitotenv.2018.11.421.
- [87] J. Zhang, M. N. Nguyen, Y. Li, C. Yang, and A. I. Schäfer. "Steroid hormone micropollutant removal from water with activated carbon fiber-ultrafiltration composite membranes". In: *Journal of Hazardous Materials* 391 (2020), p. 122020. DOI: 10.1016/j.jhazmat.2020.122020.
- [88] H. von Blücher, B. D. Böhringer, and J.-M. Giebelhausen. "Hochleistungsadsorbentien auf Basis von Aktivkohle mit hoher Mikroporosität". 2006. URL: <https://patents.google.com/patent/DE202007014890U1/de>.

- [89] L. Nghiem. "Removal of emerging trace organic contaminants by nanofiltration and reverse osmosis". PhD thesis. School of Civil, Mining and Environmental Engineering, University of Wollongong, 2005. URL: <http://ro.uow.edu.au/theses/377>.
- [90] F. Raposo, M. De La Rubia, and R. Borja. "Methylene blue number as useful indicator to evaluate the adsorptive capacity of granular activated carbon in batch mode: Influence of adsorbate/adsorbent mass ratio and particle size". In: *Journal of Hazardous Materials* 165.1 (2009), pp. 291–299. ISSN: 0304-3894. DOI: 10.1016/j.jhazmat.2008.09.106.
- [91] M. Tagliavini and A. I. Schäfer. "Removal of steroid micropollutants by polymer-based spherical activated carbon (PBSAC) assisted membrane filtration". In: *Journal of Hazardous Materials* (2018). DOI: 10.1016/j.jhazmat.2018.03.032.
- [92] F. E. Jones and G. L. Harris. "ITS-90 Density of water formulation for volumetric standards calibration". In: *Journal of Research of the National Institute of Standards and Technology* 97 (1992). DOI: 10.6028/jres.097.013.
- [93] R. W. Baker. "Membrane transport theory". In: *Membrane Technology and Applications*. John Wiley & Sons, Ltd, 2004, pp. 15–87. ISBN: 9780470020395. DOI: 10.1002/0470020393.ch2.
- [94] L. Paredes, C. Alfonsin, T. Allegue, F. Omil, and M. Carballa. "Integrating granular activated carbon in the post-treatment of membrane and settler effluents to improve organic micropollutants removal". In: *Chemical Engineering Journal* 345 (2018), pp. 79–86. DOI: 10.1016/j.cej.2018.03.120.
- [95] F. Zietzschmann, C. Stützer, and M. Jekel. "Granular activated carbon adsorption of organic micro-pollutants in drinking water and treated wastewater – aligning breakthrough curves and capacities". In: *Water Research* 92 (2016), pp. 180–187. DOI: 10.1016/j.watres.2016.01.056.
- [96] L. Pan, Y. Matsui, T. Matsushita, and N. Shirasaki. "Superiority of wet-milled over dry-milled superfine powdered activated carbon for adsorptive 2-methylisoborneol removal". In: *Water Research* 102 (2016), pp. 516–23. DOI: 10.1016/j.watres.2016.06.062.
- [97] L. Pan, Y. Nishimura, H. Takaesu, Y. Matsui, T. Matsushita, and N. Shirasaki. "Effects of decreasing activated carbon particle diameter from 30 μm to 140 nm on equilibrium adsorption capacity". In: *Water Research* 124 (2017), pp. 425–434. DOI: 10.1016/j.watres.2017.07.075.
- [98] E. Partlan, K. Davis, Y. Ren, O. G. Apul, O. T. Mefford, T. Karanfil, and D. A. Ladner. "Effect of bead milling on chemical and physical characteristics of activated carbons pulverized to superfine sizes". In: *Water Research* 89 (2016), pp. 161–70. DOI: 10.1016/j.watres.2015.11.041.

- [99] Y. Matsui, N. Ando, H. Sasaki, T. Matsushita, and K. Ohno. "Branched pore kinetic model analysis of geosmin adsorption on super-powdered activated carbon". In: *Water Research* 43.12 (2009), pp. 3095–103. DOI: 10.1016/j.watres.2009.04.014.
- [100] Y. Matsui, S. Nakao, A. Sakamoto, T. Taniguchi, L. Pan, T. Matsushita, and N. Shirasaki. "Adsorption capacities of activated carbons for geosmin and 2-methylisoborneol vary with activated carbon particle size: Effects of adsorbent and adsorbate characteristics". In: *Water Research* 85 (2015), pp. 95–102. DOI: 10.1016/j.watres.2015.08.017.
- [101] H. Takaesu, Y. Matsui, Y. Nishimura, T. Matsushita, and N. Shirasaki. "Micro-milling super-fine powdered activated carbon decreases adsorption capacity by introducing oxygen/hydrogen-containing functional groups on carbon surface from water". In: *Water Research* 155 (2019), pp. 66–75. DOI: 10.1016/j.watres.2019.02.019.
- [102] M. N. Nguyen, P. G. Weidler, H.-M. Bruns, R. Schwaiger, and A. I. Schäfer. "Interactions between carbon-based nanoparticles and steroid hormone micropollutants in water". In: *Journal of Hazardous Materials* (2020). DOI: 10.1016/j.jhazmat.2020.122929.
- [103] S. Zhang, T. Shao, S. S. K. Bekaroglu, and T. Karanfil. "The impacts of aggregation and surface chemistry of carbon nanotubes on the adsorption of synthetic organic compounds". In: *Environmental Science & Technology* 43.15 (2009), pp. 5719–5725. DOI: 10.1021/es900453e.
- [104] H. Klefer, M. Munoz, A. Modrow, B. Böhringer, P. Wasserscheid, and B. J. M. Etzold. "Polymer-based spherical activated carbon as easy-to-handle catalyst support for hydrogenation reactions". In: *Chemical Engineering and Technology* 39.2 (2016), pp. 276–284. DOI: 10.1002/ceat.201500445.
- [105] M. Sobiesiak, B. Gawdzik, A. M. Puziy, and O. I. Poddubnaya. "Polymer-based carbon adsorbents obtained from copolymer of 4,4'-bis(maleimidodiphenyl)methane and divinylbenzene for use in SPE". In: *Chromatographia* 64.3 (2006), pp. 1–7. DOI: 10.1365/s10337-006-0798-6.
- [106] H. Marsh and F. Rodríguez-Reinoso. *Activated Carbon*. Elsevier, 2006. ISBN: 9780080444635. DOI: 10.1016/B978-0-08-044463-5.X5013-4.
- [107] M. J. Prauchner and F. Rodríguez-Reinoso. "Chemical versus physical activation of coconut shell: A comparative study". In: *Microporous and Mesoporous Materials* 152 (2012), pp. 163–171. DOI: 10.1016/j.micromeso.2011.11.040.
- [108] W. Li, K. Yang, J. Peng, L. Zhang, S. Guo, and H. Xia. "Effects of carbonization temperatures on characteristics of porosity in coconut shell chars and activated carbons derived from carbonized coconut shell chars". In: *Industrial Crops and Products* 28.2 (2008), pp. 190–198. DOI: 10.1016/j.indcrop.2008.02.012.

- [109] L. Li, P. A. Quinlivan, and D. R. U. Knappe. "Effects of activated carbon surface chemistry and pore structure on the adsorption of organic contaminants from aqueous solution". In: *Carbon* 40.12 (2002), pp. 2085–2100. DOI: 10.1016/S0008-6223(02)00069-6.
- [110] L. Li, F. Sun, J. Gao, L. Wang, X. Pi, and G. Zhao. "Broadening the pore size of coal-based activated carbon via a washing-free chem-physical activation method for high-capacity dye adsorption". In: *RSC Advances* 8.26 (2018), pp. 14488–14499. DOI: 10.1039/c8ra02127a.
- [111] H. Benaddi, T. J. Bandosz, J. Jagiello, J. A. Schwarz, J. N. Rouzaud, D. Legras, and F. Béguin. "Surface functionality and porosity of activated carbons obtained from chemical activation of wood". In: *Carbon* 38.5 (2000), pp. 669–674. DOI: 10.1016/S0008-6223(99)00134-7.
- [112] T. Budinova, E. Ekinici, F. Yardim, A. Grimm, E. Björnbom, V. Minkova, and M. Goranova. "Characterization and application of activated carbon produced by H₃PO₄ and water vapor activation". In: *Fuel Processing Technology* 87.10 (2006), pp. 899–905. DOI: 10.1016/j.fuproc.2006.06.005.
- [113] N. H. Phan, S. Rio, C. Faur, L. Le Coq, P. Le Cloirec, and T. H. Nguyen. "Production of fibrous activated carbons from natural cellulose (jute, coconut) fibers for water treatment applications". In: *Carbon* 44.12 (2006), pp. 2569–2577. DOI: 10.1016/j.carbon.2006.05.048.
- [114] S. Wang, Z. H. Zhu, A. Coomes, F. Haghseresht, and G. Q. Lu. "The physical and surface chemical characteristics of activated carbons and the adsorption of methylene blue from wastewater". In: *Journal of Colloid and Interface Science* 284.2 (2005), pp. 440–6. DOI: 10.1016/j.jcis.2004.10.050.
- [115] D. J. de Ridder, L. Villacorte, A. R. Verliefde, J. Q. Verberk, S. G. Heijman, G. L. Amy, and J. C. van Dijk. "Modeling equilibrium adsorption of organic micropollutants onto activated carbon". In: *Water Resources* 44.10 (2010), pp. 3077–86. DOI: 10.1016/j.watres.2010.02.034.
- [116] B. Böhringer, O. G. Gonzalez, I. Eckle, M. Müller, J.-M. Giebelhausen, C. Schrage, and S. Fichtner. "Polymer-based spherical activated carbons - From adsorptive properties to filter performance". In: *Chemie Ingenieur Technik* 83.1-2 (Jan. 2011), pp. 53–60. DOI: 10.1002/cite.201000166.
- [117] J. H. Scofield. "Hartree-slater subshell photoionization cross-sections at 1254 and 1487 eV". In: *Journal of Electron Spectroscopy and Related Phenomena* 8 (1979), pp. 129–137. DOI: 10.1016/0368-2048(76)80015-1.
- [118] Y. Zou, A. S. Walton, I. A. Kinloch, and R. A. W. Dryfe. "Investigation of the Differential Capacitance of Highly Ordered Pyrolytic Graphite as a Model Material of Graphene". In: *Langmuir* 32.44 (2016), pp. 11448–11455. DOI: 10.1021/acs.langmuir.6b02910.

- [119] C. Song, P. Wang, and H. A. Makse. "A phase diagram for jammed matter". In: *Nature* 453.7195 (2008), pp. 629–632. DOI: 10.1038/nature06981.
- [120] T. Susi, T. Pichler, and P. Ayala. "X-ray photoelectron spectroscopy of graphitic carbon nanomaterials doped with heteroatoms". In: *Beilstein Journal of Nanotechnology* 6 (2015), pp. 177–192. DOI: 10.3762/bjnano.6.17.
- [121] S. Tardio, M.-L. Abel, R. H. Carr, and J. F. Watts. "Polystyrene-silicon bonding through π electrons: a combined XPS and DFT study". In: *Surface and Interface Analysis* 48.7 (2016), pp. 556–560. DOI: 10.1002/sia.5879.
- [122] U. Zielke, K. J. Hüttinger, and W. P. Hoffman. "Surface-oxidized carbon fibers: I. Surface structure and chemistry". In: *Carbon* 34.8 (1996), pp. 983–998. DOI: 10.1016/0008-6223(96)00032-2.
- [123] E. Worch. "Fixed-bed adsorption in drinking water treatment: a critical review on models and parameter estimation". In: *Journal of Water Supply: Research and Technology-Aqua* 57.3 (2008), pp. 171–183. DOI: 10.2166/aqua.2008.100.
- [124] A. Piazzoli and M. Antonelli. "Application of the homogeneous surface diffusion model for the prediction of the breakthrough in full-scale GAC filters fed on groundwater". In: *Process Safety and Environmental Protection* 117 (2018), pp. 286–295. DOI: <https://doi.org/10.1016/j.psep.2018.04.027>.
- [125] M. Zheng, C. Xu, H. Hu, Z. Ye, and X. Chen. "A modified homogeneous surface diffusion model for the fixed-bed adsorption of 4,6-DMDBT on Ag–CeO_x/TiO₂–SiO₂". In: *RSC Advances* 6.114 (2016), pp. 112899–112907. DOI: 10.1039/c6ra23967f.
- [126] C. Boi, S. Dimartino, and G. C. Sarti. "Modelling and simulation of affinity membrane adsorption". In: *Journal of Chromatography A* 1162.1 (2007), pp. 24–33. DOI: <https://doi.org/10.1016/j.chroma.2007.02.008>.
- [127] S. Dimartino, C. Boi, and G. C. Sarti. "A validated model for the simulation of protein purification through affinity membrane chromatography". In: *Journal of Chromatography A* 1218.13 (2011), pp. 1677–1690. DOI: <https://doi.org/10.1016/j.chroma.2010.11.056>.
- [128] T. Kataoka, H. Yoshida, and K. Ueyama. "Mass transfer in laminar region between liquid and packing material surface in the packed bed". In: *Journal of Chemical Engineering of Japan* 5.2 (1972), pp. 132–136. DOI: 10.1252/jcej.5.132.
- [129] H. Ohashi, T. Sugawara, K.-I. Kikuchi, and H. Konno. "Correlation of liquid-side mass transfer coefficient for single particles and fixed-beds". In: *Journal of Chemical Engineering of Japan* 14.6 (1981), pp. 433–438. DOI: 10.1252/jcej.14.433.

- [130] E. J. Wilson and C. J. Geankoplis. "Liquid mass transfer at very low Reynolds numbers in packed beds". In: *Industrial & Engineering Chemistry Fundamentals* 5.1 (1966), pp. 9–14. DOI: 10.1021/i160017a002.
- [131] J. Fettig and H. Sontheimer. "Kinetics of adsorption on activated carbon: I. Single solute systems". In: *Journal of Environmental Engineering* 113.4 (1987), pp. 764–779. DOI: doi:10.1061/(ASCE)0733-9372(1987)113:4(764).
- [132] J. M. P. Q. Delgado. "A critical review of dispersion in packed beds". In: *Heat and Mass Transfer* 42.4 (2005), pp. 279–310. DOI: 10.1007/s00231-005-0019-0.
- [133] L. K. Shekhawat and A. S. Rathore. "An overview of mechanistic modeling of liquid chromatography". In: *Preparative Biochemistry & Biotechnology* 49.6 (2019), pp. 623–638. DOI: 10.1080/10826068.2019.1615504.
- [134] S. O. Rastegar and T. Gu. "Empirical correlations for axial dispersion coefficient and Peclet number in fixed-bed columns". In: *Journal of Chromatography A* 1490 (2017), pp. 133–137. DOI: 10.1016/j.chroma.2017.02.026.
- [135] D. J. Gunn. "Axial and radial dispersion in fixed beds". In: *Chemical Engineering Science* 42.2 (1987), pp. 363–373. DOI: [https://doi.org/10.1016/0009-2509\(87\)85066-2](https://doi.org/10.1016/0009-2509(87)85066-2).
- [136] J. J. Carberry and R. H. Bretton. "Axial dispersion of mass in flow through fixed beds". In: *AIChE Journal* 4.3 (1958), pp. 367–375. DOI: 10.1002/aic.690040327.
- [137] P. V. Danckwerts. "Continuous flow systems: Distribution of residence times". In: *Chemical Engineering Science* 2.1 (1953), pp. 1–13. DOI: [https://doi.org/10.1016/0009-2509\(53\)80001-1](https://doi.org/10.1016/0009-2509(53)80001-1).
- [138] T. Hahn. "Advances in model-based downstream process development". PhD thesis. Institut für Bio- und Lebensmitteltechnik (BLT), Karlsruher Institut für Technologie (KIT), 2015. URL: <https://publikationen.bibliothek.kit.edu/1000051444>.
- [139] G. D. Scott and D. M. Kilgour. "The density of random close packing of spheres". In: *Journal of Physics D: Applied Physics* 2.6 (1969), pp. 863–866. DOI: 10.1088/0022-3727/2/6/311.
- [140] S. Qamar, J. N. Abbasi, A. Mehwish, and A. Seidel-Morgenstern. "Linear general rate model of chromatography for core-shell particles: Analytical solutions and moment analysis". In: *Chemical Engineering Science* 137 (2015), pp. 352–363. DOI: 10.1016/j.ces.2015.06.053.
- [141] S. Salvestrini, V. Leone, P. Iovino, S. Canzano, and S. Capasso. "Considerations about the correct evaluation of sorption thermodynamic parameters from equilibrium isotherms". In: *Journal of Chemical Thermodynamics* 68 (2014), pp. 310–316. DOI: 10.1016/j.jct.2013.09.013.

- [142] G. Wang, X. Su, Y. Hua, S. Ma, J. Wang, X. Xue, Q. Tao, and S. Komarneni. "Kinetics and thermodynamic analysis of the adsorption of hydroxy-Al cations by montmorillonite". In: *Applied Clay Science* 129 (2016), pp. 79–87. ISSN: 0169-1317. DOI: <https://doi.org/10.1016/j.clay.2016.04.023>. URL: <https://www.sciencedirect.com/science/article/pii/S0169131716301995>.
- [143] N.-W. Han, J. Bhakta, and R. G. Carbonell. "Longitudinal and lateral dispersion in packed beds: Effect of column length and particle size distribution". In: *AIChE Journal* 31.2 (1985), pp. 277–288. DOI: <https://doi.org/10.1002/aic.690310215>. eprint: <https://aiche.onlinelibrary.wiley.com/doi/pdf/10.1002/aic.690310215>. URL: <https://aiche.onlinelibrary.wiley.com/doi/abs/10.1002/aic.690310215>.
- [144] J. Wolters, M. Tagliavini, and A. I. Schäfer. "Removal of steroid hormone micropollutants by UF-PBSAC composite in presence of organic matter". In: *Journal of Membrane Science* 592 (2019), p. 117315. ISSN: 0376-7388. DOI: 10.1016/j.memsci.2019.117315.
- [145] J. E. Kilduff, T. Karanfil, and W. J. Weber. "Competitive interactions among components of humic acids in granular activated carbon adsorption systems: effects of solution chemistry". In: *Environmental Science & Technology* 30.4 (1996), pp. 1344–1351. DOI: 10.1021/es950546z.
- [146] J. J. McCreary and V. L. Snoeyink. "Characterization and activated carbon adsorption of several humic substances". In: *Water Research* 14.2 (1980), pp. 151–160. DOI: 10.1016/0043-1354(80)90231-6.
- [147] F. Zietzschmann, E. Worch, J. Altmann, A. S. Ruhl, A. Sperlich, F. Meinel, and M. Jekel. "Impact of EfOM size on competition in activated carbon adsorption of organic micro-pollutants from treated wastewater". In: *Water Research* 65 (2014), pp. 297–306. DOI: 10.1016/j.watres.2014.07.043.
- [148] Y. Matsui, T. Yoshida, S. Nakao, D. R. Knappe, and T. Matsushita. "Characteristics of competitive adsorption between 2-methylisoborneol and natural organic matter on superfine and conventionally sized powdered activated carbons". In: *Water Research* 46.15 (2012), pp. 4741–9. DOI: 10.1016/j.watres.2012.06.002.
- [149] G. Newcombe, J. Morrison, C. Hepplewhite, and D. R. U. Knappe. "Simultaneous adsorption of MIB and NOM onto activated carbon: II. Competitive effects". In: *Carbon* 40.12 (2002), pp. 2147–2156. DOI: 10.1016/S0008-6223(02)00098-2.
- [150] C. Pelekani and V. L. Snoeyink. "Competitive adsorption in natural water: role of activated carbon pore size". In: *Water Research* 33.5 (1999), pp. 1209–1219. DOI: 10.1016/S0043-1354(98)00329-7.

- [151] J. Shen, X. J. Yang, and A. I. Schäfer. "Quantification of hormone–humic acid interactions in nanofiltration". In: *Environmental Science & Technology* 46.19 (Sept. 2012), pp. 10597–10604. DOI: 10.1021/es301843s.
- [152] P. A. Neale and A. I. Schäfer. "Quantification of solute–solute interactions in steroidal hormone removal by ultrafiltration membranes". In: *Separation and Purification Technology* 90 (Apr. 2012), pp. 31–38. DOI: 10.1016/j.seppur.2012.02.011.
- [153] Lenntech. *Ultrafiltration Membranes*. Tech. rep. 2008. URL: <https://www.lenntech.com/Data-sheets/Millipore-Ultrafiltration-Membranes-L.pdf>.
- [154] E. Worch. "Eine neue gleichung zur berechnung von diffusionskoeffizienten gelöster stoffe". In: *Vom Wasser* 81 (1993), pp. 289–297.
- [155] I. Christl, H. Knicker, I. Kögel-Knabner, and R. Kretzschmar. "Chemical heterogeneity of humic substances: Characterization of size fractions obtained by hollow-fibre ultrafiltration". In: *European Journal of Soil Science* 51.4 (2000), pp. 617–625. DOI: 10.1111/j.1365-2389.2000.00352.x.
- [156] R. M. B. O. Duarte, E. B. H. Santos, and A. C. Duarte. "Spectroscopic characteristics of ultrafiltration fractions of fulvic and humic acids isolated from an eucalyptus bleached Kraft pulp mill effluent". In: *Water Research* 37.17 (2003), pp. 4073–4080. DOI: 10.1016/S0043-1354(03)00411-1.
- [157] A. Rodrigues, A. Brito, P. Janknecht, M. F. Proença, and R. Nogueira. "Quantification of humic acids in surface water: effects of divalent cations, pH, and filtration". In: *Journal of Environmental Monitoring* 11.2 (2009), pp. 377–382. DOI: 10.1039/B811942B.
- [158] A. I. Schäfer. *Natural organics removal using membranes: principles, performance, and cost*. Technomic Publishing Lancaster, Pa, 2001. ISBN: 1420031635.
- [159] S. A. Huber, A. Balz, M. Abert, and W. Pronk. "Characterisation of aquatic humic and non-humic matter with size-exclusion chromatography – organic carbon detection – organic nitrogen detection (LC-OCD-OND)". In: *Water Research* 45.2 (2011), pp. 879–885. DOI: 10.1016/j.watres.2010.09.023.
- [160] P. A. Neale, A. Antony, W. Gernjak, G. Leslie, and B. I. Escher. "Natural versus wastewater derived dissolved organic carbon: implications for the environmental fate of organic micropollutants". In: *Water Research* 45.14 (2011), pp. 4227–37. DOI: 10.1016/j.watres.2011.05.038.
- [161] L. Li, H. E. Wray, R. C. Andrews, and P. R. Bérubé. "Ultrafiltration fouling: Impact of backwash frequency and air Sparging". In: *Separation Science and Technology* 49.18 (2014), pp. 2814–2823. DOI: 10.1080/01496395.2014.948964.

- [162] H. Chang, H. Liang, F. Qu, B. Liu, H. Yu, X. Du, G. Li, and S. A. Snyder. "Hydraulic backwashing for low-pressure membranes in drinking water treatment: A review". In: *Journal of Membrane Science* 540 (2017), pp. 362–380. ISSN: 0376-7388. DOI: 10.1016/j.memsci.2017.06.077.
- [163] X. Shi, G. Tal, N. P. Hankins, and V. Gitis. "Fouling and cleaning of ultrafiltration membranes: A review". In: *Journal of Water Process Engineering* 1 (2014), pp. 121–138. ISSN: 2214-7144. DOI: 10.1016/j.jwpe.2014.04.003.
- [164] G. Zin, J. Wu, K. Rezzadori, J. C. C. Petrus, M. Di Luccio, and Q. Li. "Modification of hydrophobic commercial PVDF microfiltration membranes into superhydrophilic membranes by the mussel-inspired method with dopamine and polyethyleneimine". In: *Separation and Purification Technology* 212 (2019), pp. 641–649. DOI: 10.1016/j.seppur.2018.10.014.
- [165] R. Lyubimenko, D. Busko, B. S. Richards, A. I. Schäfer, and A. Turshatov. "Efficient Photocatalytic Removal of Methylene Blue Using a Metalloporphyrin–Poly(vinylidene fluoride) Hybrid Membrane in a Flow-Through Reactor". In: *ACS Applied Materials & Interfaces* 11.35 (2019), pp. 31763–31776. DOI: 10.1021/acsami.9b04601.
- [166] B. Kruczek. "Carman–Kozeny equation". In: *Encyclopedia of Membranes*. Ed. by E. Drioli and L. Giorno. Berlin, Heidelberg: Springer Berlin Heidelberg, 2015, pp. 1–3. ISBN: 978-3-642-40872-4. DOI: 10.1007/978-3-642-40872-4_1995-1.